Baltic State Technical University “VOENMEH” named after D.F. Ustinov

Karina Eduardovna Savelova

Regular and Mach reflection of gas-dynamic discontinuities with energy release

Scientific specialization: 1.1.9.
Mechanics of liquid, gases and plasma

Dissertation for the degree
of candidate of physical and mathematical sciences

Translation from Russian

Scientific supervisor:
Doctor of Technical Sciences
Mikhail V. Chernyshov

Saint Petersburg – 2024

Contents

Introduction

Supersonic gas flows, which realizes in jets, nozzles, air intakes, when flowing around various surfaces and at their aerodynamic interference, are accompanied by the formation of gasodynamic discontinuities (such as shock waves, slipstreams, weak discontinuities, etc.), their reflection and interaction, both regular and irregular. When gasodynamic discontinuities reflect and interact, numerous shock-wave structures appear [1-3], i.e. the systems of gasodynamic discontinuities which have one common point. A widespread example of the shock-wave structure that occurs in steady supersonic flows is the triple configuration of steady shocks, which forms, in particular, at the irregular (Mach) reflection of an oblique shock from a solid surface, symmetry plane or axis.

The phenomena of regular and irregular reflection of steady shocks (in the nonstationary case, of unsteady shock waves) were first described by E. Mach and his colleagues ([4, 5], see also [6, 7]). The development of jet aviation, rocket technology and cosmonautics, as well as the increased interest in the interactions of strong blast waves with various objects and structures caused a splash of interest in this phenomenon in the 1940s and 1950s, including one from world-famous scientists [8-12]. In particular, J. von Neumann [8] identified two criteria for changing the type of reflection of a steady or unsteady shock wave: the criterion of “mechanical equilibrium”, later named him (so-called von Neumann criterion), and the “detachment criterion”, which can be more correctly called the criterion of the maximum angle of flow deflection (on a reflected hock). He also identified the area of “dualism of solutions” (“dual solution domain”) – the parameters of the incoming flow and the incident shock, in which both regular and Mach reflection are possible. The development of the theory of reflection of oblique shocks in the 20th century was presented in review articles [13-16] and monographs [17-20]. The consensus established by the early 1990s in the scientific community was that the “detachment” criterion of maximum flow deflection was applicable to reflection of propagating shock waves (for example, relative to an inclined wedge [17]), and the von Neumann criterion, associated with the formation of so-called stationary Mach configuration

[1, 20] with a normal main (Mach) shock, is primarily applicable to shock reflection in steady flows. In this case, the size of the resulting Mach shock (Mach stem) turned out to be a continuous function of the problem parameters (in particular, the intensity of the incident shock, or its angle of incidence, or the angle of flow deflection on its surface) and tended to zero when the von Neumann criterion was fulfilled, which corresponded to the continuous transition to regular reflection. Thus, according to the established concept, the Mach reflection in steady flows continuously switched to regular one and back, and the Mach reflection was also implemented throughout the "dual solution domain" of parameters. According to the milestone work [16], the problems of estimating the size of the Mach stem and the flow separation at the interaction of the incident shock with the surface were declared almost only unresolved in the theory of steady shock reflection, but not the problem of criteria determining the type of reflection. The theoretical assumptions about the existence of hysteresis phenomenon in a reflection type change (regular or Mach one), presented in [21], were not confirmed experimentally [22-24] and were temporarily forgotten.

The development of computational possibilities and, in part, of experimental techniques has made it possible to identify hysteresis phenomena in dual solution domain, first by numerical simulation [25-34], and then experimentally [34-37]. A variety of numerical methods (solving the Euler equations and Navier-Stokes equations supplemented by various turbulence models, direct statistical Monte Carlo simulation) left no doubt about the existence of hysteresis, which became more complete as the Knudsen number increased (the rarefied gas model approximated the continuum model). A detailed analysis of the experimental results [25-34] using theoretical and numerical methods [36, 37] have shown that the revealed incompleteness of the hysteresis loop (manifested in the fact that a sudden transition from regular reflection to Mach reflection with a major jump of finite magnitude occurs somewhere inside the domain of the dualism of solutions, and not near its upper boundary, which corresponds to the detachment criterion) indicates the influence of disturbances from aside (i.e., three-dimensionality of the flow) or the effects of reflection of disturbances from the walls of a closed supersonic wind tunnel

[36, 37]. The effect of three-dimensionality has been studied in detail in [36-40], and the completeness of the hysteresis loop currently serves as one of the characteristics of the quality of experimental data obtained in wind tunnels [37]. At the same time, both regular and Mach reflection, observed in the domain of dual solution, occurred resistant to small perturbations of flow parameters [41-46]. However, as shown in [28, 29, 46, 47], Mach reflection is more resistant to finite disturbances (such as sudden change in flow velocity, gas density, introduction of an obstacle into the flowfield with its subsequent removal). It was explained in [41, 48] by a more significant increase in the entropy of the gas stream as a whole at Mach reflection than at regular reflection. Later, hysteresis phenomena with a change in the type of reflection of oblique shocks were mathematically justified by topological methods [49, 50].

Experimentally and numerically obtained data [26, 28, 29, 31, 32, 34, 43, 46, 51], as well as the results of the application of various approximate analytical models [52-58], indicated that in the domain of dual solution, either regular reflection or Mach reflection with some definite height of the main shock is observed, if only the parameters of the problem (the shape of the streamlined body, the Mach number of the incoming flow, the angle of incidence of the oblique jump, the gas adiabatic index, etc.) are uniquely determined. The background of the flowfield (its past) influences only the type of shock reflection, but not Mach stem size, if only the Mach reflection really occurs. Mach stem height can be determined uniquely both in the domain of the problem parameters corresponding only to the Mach reflection, and in dual solution domain, if only this type of shock reflection, and not regular reflection realizes. In addition, in the problems of supersonic aerodynamics, rocket technology and cosmonautics, which have significant practical significance (for example, when a supersonic aircraft accelerates [59] or when launch vehicle starts with a corresponding decrease in the degree of overexpansion of the expiring jet [27]), there is an entry into the dual solution domain from the Mach reflection domain. In this direction of changing the parameters (such as external pressure, flight Mach number, etc.), according to the established reliable concept, it is the Mach reflection that

persists throughout the dual solution domain until the parameters corresponding to the von Neumann criterion are reached. This means that of practical interest are only those methods for estimating the parameters of the shock-wave structure of flows with steady Mach reflection of oblique shocks, in which the Mach stem height is determined in a unique way in the entire domain of existence of Mach reflection (including the dual solution domain) and tends to zero at the lower boundary of this region which corresponds to von Neumann criterion.

Quick engineering estimation of the height of the main shock, as a key parameter which determines the properties of the forming shock-wave structure and flow parameters behind it, was declared one of the two key problems in steady shock reflection studies already in [16]. The assumptions made in the first approximate analytical models [52, 53] led to a significant (by 50-90%) underestimation of the Mach stem height compared with experimentally observed values [24, 37, 40]. However, they were based on the correct (experimentally and numerically confirmed) concept of the formation of a “virtual nozzle” – the flow region behind the Mach stem, in which the transition from subsonic flow velocity (immediately after the Mach shock) to supersonic one with simultaneous (as in the classical geometric dual-bell de Laval nozzle) transition from narrowing its cross-section to its expansion, which is accompanied by a corresponding turn of the slipstream limiting this area. Subsequently, the model [53] was supplemented with various ratios averaging the Mach number behind the main shock [57, 58], the shape of the reflected oblique shock [60, 61] and turning slipstream [54, 55], which slightly increased the accuracy of the results achieved. The model proposed in [56, 62] was based on analytical solutions to the problems of overtaking [63] and counter [60, 61] interaction of oblique shocks and isentropic waves, conjugation of the quasi-one-dimensional flow region with an expansion/compression Prandtl-Meyer wave [64, 65], the incidence of a rarefaction wave on the slipstream, taking into account the existence of a reflected compression wave. This model [56, 62] differs in the greatest accuracy (compared with the results of numerical and physical experiments) of the approximation of the supersonic part of the flowfield. In the presented dissertation study, the analytical

model summarized in [56] is generalized to the case of the presence of a pulsed energy supply (for example, caused by exothermic chemical reactions) and changes in the chemical composition of the gas mixture behind the Mach shock [143, 145, 147].

Interest to the analytical models for rapid assessment of the parameters of the shock-wave structure of flows with Mach reflection and/or irregular interaction of steady shocks has increased markedly in recent years [57, 58, 66-68]. It is probably explained by the development of vehicles flying at high supersonic speeds in the atmosphere and air intake devices for their propulsion systems. With an accuracy acceptable for applied research, a model of a perfect gas with a reduced (compared to air) “effective” adiabatic index can be used to describe flows with high supersonic velocity whish shock reflections and interactions. It is in such steady flows (along with flows of polyatomic gases) that a special shock-wave structure can exist, which was discovered by L.G. Gvozdeva [69] and later studied in [70-75] – the Mach reflection with a negative (relative to the incoming flow) slope angle of the reflected shock. In the presented thesis, the conditions of existence and unambiguity of the solution for such structures of “negative”: Mach reflection are analyzed, and the corresponding analytical relations are derived [144]. The obtained results are compared with the data of a numerical experiment [70, 76], including in the presence of the solution ambiguity.

The triple configuration of steady shocks (a special case of which is the triple configuration of the Mach reflection), divides the incoming flow into two streams that differ significantly in the values of the velocity and flow Mach number of the flow, impulse and dynamic pressure, stagnation pressure and static temperature, and many other parameters [76, 78, 79]. This fully applies to triple configurations of irregular reflection realized in a flow with large Mach numbers and reduced gas adiabatic indices, including “negative” configurations [75]. In particular, the supersonic gas flow behind the reflected shock has a significantly higher (sometimes in tens of times) stagnation pressure than the subsonic flow behind the Mach stem. Under the condition of further deceleration in the system of oblique shocks [80-83],

this flow can be effectively used in the thermodynamic cycle of a ramjet engine (the Brayton cycle). The subsonic flow behind the main (Mach) stem, despite the small value of its total pressure, has another advantage – a significantly higher static temperature, which can initiate the detonation of the fuel-air mixture supplied to the surface of the main shock and thus stimulates its use in the thermodynamic cycle of a ramjet detonation engine (the Fickett-Jacobs cycle [84, 85]).

The idea of a combined ramjet engine, expressed for the first time in [86], was analyzed and justified in the cycle of studies [150-156, 159, 160, 165] which the author and her supervisor provided. For its effective implementation, it is necessary to separate the streams formed behind the main shock and reflected one after the Mach reflection with a pulsed energy supply and a change in the chemical composition of the gas mixture at the main shock. Separation along the slipstream emanating from the triple point seems most evident. To solve this problem, in turn, it is necessary to determine the condition of existence of the Mach reflection, as well as the height of the main shock, the shape and other parameters of the slipstream, of other gasodynamic discontinuities in the flowfield for any arbitrarily selected parameters of the problem. The presented study is largely aimed to solving this important problem – the development of an approximate analytical model for rapid estimation of the parameters of the shock-wave structure of supersonic flows with Mach reflection in the presence of a pulsed energy supply and a change in the chemical composition of the gas mixture at the main shock, which thus turns into a stationary detonation wave. The small (in comparison with the characteristic lengths of technical devices) thickness of the “himpik” (“von Neumann peak”, or “von Neumann spike”) zone makes it possible to neglect the kinetics of chemical reactions behind the main shock for the sake of derivation of analytical relations. Thus, the main shock is considered within the framework of the classical Chapman-Jouguet model as an oblique (in general) stationary detonation wave with instantaneous energy supply and a change in the chemical composition, manifesting itself primarily in a change in its adiabatic index. Using the Chapman-Jouguet model to the Mach stem allows us to obtain a number of analytical solutions describing the flowfield.

Comparison with numerical simulation data [152, 158, 160, 165], including the results of other authors [87-90], shows that the constructed analytical model leads to qualitatively correct and quantitatively fairly accurate results.

To determine the domain of existence of the solution and calculate the flow parameters in the vicinity of the triple point of the Mach reflection, this work uses a graphical technique of detonation shock polars [91] describing stationary detonation waves within the framework of the Champan-Jouguet model. The mathematical model of stationary detonation has been repeatedly used (without full parametric analysis) to describe the Mach reflection (in [88-90] – in relation to the incident shock and the main one, and in [87] – for all jumps in the flowfield). Unlike the above-mentioned studies, this work takes into account pulsed energy supply and changes in the chemical composition exclusively at the main (Mach) shock. It is assumed that, as was shown earlier [76, 79, 92], a significantly higher temperature behind the main shock stimulates, first of all, pulsed energy release behind its surface in the immediate vicinity of it.

In this study and, as well as in other publications of its author [145-147, 164, 167, 169], it is shown that the presence of a pulsed energy supply leads to a significant shift in the lower boundary of the region of existence of the Mach reflection, which under “normal” conditions corresponds to the von Neumann criterion. It leads to a possibility of a Mach reflection of rather weak oblique shocks that reflect only regularly under “normal” conditions (if pulsed power supply at the main shock is not possible). The decrease in the gas adiabatic index, typical for the combustion of a fuel-air mixture, has a similar, but much weaker effect. The results of the application of the developed approximate analytical model and their computational verification show that a pulsed energy supply (within the limits allowing stationary detonation) leads to a noticeable increase in the Mach stem size and in the width of the subsonic flow region behind it, potentially suitable for subsequent use in the Fickett-Jacobs thermodynamic cycle. In addition, the developed analytical model makes it possible to quickly determine the shape of all gasodynamic discontinuities in the flowfield, including a slipstream emanating from a triple point.

It can be practically useful for separating flows with different thermal and gasodynamic properties.

Further development of this study can lead to a general theory of shock-wave structures (including triple-shock configurations) with pulsed energy release at the constituent gasodynamic discontinuities.

General characteristics and structure of the study

The relevance of the research topic is the need to extend the theory of interaction of gasodynamic discontinuities to cases of reflection and interaction of those discontinuities with a possible pulsed energy supply and a change in the chemical composition of the gas mixture. The need for such an expansion of the range of theoretically solvable tasks bases on the development of aviation, rocket and space technologies, the design of prospective propulsion systems of aircraft for flights with high supersonic speeds. In view of this, it becomes necessary to study the interaction of gasodynamic discontinuities in supersonic flows of reactive gas mixtures, to analyze the flowfield and to optimize the resulting shock-wave systems and structures, rapidly evaluating new aerodynamic schemes and designs of jet engines.

The aim of this study is to analyze shock-wave structures that occur when oblique shocks reflects, including under conditions of pulsed energy supply and changes in the chemical composition of the gas mixture at the main shock (Mach stem), as well as to create a reliable mathematical technique for rapid assessment and analysis of the flowfield with resulting shock-wave structures.

The reliability of the obtained results is ensured applying strict and well-tested mathematical apparatus of classical gas dynamics, dynamics of detonation waves, compatibility conditions at gasodynamic discontinuities and exact solutions of classical problems of their interaction. The author also obtained the data of theoretical analysis and numerical simulation which mutually verify each other. The available experimental data from other authors also confirm the reliability of the results obtained.

The scientific novelty of the research is as follows:

- analytical relations describing shock-wave structures of regular reflection with minimal dynamic loading and, for the first time, with minimal thermal loading of the affected object are obtained;

- the areas of ambiguity of the solution for shock wave-structures resulting in the reflection of oblique shocks in flows with large Mach numbers and reduced adiabatic indices are identified and analytically described;

- the conditions of existence are revealed and a parametric analysis of triple configurations of steady shocks at Mach reflection with pulsed energy supply and a change in the chemical composition at the main shock is obtained;

- for the first time, an approximate analytical model of the flow with Mach reflection with the possible presence of a pulsed energy supply and a change in the chemical composition of the mixture at the main shock has been developed;

- the laws of change in the shock-wave structure of the steady Mach reflection under conditions of pulsed energy supply at the main shock are analytically and numerically revealed.

The scientific value of the study consists in the following:

- theoretical analysis and optimization of shock-wave structures of steady regular reflection of oblique shocks are obtained according to the criteria of dynamic and thermal load on the object of impact, interpretation of the results obtained for unsteady reflection of propagating shock waves is given;

- a theoretical analysis of the ambiguity of solutions for shock-wave structures which can form at oblique shock reflection at large Mach numbers and reduced adiabatic indices is carried out;

- a novel approximate analytical model of gas flow with Mach reflection has been developed, which allows for a theoretical analysis of flows with energy supply and a sudden change in the chemical composition of the gas mixture exclusively at the main shock (Mach stem);

- the analysis of the influence of pulsed energy supply and changes in the chemical composition on the feasibility of Mach reflection, as well as on the

gasodynamic parameters of the flowfield and on the geometric parameters of the shock-wave structure which forms in this case is obtained.

The practical value of the dissertation is as follows:

a) the results of the optimization of the shock-wave structure of regular reflection can significantly reduce the dynamic and thermal loads on aerodynamic surfaces and objects affected by shock and blast waves;

b) the analyzed ambiguity of solutions for shock-wave structures of Mach reflection should be taken into account in the gasodynamic design of supersonic air intakes, airframes of aircraft and other technical objects;

c) model developed for rapid estimation of the parameters of the shock-wave structure of the Mach reflection, allowing pulsed power supply and a change in the chemical composition of the gas at the main shock, can be used in the design of various technical devices, including prospective ramjet engines.

Publications. The results presented in this study were published in papers [148-169] of which 3 are in peer-reviewed scientific journals recommended by the Higher Attestation Commission, 8 are indexed in the international citation databases Web of Science and SCOPUS, 17 are in conference materials indexed in the Russian scientific citation index (RINTs). The author's personal contribution is described in Appendix A.

Approbation of the results. The results achieved during the study were presented at the following national and international conferences, and other scientific and technical events:

a) All-Russian Youth Scientific and Technical Conference «Start-2018» (Saint Petersburg, 2018);

b) VII All-Russian Youth Scientific Conference with International Participation «Current Issues of Continuum Mechanics and Celestial Mechanics – 2023» (Tomsk, 2018);

c) All-Russian Scientific and Technical Conference «The Eight Utkin's Readings» (Saint Petersburg, 2019);

d) XLIV Academic Space Conference dedicated to the memory of academician S.P. Korolev and other outstanding national scientists – pioneers of space exploration (Moscow, 2019);

e) XXII All-Russian Scientific and Practical Conference “Actual Problems of Protection and Security” (Saint Petersburg, 2019);

f) the 19th International Conference “Aviation and Cosmonautics” (Moscow, 2020);

g) the International Scientific Conference on Mechanics “The Ninth Polyakhov’s Reading” (Saint Petersburg, 2021);

h) International Scientific Conference “PETER 2021: New Models and Hydrocodes for Shock Wave Physics” (London, 2021)

i) the 20th International Conference “Aviation and Cosmonautics” (Moscow, 2021);

j) XLV Academic Space Conference dedicated to the memory of academician S.P. Korolev and other outstanding national scientists – pioneers of space exploration (Moscow, 2021);

k) the Twenty-Second International Conference on Computational Mechanics and Modern Applied Software Systems (CMMASS'2021), Alushta, 2021;

l) the Second All-Russian Scientific and Technical Conference “Scientific Readings in Memory of Academician V.P. Glushko” (Saint Petersburg, 2021);

m) the 21st International Conference “Aviation and Cosmonautics” (Moscow, 2022);

n) XXV All-Russian Scientific and Practical Conference “Actual Problems of Protection and Security” (Saint Petersburg, 2022);

o) XXVI All-Russian Seminar with International Participation on Jet, Separated and Unsteady Flows (Saint Petersburg, 2022);

p) XXXIII Scientific and Technical Conference on Aerodynamics (Zhukovsky, 2022);

q) XLVII Academic Space Conference dedicated to the memory of academician S.P. Korolev and other outstanding national scientists – pioneers of space exploration (Moscow, 2023);

r) All-Russian Scientific Symposium on Problems of Aeromechanics and Gas Dynamics, Dedicated to the 100th Anniversary of the Birth of Academician Gorimir Gorimirovich Cherny (Moscow, 2023);

s) XXVI All-Russian Scientific and Practical Conference "Actual Problems of Protection and Security" (Saint Petersburg, 2023);

t) X International Symposium "Space Flight Safety" (Saint Petersburg, 2023);

u) the XXXIX Siberian Thermophysical Seminar (Novosibirsk, 2023);

v) the XIIIth All-Russian Congress on Theoretical and Applied Mechanics (Saint Petersburg, 2023);

w) II Seminar School "Mechanics, Chemistry and New Materials" under the Guidance of the Corresponding Member of RAS Yu.V. Petrov (Saint Petersburg, 2023);

x) VII Minsk International Colloqium on Physics of Shock Waves, Combustion and Detonation (Minsk, 2023).

The oral lectures which the author presented at events (b), (o) and (u) were awarded honorary diplomas.

The structure and scope of the PhD thesis. The study consists of an introduction, three chapters, a conclusion, a list of 169 references and an appendix. The total length of the study is 164 pages, including 34 figures and 1 table.

Main scientific achievements:

a) The results of optimization of the shock-wave structure of regular reflection, analytically obtained in the presented study, which can significantly reduce not only dynamic [93], but also thermal loads on bodies subjected to shock-wave action during aerodynamic interference, as well as (when reversing motion) – on objects subjected to traveling shock and blast waves [148]. Personal contribution of the author in obtaining those results: literature analysis, numerical and analytical calculations, interpretation of results, writing the article.

b) The results [144, 166] of the analysis of the ambiguity of solutions for shock-wave structures of Mach reflection (including “negative” triple configurations), which must be taken into account in the gasodynamic design of various technical devices [149, 151, 157]. In particular, the coexistence of solutions for “negative” configurations of Mach reflection, regular reflection, and solutions with detached bow shocks can lead to the practical unfeasibility or instability of “negative” configurations. [144]. Personal contribution of the author in obtaining those results: literature analysis, numerical and analytical calculations, interpretation of results, writing articles.

c) An approximate analytical model of the shock-wave structure of the flow with Mach reflection [143, 145, 162, 167, 169], taking into account the possible presence of a pulsed energy supply and changes in the chemical composition of the gas mixture at the main shock [146, 147, 161, 163, 164], which allows for a fairly accurate and reliable assessment of the main flow parameters, including the size of the main (Mach) shock, and can be used for the gas dynamic design of various technical devices, including advanced ramjet engines [150, 152, 153-156, 165] (all analytical calculations were carried out personally by the author of the dissertation, the total contribution is at least 80%).

d) The presence of a pulsed energy supply (within the established limits of the solution existence) leads to a significant increase in Mach stem size [147, 158-160], as well as to the realization of the Mach reflection in conditions when, in the absence of a pulsed energy supply, only regular reflection is realized [146, 169]. The effect of changes in the chemical composition of the mixture on the height of the main shock and other parameters of the shock-wave structure is significantly weaker [146, 147]. Personal participation of the author in obtaining these results: literature analysis, numerical and analytical calculations, interpretation of results, writing articles (personal contribution is at least 80%).

Results submitted for defense

a) an approximate analytical model of the shock-wave structure of a flow with Mach reflection, including in the presence of pulsed energy release and changes in the chemical composition of the gas mixture at the main shock;

b) the presence of pulsed energy release leads to a significant increase in the size of the Mach stem and also to the implementation of Mach reflection of oblique shocks which can reflect only regularly, if energy realase is impossible;

c) results of analysis of the ambiguity of solutions for shock-wave structures of Mach reflection (including “negative” triple configurations). In particular, the coexistence of solutions for “negative” configurations of Mach reflection, regular reflection and solutions with separated shock waves;

d) results of optimization of the shock-wave structure of regular reflection.

Acknowledgment. The work was supported by the Ministry of Science and Higher Education of the Russian Federation (the project “Creating a leading scientific and technical reserve in the development of advanced technologies for small gas turbine, rocket and combined engines of ultra-light launch vehicles, small spacecraft and unmanned aerial vehicles that provide priority positions for Russian companies in emerging global markets of the future”, No. FZWF-2020-0015).

Chapter 1. Mathematical models and basic relationships

Modern achievements of the theory of interaction of gas-dynamic discontinuities [1, 18, 20, 44, 50, 62, 69], as wel as in the theory of optimal shock-wave systems and structures [23, 78, 79, 83] make it possible to solve complex problems research and control of flows with various types of reflection and interaction of gas-dynamic discontinuities analytically and numerically. Chapter 1 shows the basic terms and relationships used in this study which form the basis of the mathematical apparatus. In this case, a thermodynamic model of a perfect gas is used, which is also (with the exception of calculations of model flows using the methods of computational fluid dynamics) assumed to be inviscid and non-heat-conducting.

1.1. Steady shock wave

A normal or oblique steady shock (Figure 1.1) is the surface of a gas-dynamic discontuinuity located at a non-zero angle to the direction of upstream flow (so-called surface of a normal discontinuity). At the shock wave, a finite break of a number of flow parameters occurs. The relations used below that connect the shape of the shock and the change in flow parameters on its sides are given below.

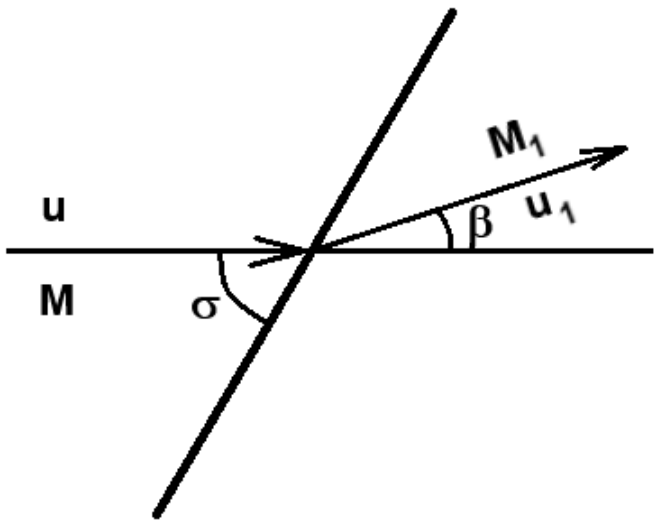

Figure 1.1. Diagram of the flow with a steady shock

One of the main parameters of a shock wave is its intensity (shock strength) J. It is the ratio of static pressures behind the shock (p_1) and in front of him (p), which

is related to the angle σ of the shock slope to the upstream velocity vector by the well-known relation

$$J_1 = p_1/p = (1+\varepsilon)M^2 \sin^2\sigma - \varepsilon. \tag{1.1}$$

Here $\varepsilon = (\gamma-1)/(\gamma+1)$, and γ is gas adiabatic index (wherever this is not specified separately, all examples of calculations correspond to the value $\gamma = 1.4$). In particular, the intensity J_m of a steady shock normal to the oncoming flow is

$$J_m = (1+\varepsilon)M^2 - \varepsilon. \tag{1.2}$$

Shock wave which degenerates into a weak disturbance ($J \to 1$) is directed at Mach angle

$$\alpha = \arcsin(1/M). \tag{1.3}$$

Angle β of flow rotation of on the surface of the steady shock is also determined by its intensity:

$$|\beta| = \arctan\left[\sqrt{\frac{J_m(M)-J}{J+\varepsilon}} - \frac{(1-\varepsilon)(J-1)}{(1+\varepsilon)M^2-(1-\varepsilon)(J-1)}\right]. \tag{1.4}$$

Relation (1.4) is graphically displayed on the plane ($\beta; \Lambda = \ln J$) in the form of a shock polar (for example, heart-shaped curve I in Figure 1.2). Maximum flow deflexction angle for a given fixed Mach number M at a single shock is achieved at shock intensity

$$J_l = \frac{M^2-2}{2} + \sqrt{\left(\frac{M^2-2}{2}\right)^2 + (1+2\varepsilon)(M^2-1) + 2} \tag{1.5}$$

and corresponds to the extreme left and right points l on shock polar I. Those points divide the shock polar into its upper (which corresponds to the so-called strong shocks) and lower (corresponding to weak shocks) branches.

Mach number M_1 of the flow behind the shock is determined by the relation

$$M_1 = \sqrt{\left[(J+\varepsilon)M^2 - (1-\varepsilon)(J^2-1)\right]/\left[J(1+\varepsilon J)\right]}. \tag{1.6}$$

The relation obtained from (1.6) at $M_1 = 1$

$$J_*(M) = \frac{M^2-1}{2} + \sqrt{\left(\frac{M^2-1}{2}\right)^2 + \varepsilon(M^2-1) + 1} \tag{1.7}$$

determines the strength of the oblique shock with the critical velocity of the flow downstream it. The flow behind the shock wave is supersonic at $J < J_*$ and subsonic in the opposite case (in particular, behind all "strong" waves, since $J_* < J_l$ at the same Mach number, and the corresponding point "*"on the shock polar is always located slightly below the point l, which corresponds to the maximum flow turn).

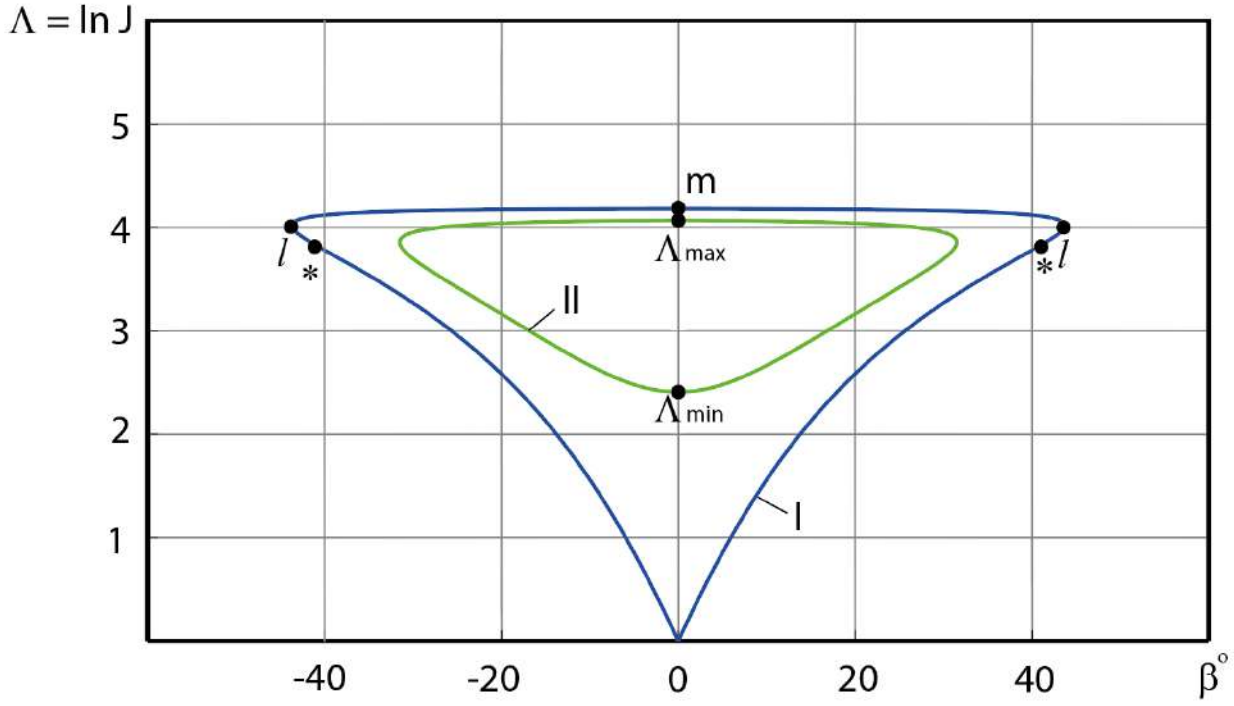

Figure 1.2. Graphical representation of stationsry shocks on the plane of shock polars

Rankine-Hugoniot adiabat describing the changes in density (ρ) and pressure at the shock wave, for a perfect gas is written in the following form:

$$E = \rho/\rho_1 = (1+\varepsilon J)/(J+\varepsilon).$$

It determines the change in static gas temperature (T)

$$\Theta = T_1/T = J(1+\varepsilon J)/(J+\varepsilon), \qquad (1.8)$$

speed of sound, acoustic impedance and other thermodynamic parameters. Stagnation pressure ratio (p_0) for gas flow (so-called coefficient of losses, or coefficient of recovery of this total pressure at the shock wave) is determined by the relation

$$I = p_{01}/p_0 = \left(JE^{\gamma}\right)^{-\frac{1-\varepsilon}{2\varepsilon}}. \qquad (1.9)$$

It is a monotonically decreasing function of the shock intensity.

Differential conditions of dynamic compatibility [1, 61-63] make it possible to relate the gradients of flow parameters in a non-uniform gas flow (the so-called main non-uniformities $N_1 = \partial \ln p / \partial s$ – flow non-isobaricity, $N_2 = \partial \theta / \partial s$ – streamline curvature, $N_3 = \partial \ln p_0 / \partial n$ – vorticity degree of the isoenergetic flow) in the most convenient form:

$$\widetilde{N}_i = C_i \sum_{j=1}^{5} A_{ij} N_j \, .$$

Here $\widetilde{N}_i$ $(i = 1..3)$ are the main non-uniformiities in the flow behind the shock, N_j are the non-uniformiities in front of it, $N_4 = \delta / y$ is the flow symmetry index, $N_5 \equiv K_\sigma$ is the geometric curvature of the shock (which is non-zero in the general case), $\delta = 0$ in planar flow and $\delta = 1$ in axisymmetric one, y is the distance from the axis or the plane of symmetry, θ is the flow angle, (s, n) are the "natural" coordinates associated with the direction of gas flow.

1.2. Stationary shock with pulsed energy release and changes in the chemical composition of the gas

A significant increase in temperature at a strong shock wave can lead to detonation of a reactive gas mixture with a corresponding pulsed energy release and a change in chemical composition. The simplest model that allows a qualitative analytical study of the reflection and interaction of shock waves with pulsed energy release is the Chapman-Jouguet relationship for stationary detonation:

$$\begin{gathered} \rho u_n = \rho_1 u_{1n}, \; p + \rho u_n^2 = p_1 + \rho_1 u_{1n}^2, \; u_\tau = u_{1\tau}, \\ \frac{u_n^2 + u_\tau^2}{2} + \frac{\gamma}{\gamma - 1} \frac{p}{\rho} + \phi = \frac{u_{1n}^2 + u_{1\tau}^2}{2} + \frac{\gamma_1}{\gamma_1 - 1} \frac{p_1}{\rho_1} . \end{gathered} \tag{1.10}$$

Here, the indices «n» and «τ» refer to the normal and tangential (to the shock surface) components of the flow velocity u, the adiabatic index of the gas mixture (products of stationary detonation) behind the wave is equal to γ_1, and ϕ is pulsed energy release per unit mass of a gas mixture, determined by specific heat λ of fuel combustion related to the entire gas mixture in the oncoming flow.

Pulse energy release ϕ can be represented by its dimensionless quantity

$$\bar{\phi} = \frac{\phi}{(p/\rho)} = \frac{\gamma\phi}{(\gamma-1)c_p T}, \tag{1.11}$$

where the values of temperature T and specific isobaric heat capacity c_p refer to the mixture in the free flow upstream the shock.

Model (1.10) transforms the relations (1.1-1.9) on shock waves. In particular, the formula [88]

$$|\beta| = \operatorname{arctg}\left[\frac{(J-1)\sqrt{F-1}}{\gamma M^2-(J-1)}\right],\ F = \frac{2\gamma M^2\left[(\gamma-\gamma_1)+(\gamma-1)\left((J-1)-(\gamma_1-1)\bar{\phi}\right)\right]}{(\gamma-1)(J-1)\left[(\gamma_1+1)(J-1)+2\gamma_1\right]} \tag{1.12}$$

describes the the flow deflection at a strong shock with energy release, transforming at $\gamma_1 = \gamma$ and $\bar{\phi} = 0$ into the formula (1.4).

As it is shown in [146], a fairly large pulsed energy release $\bar{\phi}$ shifts the "detonation" polar II ([21], Figure 1.2), displayed by relation (1.12), inside the shock polar I, corresponding to the equation (1.4). At the same time, the intensity J of the shock j (i.e., of the stationary detonation wave) must belong to the gap

$$J_{\min} \le J \le J_{\max}. \tag{1.13}$$

Here, the value $J = J_{\max}$ corresponds to a normal steady shock with pulsed energy release. Values $J_{\min}$ and $J_{\max}$ are determined by the formula [146]

$$J_{\min,\max} = \frac{\gamma+1}{\gamma_3+1}\cdot\frac{J_m(M)+1}{2} \mp \frac{\sqrt{\gamma^2M^4+\gamma_3^2-2\gamma M^2\left[\left(\gamma_3^2-1\right)\bar{\phi}+\left(\gamma_3^2-\gamma\right)/(\gamma-1)\right]}}{\gamma_3+1}, \tag{1.14}$$

where $J_m(M) = (1+\varepsilon)M^2 - \varepsilon$.

Mach number M_1 behind a shock with energy release, instead of (1.6), is determined by the relation

$$M_1 = \sqrt{\frac{\gamma M^2\left(E^2\sin^2\sigma+\cos^2\sigma\right)}{\gamma_1 EJ}}, \tag{1.15}$$

where is the dependency

$$\sigma = \arcsin\sqrt{\frac{J-1}{\gamma(1-E)M^2}} \tag{1.16}$$

determines the shock slope angle to the flow in front of it instead (1.1), and

$$E = 1 - \frac{2\left[J - (\gamma_1 - 1)/(\gamma - 1) - (\gamma_1 - 1)\bar{\phi}\right]}{(\gamma_1 - 1) + (\gamma_1 + 1)J} \tag{1.17}$$

is the inverse ratio of gas densities on the both shock sides, which converges at $\bar{\phi} = 0$ and $\gamma_1 = \gamma$ to the usual Rankine-Hugoniot adiabat.

1.3. Triple-shock configurations

Triple shock configurations (TC) are the shock-wave structures consisting of three shocks ($j_1 - j_3$, see Fig. 1.3,a-e), which have a common (triple) point (*T*), and the slipstream (τ), outcoming from this triple point.

Consistency conditions on a slipstream (equality of static pressures and collinearity of flow velocity vectors on its sides) connect the intensities of shocks and the angles of flow deflection on their sides by the system

$$J_1 J_2 = J_3, \quad \beta_1 + \beta_2 = \beta_3 \tag{1.18}$$

or

$$\Lambda_1 + \Lambda_2 = \Lambda_3, \quad \beta_1 + \beta_2 = \beta_3, \tag{1.19}$$

where $\Lambda_i = \ln J_i$, $i = 1..3$, J_i is the strength of the shock j_i, β_i is angle of flow deflection on its surface, determined by a formula similar to (1.4).

Depending on the directions of flow deflection at individual shocks, there are [1, 10] triple configurations of the first type (TC-1, $\beta_1\beta_2 < 0$, $\beta_1\beta_3 < 0$, Figure 1.3,a), the second type (TC-2, $\beta_1\beta_2 < 0$, $\beta_1\beta_3 > 0$, Figure 1.3,c) and the third one (TC-3, $\beta_1\beta_2 > 0$, $\beta_1\beta_3 > 0$, Figure 1.3,e) type. It is usually assumed that triple configurations of the first type form in some special cases of interaction of counter shocks, configuretions of the third type – at interaction of overtaking shocks, and of the second type – in the case of irregular (Mach) reflection of a shock j_1. However, in complex supersonic flows that occur in real gas-dynamic devices, highly branched shock-wave structures with numerous triple configurations of all types occur very often.

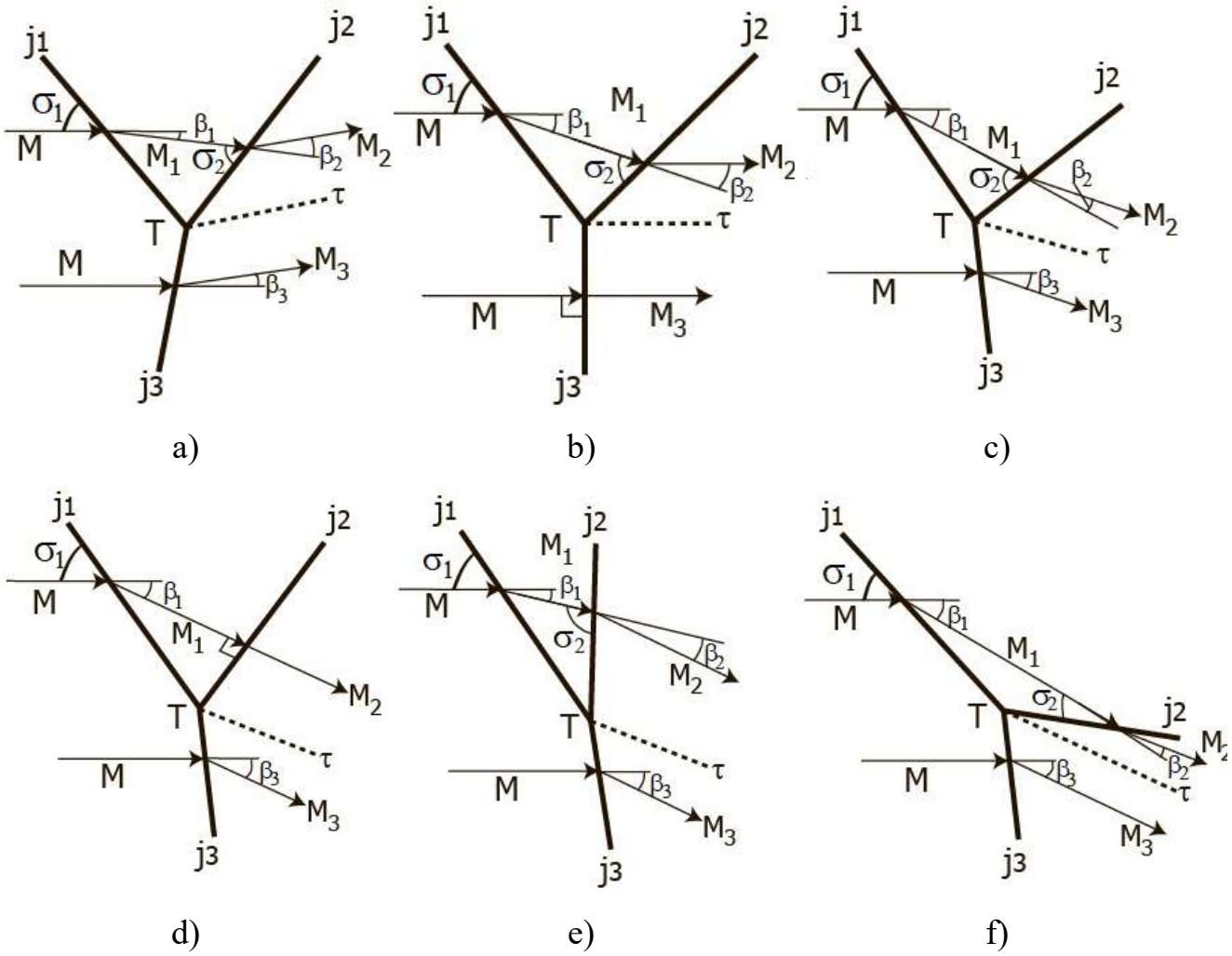

Figure 1.3. Classification of the triple configurations of the steady shocks: a) triple configuration of the first type (TC-1); b) stationary Mach configuration (SMC); c) TC-2; d) transitional TC-2-3; e) TC-3; f) "negative" triple configuration (NTC)

Triple-shock configuration with the normal main shock j_3 (stationary Mach configuration, or SMC), shown in Figure 1,b, borders TC-1 and TC-2. According to the von Neumann criterion for transition of the type of shock reflection, which is traditionally used for steady supersonic flows, the formation of SMC corresponds to the transition from Mach reflection to regular one, as the main shock j_3 decreases in size and disappears. Intensity $J_1 = J_N$ for incident shock j_1 which forms the SMC at its reflection, obeys the equation [79]

$$\sum_{n=0}^{3} E_n J_N^n = 0, \tag{1.20}$$

$$E_3 = 1-\varepsilon, \quad E_2 = -\left[\left(1+\varepsilon-\varepsilon^2+\varepsilon^3\right)M^2 + (1-\varepsilon)\left(1-\varepsilon+\varepsilon^2\right)\right],$$

$$E_1 = \varepsilon\left[(1+\varepsilon)M^2 + 1 - \varepsilon\right]\cdot\left[(1-\varepsilon)M^2 - 2 + \varepsilon\right],\quad E_0 = (1-\varepsilon)\left(M^2-1\right)\left((1+\varepsilon)M^2 - \varepsilon\right)$$

According to the results of the studies [62, 76, 78, 79], the temperature of the flow behind the main shock of the Mach reflection (in TC-2 or SMC) is significantly higher than one in the flow behind the reflected shock on the other side of the slipstream. This effect is especially pronounced at reduced gas adiabatic indices and high free-stream Mach numbers. A significant increase in temperature at the main shock can lead to pulsed energy release and a change in the chemical composition of the reactive gas mixture. In this case, the angle β_3 of flow deflection at a shock j_3 in systems (1.18) or (1.19) is determined by a relation of the form (1.12), and not (1.4), and the Mach number behind its surface obeys a formula of the form (1.15), and not (1.6), as Mach numbers behind the incident (j_1) and reflected (j_2) shocks.

The transition triple configuration with a direct reflected shock (TC-2-3, see Figure 1.3,d) limits the region of existence of the TC-2 configurations formed at Mach reflection, from the upper side. Strength $J_1 = J_T$ of the shock j_1 which forms TCC-2-3, obeys the relation [79]

$$M^4 - rM^2 + \left(J_T - 1\right)\left(J_T + 2 - \varepsilon\right)/\left(1-\varepsilon\right) = 0,$$
$$r = \left(J_T - 1\right)\left(J_T + 2 - \varepsilon\right)/\left(J_T + \varepsilon\right) + \left(J_T + \varepsilon\right)/\left(1+\varepsilon\right) + \left(1 + \varepsilon J_T\right)^2 \Big/ \left[\left(1-\varepsilon\right)\left(J_T + \varepsilon\right)^2\right] \qquad (1.21)$$

The possibility of Mach reflection with the formation of TC-1 or TC-3 (which is presumably non-stable) is not considered in this work.

In the article [69], triple configurations of steady Mach reflection with a negative (to the oncoming flow) inclination angle of the reflected shock ("negative" TC, or NTC), were discovered for steady supersonic flows (see Fig. 1.3,f). Subsequently, they were studied in [70-77]. It is known from [75] that the NTCs for at high free-stream Mach numbers and low (compared to $\gamma = 1.4$) ratios of gas specific eats. In the presence of high-temperature effects, the formation of NTC in flows of not only polyatomic, but also diatomic gases and their mixtures is not excluded. Indeed, the results of [76] indicate a very high temperature of the flow behind the main shock of the NTC (compared to the temperature downstream the

incident shock and the reflected one). At the same time, the problem of the sustainability of the NTCs, the unambiguousness of their formation and the conditions of their implementation requires additional thorough research. In particular, the conditions for the existence and uniqueness of the solution for triple configurations and some other shock-wave structures are considered in the Subsection 2.3 of this thesis.

1.4. Quasi-one-dimensional flow region

It has been repeatedly shown [40, 52-58, 62] that the flow behind the main shock of the Mach reflection (for example, behind the shock j_3 in Figure 1.3,c) in nozzle, jet and channel flows is described by the quasi-one-dimensional flow (QODF) model with quite satisfactory accuracy. Condition for constant gas mass flow rate Q through an arbitrary cross section F of such a region

$$Q = \rho u F = \text{const}$$

together with the isentropic flow functions [94] lead to an equation relating the width $y(x)$ channel and Mach number M along it:

$$q(M) \cdot y(x) = \text{const}, \tag{1.22}$$

or

$$\frac{y_1}{y_2} = \frac{y(x_1)}{y(x_2)} = \frac{q(M_2)}{q(M_1)},$$

or

$$y(x) = q(M) \cdot y_*.$$

Here, the values $y(x)$, $y_1 = y(x_1)$ and $y_2 = y(x_2)$ correspond to the channel width with the flow Mach number equal to, respectively, M, M_1 и M_2, y_* is the width of the “critical” section with a flow Mach number equal to unity, and

$$q(M) = M \cdot \left[1 + \varepsilon\left(M^2 - 1\right)\right]^{-1/2\varepsilon}$$

is the dimensionless isentropic flow rate function. The change in Mach number along the channel determines the corresponding change in static pressure:

$$\frac{p_1}{p_2}=\frac{p(x_1)}{p(x_2)}=\frac{\pi(M_1)}{\pi(M_2)}, \tag{1.23}$$

where

$$\pi(M)=\left(1+\frac{\gamma-1}{2}M^2\right)^{-\gamma/(\gamma-1)}$$

is the isentropic pressure function.

It has been repeatedly shown in [62, 64, 65, 143, 145, 147] that the application of a quasi-one-dimensional flow model to a channel of variable width $y(x)$ (for example, to the "virtual de Laval nozzle" formed behind the Mach stem) is equivalent to the following system of ordinary differential equations to describe the change in flow parameters:

$$\frac{dy}{dx}=\mathrm{tg}\,\theta, \tag{1.24}$$

$$\frac{dM}{dx}=\frac{\mu(M)M^2\tan\theta}{(1-\varepsilon)(M^2-1)y}, \tag{1.25}$$

directly following from the relations (1.22) and (1.23). Here $\mu(M)=1+\varepsilon(M^2-1)$ if the function of flow Mach number M; $\theta(x)$ is the positive or negative angle of inclination of the channel boundary to the plane of flow symmetry. If we consider the Mach number as an independent variable (which makes sense if the integration is carried out up to the value $M=1$), equations (1.24) and (1.25) take the form

$$\frac{dx}{dM}=\frac{(1-\varepsilon)(M^2-1)y}{\mu(M)M^2\tan\theta}, \tag{1.26}$$

$$\frac{dy}{dM}=\frac{(1-\varepsilon)(M^2-1)y}{\mu(M)M^2}. \tag{1.27}$$

In this case, as follows from (1.23-1.25), the main non-uniformity $N_1=\partial\ln p/\partial s$ (flow non-isobaricity along the boundary of the QODF region) obeys the expression

$$N_1=\frac{\partial\ln p}{\partial s}=-\frac{\gamma M^3\sin\theta}{(M^2-1)y}. \tag{1.28}$$

1.5. Prandtl-Meyer wave

As certain conditions [94, 95] are satisfied, a Prandtl-Meyer flow (an expansion wave or a compression one) with straight acoustic characteristics of the first or second family forms in a planar supersonic flow of a perfect gas (Figure 1.4). Mach number M_2 on an arbitrary straight acoustic characteristic of such a flow, as well as the Mach number M_1 behind the whole wave, depends on the Mach number M in front of the Prandtl-Meyer wave and the angle of the flow deflection on the whole wave or on its corresponding part:

$$\nu(M_2)=\nu(M)+\chi(\theta_2-\theta), \tag{1.29}$$

or

$$\nu(M_1)=\nu(M)+\chi(\theta_1-\theta)=\nu(M)-\chi\beta. \tag{1.30}$$

Here $\nu(M)=1/\sqrt{\varepsilon}\arctan\sqrt{\varepsilon(M^2-1)}-\arctan\sqrt{M^2-1}$ is the Prandtl-Meyer function, θ is the fow angle in front of the wave, θ_1 is the flow angle after it, θ_2 is the flow angle on an arbitrary acoustic characteristic with Mach number M_2, $\chi=1$ and $\chi=-1$ for waves with rectilinear acoustic characteristics of the first and second families, respectively; β is the angle of flow deflection on the wave (for example, $\beta<0$ on the expansion wave with straight acoustic characteristics of the first family, which is shown in Fig. 1.4).

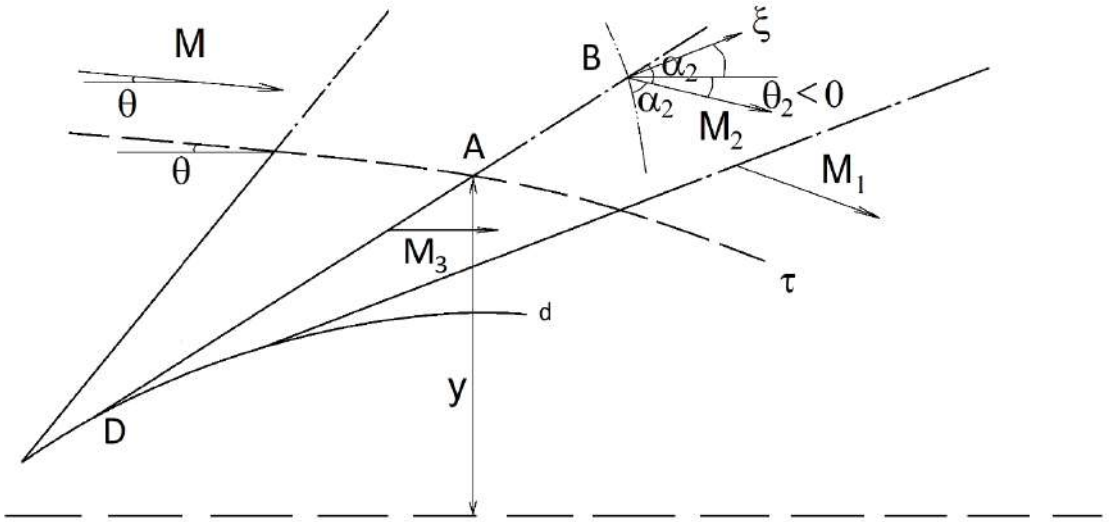

Figure 1.4. Flow parameters in a Prandtl-Meyer wave bordering the quasi-one-dimensional flow region

Static pressure p_2 on an arbitrary straight acoustic characteristic, as well as pressure p_1 behind the wave as a whole, relates to pressure p in front of the wave with the corresponding isentropic function:

$$p_2/p = \pi(M_2)/\pi(M), \tag{1.31}$$

or

$$p_1/p = \pi(M_1)/\pi(M). \tag{1.32}$$

In this case, an arbitrary linear characteristic is inclined at an angle $\theta_2 + \chi\alpha_2 = \theta_2 + \chi\alpha(M_2)$ to the horizontal plane, and the trailing (last, tail) characteristic is inclined at an angle $\theta_1 + \chi\alpha(M_1)$, where $\alpha(M) = \arcsin(1/M)$ is the Mach angle.

It has been repeatedly shown [1] and subsequently used in works [2, 56, 61-65] that the flow gradients (in particular, its non-isobaricity N_1 in a Prandtl-Meyer wave) are inversely proportional to the distance r to the center of the wave (if the wave is centered) or to the discriminant curve d of its linear characteristics (see Figure 1.4):

$$|N_1| = \left|\frac{\partial \ln p}{\partial s}\right| = \frac{(1-\varepsilon)\sqrt{M_2^2 - 1}}{rM_2}. \tag{1.33}$$

This non-isobaricity value is negative or positive for the expansion or compression waves, respectively. A similar relationship describes geometric curvature N_2 of an arbitrary streamline which crosses a straight acoustic characteristic:

$$|N_2| = \left|\frac{\partial \theta_2}{\partial s}\right| = \frac{(1-\varepsilon)\left(M_2^2 - 1\right)}{rM_2^3}. \tag{1.34}$$

At the same time, the main non-uniformity N_1 in the Prandtl-Meyer flow field obeys the relation [1]:

$$N_1 - \chi\Gamma(M_2)N_2 = 0.$$

Here, $\Gamma(M) = \gamma M^2/\sqrt{M^2 - 1}$ is the characteristic complex.

In many cases of Mach reflection (see [40, 52-58, 62, 143, 145, 147)], the flow behind the reflected shock (for example, in region II in Figure 1.4) is described with satisfactory accuracy by the Prandtl-Meyer wave flow model, and the flow behind the

main shock (in region III) fits for a model of quasi-one-dimensional flow. In this case, the flow parameters in regions II and III are related by the condition of equality of pressures on the sides of the sleepstream τ, described by the equation $y(x)$. It can also be assumed that the gas in region II has an adiabatic index γ_2, and the gas in region III has a different adiabatic index γ_3 (for example, due to reactions that changed the chemical composition of the gas immediately behind the main shock). In this case, as $\chi = 1$, the shape $y(x)$ of slipstream, angle $\theta_2(x)$ of its inclination and change in Mach numbers $M_2(x)$ and $M_3(x)$ on both its sides obeys the ordinary differential equations [147], which follow from (1.22), (1.23), (1.29) and (1.31):

$$\frac{dy}{dx} = \tan\theta_2, \tag{1.35}$$

$$\frac{d\theta_2}{dx} = -\frac{\gamma_3 M_3^2 \sqrt{M_2^2 - 1}\tan\theta_2}{\gamma_2 M_2^2 \left(M_3^2 - 1\right) y}, \tag{1.36}$$

$$\frac{dM_2}{dx} = \frac{\gamma_3 M_3^2 \left[1 + \varepsilon_2 \left(M_2^2 - 1\right)\right]\tan\theta_2}{(1+\varepsilon_2) M_2 \left(M_3^2 - 1\right) y}, \tag{1.37}$$

$$\frac{dM_3}{dx} = \frac{M_3^2 \left[1 + \varepsilon_3 \left(M_3^2 - 1\right)\right]\tan\theta_2}{(1-\varepsilon_3)\left(M_3^2 - 1\right) y}. \tag{1.38}$$

(in this case, equations (1.35) and (1.38) correspond to the previously obtained relations (1.24) and (1.25) for the region of quasi-one-dimensional flow).

If we consider the Mach number M_3 below the slipstream as an independent variable, equations (1.35-1.38) look as it follows:

$$\frac{dx}{dM_3} = \frac{(1-\varepsilon_3)\left(M_3^2 - 1\right) y}{M_3^2 \left[1 + \varepsilon_3 \left(M_3^2 - 1\right)\right]\tan\theta_2}, \tag{1.39}$$

$$\frac{dy}{dM_3} = \frac{(1-\varepsilon_3)\left(M_3^2 - 1\right) y}{M_3^2 \left[1 + \varepsilon_3 \left(M_3^2 - 1\right)\right]}, \tag{1.40}$$

$$\frac{d\theta_2}{dM_3} = -\frac{(1+\varepsilon_3) M_3 \sqrt{M_2^2 - 1}}{\gamma M_2^2 \left[1 + \varepsilon_3 \left(M_3^2 - 1\right)\right]}, \tag{1.41}$$

$$\frac{dM_2}{dM_3} = \frac{(1+\varepsilon_3) M_3 \left[1 + \varepsilon \left(M_2^2 - 1\right)\right]}{(1+\varepsilon) M_2 \left[1 + \varepsilon_3 \left(M_3^2 - 1\right)\right]}. \tag{1.42}$$

Condition $\gamma_2 = \gamma_3 = \gamma$ of equality of gas adiabatic indices on both sides of the slipstream simplifies the system (1.35-1.38) to the following form [56, 62, 64, 65, 143, 145]:

$$\frac{dy}{dx} = \tan\theta_2, \tag{1.43}$$

$$\frac{d\theta_2}{dx} = -\frac{M_3^2\sqrt{M_2^2-1}\tan\theta_2}{M_2^2\left(M_3^2-1\right)y}, \tag{1.44}$$

$$\frac{dM_2}{dx} = \frac{M_3^2\left[1+\varepsilon\left(M_2^2-1\right)\right]\tan\theta_2}{(1-\varepsilon)M_2\left(M_3^2-1\right)y}, \tag{1.45}$$

$$\frac{dM_3}{dx} = \frac{\left[1+\varepsilon\left(M_3^2-1\right)\right]M_3^2\tan\theta_2}{(1-\varepsilon)\left(M_3^2-1\right)y}, \tag{1.46}$$

and transforms system (1.39-1.42) to the form

$$\frac{dx}{dM_3} = \frac{(1-\varepsilon)\left(M_3^2-1\right)y}{M_3^2\left[1+\varepsilon\left(M_3^2-1\right)\right]\tan\theta_2}, \tag{1.47}$$

$$\frac{dy}{dM_3} = \frac{(1-\varepsilon)\left(M_3^2-1\right)y}{M_3^2\left[1+\varepsilon\left(M_3^2-1\right)\right]}, \tag{1.48}$$

$$\frac{d\theta_2}{dM_3} = -\frac{(1-\varepsilon)M_3\sqrt{M_2^2-1}}{M_2^2\left[1+\varepsilon\left(M_3^2-1\right)\right]}, \tag{1.49}$$

$$\frac{dM_2}{dM_3} = \frac{M_3\left[1+\varepsilon\left(M_2^2-1\right)\right]}{M_2\left[1+\varepsilon\left(M_3^2-1\right)\right]}. \tag{1.50}$$

Expressions (1.34) and (1.36) determine the distance r_A from some point A on a slipstream to the corresponding point D on the discriminant curve:

$$r_A = \frac{\left(1+\varepsilon_2\right)\sqrt{M_2^2-1}\left(M_3^2-1\right)y_A}{\gamma_3 M_2 M_3^2\sin\theta_2}, \tag{1.51}$$

so

$$x_D = x_A - r_A\cos\left(\alpha_2+\theta_2\right), \tag{1.52}$$

$$y_D = y_A - r_A\sin\left(\alpha_2+\theta_2\right). \tag{1.53}$$

Relations (1.34), (1.51-1.53) allow us to determine non-uniformity N_{2B} of the Prandtl-Meyer flow at its arbitrary point B with coordinates (x_B,

$y_B = y_A + (x_B - x_A)\tan(\alpha_2 + \theta_2))$ on a straight characteristic AB with Mach number M_2:

$$N_{2B} = \left(\frac{\partial\theta_2}{\partial s}\right)_B = \frac{(1-\varepsilon)\left(M_2^2-1\right)}{r_B M_2^3} = \frac{(1-\varepsilon)\left(M_2^2-1\right)}{r_A M_2^3}\cdot\frac{r_A}{r_B} = \frac{y_A - y_D}{y_B - y_D}\cdot N_{2A}, \tag{1.54}$$

where

$$N_{2A} = -\frac{M_3^2\sqrt{M_2^2-1}\sin\theta_2}{M_2^2\left(M_3^2-1\right)y_A}. \tag{1.55}$$

Owing to equations (1.54) and (1.55), the derivatives of the flow angle θ_2 in any direction ξ to the horizontal are determined at an arbitrary point B:

$$\left(\frac{\partial\theta_2}{\partial\xi}\right)_B = \frac{\sin\left(\alpha_2+\theta_2-\xi\right)}{\sin\left(\alpha_2+\theta_2\right)}N_{2B}, \tag{1.56}$$

in particular, in the direction ($\xi = \theta_2 - \alpha_2$) of incidence of the curvilinear acoustic characteristic:

$$\frac{d\theta_2}{d\xi} = \frac{\sin 2\alpha_2}{\sin\left(\alpha_2+\theta_2\right)}N_{2B} = \frac{2\sqrt{M_2^2-1}}{M_2^2\cdot\sin\left(\alpha_2+\theta_2\right)}N_{2B}. \tag{1.57}$$

Condition (1.29), together with (1.56) and (1.57), allows us to determine also the change in the Mach number of the flow M_2 in any direction ξ:

$$\left(\frac{\partial M_2}{\partial\xi}\right)_B = -\frac{M\left[1+\varepsilon_2\left(M_2^2-1\right)\right]}{(1-\varepsilon_2)\sqrt{M_2^2-1}}\cdot\left(\frac{\partial\theta_2}{\partial\xi}\right)_B, \tag{1.58}$$

in particular, if ξ if direction of incidence of the curvilinear characteristic:

$$\frac{dM_2}{d\xi} = -\frac{M_2\left[1+\varepsilon_2\left(M_2^2-1\right)\right]}{(1-\varepsilon_2)\sqrt{M_2^2-1}}\cdot\frac{d\theta_2}{d\xi}. \tag{1.59}$$

Relations (1.39-1.42) or (1.47-1.50) allow, together with variation of the values θ_2 and M_2 in an arbitrary direction in the Prandtl-Meyer wave, “conjugating” with the quasi-one-dimensional flow region, determine the change in the Mach number M_3 on the other side of the slipstream τ and the shape $y(x)$ of the corresponding part of the slipstream. Thanks to this, the flowfield in the “conjugated” wave turns out to be completely defined.

If the gas adiabatic indices are equal on both sides of the slipstream (i.e., $\gamma_2 = \gamma_3 = \gamma$), ratios (1.51-1.59) become somewhat simpler.

Conclusions to the Chapter 1

The basic concepts and relationships given in the Subsections 1.1-1.5 provide the necessary conceptual and mathematical apparatus for the analytical study of the shock-wave structure of gas flows with Mach reflection, including one in the presence of pulsed energy release and change in the chemical composition of the gas mixture at some shock surfaces.

Chapter 2. Theoretical analysis of shock-wave systems and structures in gas flows with high supersonic velocity

2.1. Extreme regular reflection of oblique steady shocks and propagating shock waves

2.1.1. Schematic of gas flow with regular shock reflection

The simplest shock-wave structure (i.e., a set of gas-dynamic discontinuities which have a common point) forms at the regular reflection of an oblique steady wave or a propagating shock wave in a perfect gas. In [148], the conditions for the extrema of static pressure and gas temperature behind the reflection point of a shock of a given intensity are analytically determined depending on the Mach number of the free-stream flow. The results obtained are applied to the solution of the equivalent problem of the reflection of a propagating shock wave of a given intensity from an inclined obstacle. A non-monotonic change in the thermal and mechanical load on the target is shown depending on the angle of its surface inclination, and the inclination angles corresponding to the pressure and temperature extremes behind the point of shock reflection are determined analytically.

Regular reflection of steady and unsteady shocks from a solid surface or plane of symmetry of a gas flow has been known since the 19th century [4-7]. The analytical solution [96] for the parameters of a reflected steady or unsteady shock can be graphically represented on the plane of shock polars [97, 98]. The conditions for the existence of regular reflection and the criteria for the transition to irregular (Mach) reflection in both steady and unsteady flows have been well studied [8, 15, 18, 44]. If the value γ the gas adiabatic index in a steady flow is known and fixed, then the properties of the reflected shock are [1] the functions of the Mach number M of the flow in front of the incident shock (Figure 2.1,a) and of one of the parameters of this shock (for example, its intensity J_1, which is the ratio of static pressures on its sides, or its amplitude Δp_1, which is the difference between these

pressures and is especially important in problems of blast wave reflection [19, 44, 99, 100] with reversal of motion, transforming its leading front into a steady shock).

Dependencies determining the intensity (the strength) of the reflected shock $J_2(M, J_1)$ or its amplitude $\Delta p_2(M, \Delta p_1)$, are monotonic with respect to J_1 (or amplitude Δp_1): with increasing intensity J_1 (amplitude Δp_1), as the incident disturbance increases, the intensity (amplitude) of the reflected shock increases also. It was analytically shown in [148], that the parameters of the reflected shock wave are (at fixed values J_1 or Δp_1) the non-monotonic functions of the free-stream Mach number M; the conditions for the occurrence of pressure extrema behind the reflected shock have been determined.

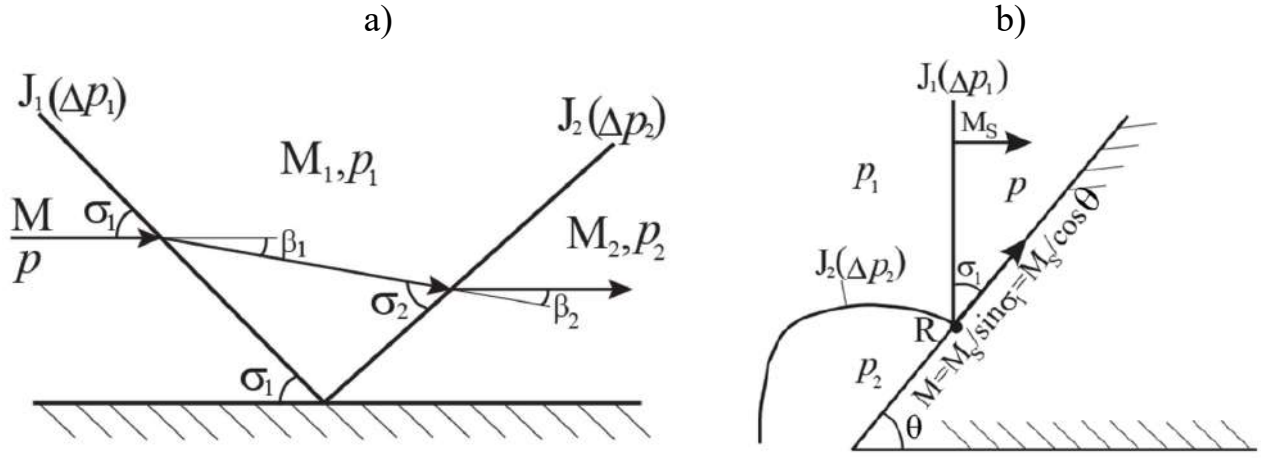

Figure 2.1. Regular reflection of an oblique steady shock (a) and the mechanically equivalent case of reflection of a propagating shock wave from an inclined barrier (b)

The practical value of the analytical solutions obtained in [148] is based on their application in equivalent problems of oblique reflection of the propagatins shock waves (in particular, blast ons, see Figure 2.1, b). Gas pressure and temperature behind the point of regular reflection of an oblique steady shock with a slope angle σ_1 (Figure 2.1,a) are equal to the pressure and temperature behind the point of reflection of an unsteady shock of the same strength (amplitude) from a wedge inclined at an angle $\theta = \pi/2 - \sigma_1$ to the direction of its propagation (Figure 2.1,b). Change in flow Mach number M in the steady shock reflection problem corresponds to a variation in the wedge angle θ in the problem of unsteady reflection of a moving wave of the same strength. From the non-monotonic change in pressure and

temperature behind the reflected shock, a non-monotonic dependence of the mechanical and thermal load behind the reflected shock on the angle of the obstacle inclination follows.

Next, first of all, we consider the regular reflection of a steady shock (Figure 2.1,a) which falls on a solid surface or plane of symmetry in a supersonic flow of an inviscid perfect gas. Free-stream flow parameters (Mach number M, pressure p, adiabatic index γ) and angle σ_1 of the shock incidence determine the incident shock intensity (1.1):

$$J_1 = p_1/p = (1+\varepsilon)M^2 \sin^2\sigma_1 - \varepsilon,$$

its amplitude (1.2):

$$\Delta p_1 = p_1 - p = p\cdot(J_1 - 1)$$

and flow deflection angle β_1 on its surface (1.4):

$$|\beta_1| = \arctan\left[\sqrt{\frac{(1+\varepsilon)M^2 - \varepsilon - J_1}{J_1 + \varepsilon}}\,\frac{(1-\varepsilon)(J_1-1)}{(1+\varepsilon)M^2 - (1-\varepsilon)(J_1-1)}\right]. \quad (2.1)$$

Mach number M_1 of the flow behind the shock is determined by relation (1.6):

$$M_1 = \sqrt{\frac{(J_1+\varepsilon)M^2 - (1-\varepsilon)\left(J_1^2-1\right)}{J_1(1+\varepsilon J_1)}}, \quad (2.2)$$

and the angle β_2 of the flow deflection on a reflected shock depends on its intensity and Mach number M_1 flow in front of him:

$$\beta_2 = \operatorname{arctg}\left[\sqrt{\frac{(1+\varepsilon)M_1^2 - \varepsilon - J_2}{J_2 + \varepsilon}}\,\frac{(1-\varepsilon)(J_2-1)}{(1+\varepsilon)M_1^2 - (1-\varepsilon)(J_2-1)}\right]. \quad (2.3)$$

Condition for regular reflection realization,

$$\beta_1 + \beta_2 = 0 \quad (2.4)$$

leads, taking into account the relations (2.1-2.3), to the following equation regarding intensity $J_2 = p_2/p_1$ of the reflected shock:

$$\sum_{n=0}^{3} C_n J_2^n = 0, \quad (2.5)$$

$$C_3 = [(1+\varepsilon J_1)J_1 M]^2,\ C_2 = -J_1(1+\varepsilon J_1)\cdot x_2,$$

$$C_1 = (1+\varepsilon)(J_1+\varepsilon)\left(1+(1+2\varepsilon)J_1^2\right)M^4 - x_1 M^2 + (1-\varepsilon)(J_1+\varepsilon)(J_1+1)(J_1-1)^3,$$

$$C_0 = -(1+\varepsilon)(J_1+\varepsilon)((1+2\varepsilon)J_1-\varepsilon)M^4 + x_0 M^2 - (1-\varepsilon)(J_1+\varepsilon)^2(J_1-1)^2,$$

$$x_2 = (1+\varepsilon)(J_1+\varepsilon)M^4 + \left(\varepsilon(2-\varepsilon)J_1^2 - \varepsilon(1-2\varepsilon)J_1 + 2\left(1-\varepsilon^2\right)\right)M^2 - (1-\varepsilon)(J_1+\varepsilon)(J_1-1)^2,$$

$$x_1 = 2(1+\varepsilon(1-\varepsilon))J_1^4 - 2\left(1-2\varepsilon^2\right)J_1^3 - \varepsilon\left(4-\varepsilon-2\varepsilon^2\right)J_1^2 + 2\varepsilon(1-\varepsilon)J_1 - \left(1-2\varepsilon^2\right),$$

$$x_0 = 2\left(1+\varepsilon-\varepsilon^2\right)J_1^3 - \left(2-6\varepsilon^2+\varepsilon^3\right)J_1^2 - 2\varepsilon(1-\varepsilon)(1+2\varepsilon)J_1 + \varepsilon\left(1-2\varepsilon^2\right),$$

first written down in [97] regarding the reflection shock slope angle σ_2.

Thermal loads acting on the obstacle from the flows downstream both shocks can be characterized by the temperature ratios $\Theta_1 = T_1/T$ и $\Theta_2 = T_2/T_1$. Here, T, T_1 and T_2 are the temperatures in the undisturbed flow, and after the first and second shocks, respectively. According to the Rankine-Hugoniot adiabatic and the equation of state of a perfect gas, the temperature ratio (1.8) on the sides of a steady or unsteady shock is a monotonic function of intensity:

$$\Theta_i = J_i\left(1+\varepsilon J_i\right)\Big/\left(J_i+\varepsilon\right),\ \ i=1,2. \tag{2.6}$$

For the same reason, the gas temperature behind the reflection point

$$T_2 = \Theta_1\Theta_2 T = J_1 J_2\left(1+\varepsilon J_1\right)\left(1+\varepsilon J_2\right)T\Big/\left[\left(J_1+\varepsilon\right)\left(J_2+\varepsilon\right)\right]$$

is also a monotonic function of the intensity of the reflected disturbance. As a result, if the intensity of the incident steady or unsteady shock, the temperature maxima and minima behind the reflected disturbance coincide with the pressure maxima and minima behind it.

Algebraic equation (2.5) has at most two real roots belonging to the range $[1; J_m(M_1))$, where $J_m(M_1)$ is the intensity of a normal steady shock in a flow with Mach number M_1. Those solutions exist if only the intensity of the incident shock satisfies the condition

$$1 \le J_1 \le J_d(M). \tag{2.7}$$

Here, the intensity $J_d(M)$ corresponds to the so-called maximum reflection angle criterion (“detachment criterion”, [9-11]) and is determined from the equation

$$\sum_{n=0}^{5} D_n J_d^n = 0, \tag{2.8}$$

$$D_5 = (1-\varepsilon)^2, \;\; D_4 = -(1-\varepsilon)\cdot\left[\left(3+4\varepsilon-\varepsilon^2\right)M^2 + \left(4-5\varepsilon+\varepsilon^2\right)\right],$$

$$D_3 = \left(3+4\varepsilon+2\varepsilon^2\right)M^4 + 4(1-\varepsilon)\left(1+2\varepsilon-\varepsilon^2\right)M^2 + 2(3-2\varepsilon)(1-\varepsilon)^2,$$

$$D_2 = -(1+\varepsilon)M^6 + \varepsilon\left(1+2\varepsilon^2\right)M^4 - 4\varepsilon(1-\varepsilon)(1-2\varepsilon)M^2 - 2(2-3\varepsilon)(1-\varepsilon)^2,$$

$$D_1 = -\left[1+\varepsilon\left(M^2-1\right)\right]\cdot\left[2(1+\varepsilon)M^4 + \varepsilon(1+4\varepsilon)M^2 - \left(1-5\varepsilon+4\varepsilon^2\right)\right],$$

$$D_0 = -\left[(1+\varepsilon)M^2 - \varepsilon\right]\cdot\left[1+\varepsilon\left(M^2-1\right)\right]^2$$

(see curve 1 in Fig. 2.2, a; here and below, all calculation examples correspond to the gas adiabatic index $\gamma = 1.4$).

The practice of operating gas-dynamic devices [20], as well as the analysis of regular reflection stability to small disturbances [41, 45], show that the smaller of the two mentioned roots of the equation (2.5), corresponding to the so-called weak branch of the reflected shock polar, realizes at the regular reflection of shock waves and shock waves,

At moderate and high Mach numbers ($M > M_a$, where $M_a = \sqrt{(2-\varepsilon)/(1-\varepsilon)} = 1.483$), the von Neumann criterion (also known as the "mechanical equilibrium criterion") of oblique shock reflection transition is also used. Equation (1.20), see curve 2 in Fig. 2a, determines the intensity $J_N(M)$ of the incident shock, corresponding to this criterion. In the region of parameters of the incident shock, located between curves 1 and 2 ("dual solution domain"), there are solutions for both regular reflection and Mach one.

a)

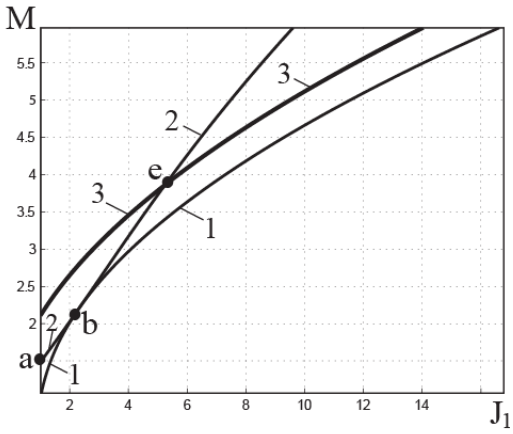

b) c)

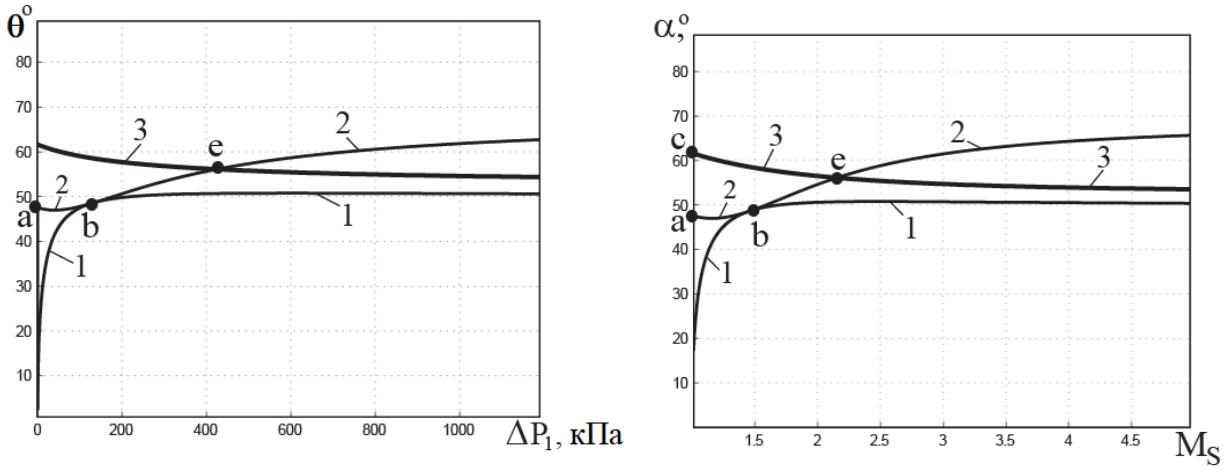

Figure 2.2. Conditions for the realizability of regular reflection, extremes of mechanical and thermal load behind reflected steady and unsteady shocks: curves 1 are the lower boundaries of the region of regular reflection according to the “detachment criterion”, curves 2 correspond to shock reflection transition according to the von Neumann (“mechanical equilibrium”)criterion, curves 3 point to the local minima of the amplitude of the reflected steady shock (a) or unsteady one (b, c), as well as the minima of pressure and temperature behind it

Numerous experiments [11, 21] reveal that the “mechanical equilibrium criterion” (1.20) is preferable when analyzing steady flows, especially in the region of solution ambiguity located above the point b of tangency of curves 1 and 2. Here the Mach number $M_b = 2.202$ is the root of the equation [79, 101]

$$\sum_{n=0}^{4} F_n M_b^{2n} = 0,$$

$$F_4 = (1-\varepsilon)\left(2 - 4\varepsilon + 2\varepsilon^3 - \varepsilon^4\right),\ F_3 = -10 + 20\varepsilon - 10\varepsilon^2 - 10\varepsilon^3 + 12\varepsilon^4 - 4\varepsilon^5,$$

$$F_2 = 12 - 24\varepsilon + 10\varepsilon^2 + 16\varepsilon^3 - 18\varepsilon^4 + 6\varepsilon^5,\ F_1 = -2(1+\varepsilon)\left(3 - 4\varepsilon + 2\varepsilon^2\right)(1-\varepsilon)^2,$$

$$F_0 = (1+\varepsilon)(1-\varepsilon)^4.$$

However, the solutions obtained for steady flows can be subsequently (after appropriate reversal of motion [102]) applied to the unsteady reflection of shock waves from structural elements, in which an another transition criterion can be used. Therefore, below we consider the entire range (2.6) of theoretically possible parameters of incident shocks.

2.1.2. Schematic of an equivalent unsteady flow with regular reflection of a shock wave

Regular reflection of a shock wave which falls on a solid surface (plane of symmetry) at an incidence angle σ_1 in a flow with Mach number M (Figure 2.1,a), is mechanically equivelent after the motion reversal, to the reflection of an unsteady shock of the same intensity

$$J_1 = p_1/p = (1+\varepsilon)M^2 \sin^2\sigma_1 - \varepsilon = (1+\varepsilon)M^2 \cos^2\theta - \varepsilon, \qquad (2.9)$$

which propagates through a stagnant medium and reflects from the wedge at an angle $\theta = \pi/2 - \sigma_1$ (Figure 2.1,b). Here, the point R of the unsteady shock wave reflection moves along the surface with the same Mach number M. This method of motion reversal was applied to the reflection of steadyand unsteady shocks was used, in particular, in [102] to analyze the Mach reflection. The shock Mach number, which characterizes the normal (relative to its own front) propagation speed of of the incident wave in Figure 2.1,b, is $M_S = M\sin\sigma_1 = M\cos\theta = \sqrt{(J_1+\varepsilon)/(1+\varepsilon)}$, so $J_1 = (1+\varepsilon)M_S^2 - \varepsilon$. In this case, the intensity of the reflected wave and the static pressure behind it are the same as in the equivalent case of steady shock reflection.

In some problems of unsteady reflection of shocks and blast waves, the pressure drops on those waves (their amplitudes) and the values of overpressure behind the reflection point are of particular importance, because they characterize the mechanical load on the target. The amplitude of the incident shock wave is

$$\Delta p_1 = p_1 - p = p\cdot(J_1 - 1), \qquad (2.10)$$

the reflected wave amplitude is

$$\Delta p_2 = p_2 - p_1 = pJ_1 \cdot (J_2 - 1),$$

and the overpressure behind the reflection point is equal to

$$\Delta p_\Sigma = p_2 - p = p \cdot (J_1 J_2 - 1).$$

As the pressure p in an undisturbed environment and the intensity J_1 (amplitudes Δp_1) of the incident shock are fixed, the amplitude Δp_2 of the reflected wave and overpressure Δp_Σ behind it depend linearly on its intensity J_2, which, in its turn, depends on the wedge angle θ at the unsteady reflection or on Mach number M in the equivalent steady case. Non-monotonic dependence $J_2(M)$ with a regular reflection of a stationary shock of a fixed intensity means that the overpressure Δp_Σ and temperature T_2 behind the point of reflection of a propagation shock wave with a given amplitude depends non-monotonically on the angle of inclination of the reflecting surface. This fact is not outwardly obvious (rather, on the contrary) and requires analytical proof.

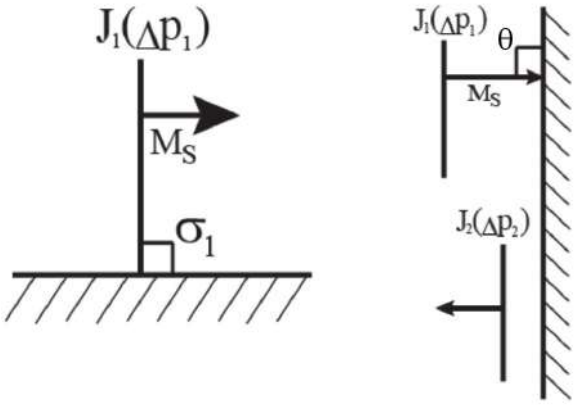

а) *б)*

Figure 2.3. Limiting cases of interaction of a propagating shock wave with a surface: a) parallel sliding ($\sigma_1 = 90°$, $\theta = 0$); *б*) normal reflection ($\sigma_1 = 0$, $\theta = 90°$): movement of the incident wave (top) and the reflected one (bottom)

The increase in pressure on the target behind the reflected shock wave can, in addition, be characterized by the pressure coefficient

$$K_2 = \Delta p_2 / \Delta p_1 = (J_2 - 1)/(J_1 - 1) \qquad (2.11)$$

or wave amplification factor

$$K_\Sigma = \Delta p_\Sigma / \Delta p_1 = (J_1 J_2 - 1)/(J_1 - 1). \qquad (2.12)$$

Those coefficients are minimal ($K_2 = 0$, $K_\Sigma = 1$), if the wave slides parallel to the surface (Figure 2.3,a), and there is no reflected wave (it degenerates into a weak disturbance, $J_2 = 1$).

At the normal ($\theta = 90°$, $\sigma_1 = 0$) reflection of a shock wave with an amplitude Δp_1 (Figure 2.3,b), the amplitude Δp_2 of the reflected wave is calculated using the Izmaylov-Crussard formula [99, 103]

$$\Delta p_2 = \Delta p_1 \cdot [1 + \Delta p_1 / (\varepsilon \Delta p_1 + (1+\varepsilon) p_0)],$$

so the coefficients of pressure and amplification of the reflected wave

$$K_2 = 1 + \Delta p_1 / (\varepsilon \Delta p_1 + (1+\varepsilon) p_0) = 1 + (J_1 - 1)/(1 + \varepsilon J_1), \qquad (2.13)$$

$$K_\Sigma = 2 + \Delta p_1 / (\varepsilon \Delta p_1 + (1+\varepsilon) p_0) = 2 + (J_1 - 1)/(1 + \varepsilon J_1). \qquad (2.14)$$

After the reverse transition to steady flow, the normal reflection of the unsteady shock ismechanically equivalent to the reflection of a steady shock of the same intensity J_1 in Mach number flow $M \to \infty$. Thus, the analysis of the reflection of steady shocks in perfect gas flows with high supersonic Mach numbers without considering additional (“hypersonic”) physical effects acquires an obvious practical value. This phenomenon is mechanically equivalent to the reflection of unsteady shock waves of quite moderate intensity from obstacles that are close to normal to shock wave front. This is, for example, the reflection of a shock wave front during a near-surface explosion, when a point of regular reflection propagates along the surface with a very high speed (at the first moment of normal reflection when touching the surface – with an infinitely high speed, see Figure 2.4 and [104]).

Similar to pressure gaps (shock wave amplitudes), temperature gaps on the surfaces of incident and reflected disturbances can be determined as it follows:

$$\Delta T_1 = T_1 - T = T \cdot (\Theta_1 - 1), \Delta T_2 = T_2 - T_1 = T \cdot \Theta_1 (\Theta_2 - 1), \Delta T_\Sigma = T_2 - T = T \cdot (\Theta_1 \Theta_2 - 1).$$

Here, the relations Θ_i ($i = 1,2$) of the static temperatures are expressed through the intensities of the corresponding shocks using relations (2.6).

Similarly to the relation K_2 of reflected and incident waves amplitudes (2.11) and the coefficient K_Σ of overpressure amplification (2.12), the relation H_2 of temperature gaps and the coefficient H_Σ of increase in thermal loads are introduced at further:

$$H_2 = \Delta T_2 / \Delta T_1 = \Theta_1 \cdot (\Theta_2 - 1)/(\Theta_1 - 1), \tag{2.15}$$

$$H_\Sigma = \Delta T_\Sigma / \Delta T_1 = (\Theta_1 \Theta_2 - 1)/(\Theta_1 - 1). \tag{2.16}$$

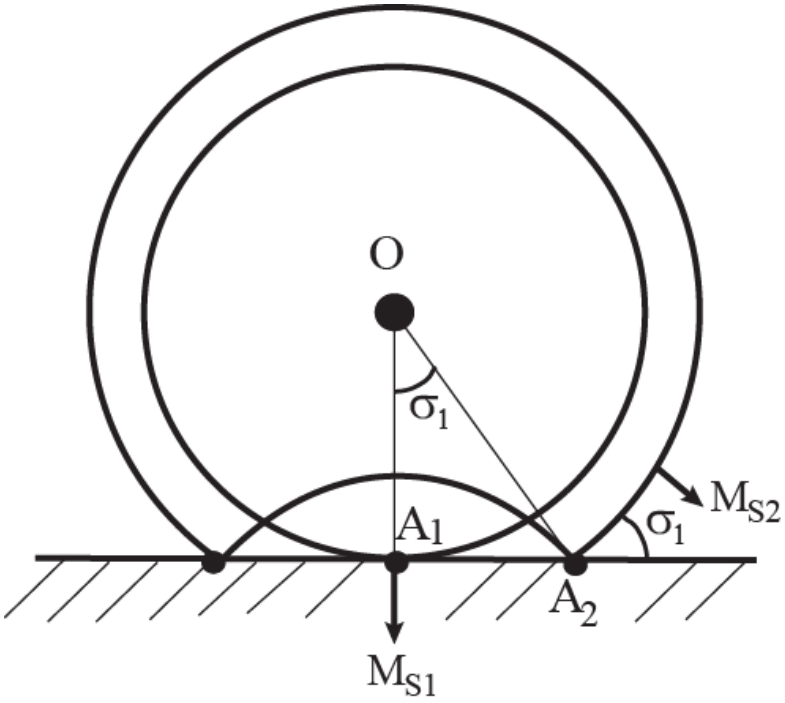

Figure 2.4. Initial stages of reflection of the blast wave front during a near-surface explosion. The velocity of movement of the reflection point along the surface is infinitely large at the initial moment of normal reflection (point A_1). It corresponds to the Mach number $M = M_S / \sin\sigma_1$ at regular reflection (point A_2). In this case, the Mach number M_S (M_{S1}, M_{S2}) of the movement of the wave front is, as a rule, variable and decreases with distance from the explosion epicenter O

2.1.3. Analytical results determining the extreme reflection of steady and unsteady shocks

Equality of the partial derivative to zero ($\partial J_2 / \partial M = 0$), being applied to solution (2.5), determines the conditions for the extreme intensity of the reflected disturbance. Those conditions can be written in the form of a cubic equation relative to the intensity of the incident shock:

$$\sum_{n=0}^{3} G_n J_1^n = 0, \tag{2.17}$$

$$G_3 = (1-\varepsilon)^2,\ G_2 = -3(1-\varepsilon)\cdot\left[(1+\varepsilon)M^2 + 1 - \varepsilon\right],$$

$$G_1 = (1-\varepsilon)\cdot\left[(1+\varepsilon)(3+2\varepsilon)M^4 + 2(1+\varepsilon)(1-2\varepsilon)M^2 + (1-\varepsilon)(1-2\varepsilon)\right],$$

$$G_0 = -\left[(1+\varepsilon)M^4 + 1 - \varepsilon\right]\cdot\left[(1+\varepsilon)(1-2\varepsilon)M^2 - (1-\varepsilon)(1+2\varepsilon)\right],$$

or as a similar equation relative to the flow Mach number:

$$\sum_{n=0}^{3} H_n M^{2n} = 0, \tag{2.18}$$

$$H_3 = (1-2\varepsilon)(1+\varepsilon)^2,\ \ H_2 = -\left(1-\varepsilon^2\right)\cdot\left[(3+2\varepsilon)J_1 + 1 + 2\varepsilon\right],$$

$$H_1 = \left(1-\varepsilon^2\right)\cdot\left[3J_1^2 - 2(1-2\varepsilon)J_1 + 1 - 2\varepsilon\right],\ \ H_0 = -(1-\varepsilon)^2\cdot(J_1-1)\cdot\left(J_1^2 - 2J_1 - 1 - 2\varepsilon\right).$$

Calculations show that the solutions of equations (2.17) or (2.18), shown by curve 3 in Figure 2.1, really corresponds to regular reflection of the incident shock.

It is appropriate to consider the equivalent reflection of an unsteady shock wave on a plane $(\Delta p_1, \theta)$, which in shown in Figure 2.2,b. The amplitude of the incident wave is related to its intensity by (2.11), and the angle of obstacle inclination relates to the Mach number and intensity by (2.10) at the condition $\theta = 90° - \sigma_1$. Here and below, for definiteness, it is assumed that the unsteady shock wave propagates through an undisturbed stagnant medium with pressure $p = 100$ kPa.

The solution for regular reflection of the incident wave exists in the range $\theta \in [\theta_d, 90°)$. Here θ_d in the wedge angle corresponding to “detachment criterion” (2.7), i.e., to the transition to irregular reflection). This limiting angle (2.8) is shown by curve 1 in Figure 2.2,b. The wedge angle corresponding to the von Neumann criterion (1.20) is shown there by curve 2. Curve 3 corresponds to the minimum pressure on the target depending on the angle of its inclination at various fixed amplitudes of the incident wave.

The extrema of the parameters of the reflected unsteady shock wave are also shown in Figure 2,c in coordinates (M_S, θ). Curve 3 corresponds to pressure minima behind the shock reflection point with a certain Mach number M_S of its front

propagation. It allows to set the angles of inclination of structural elements that deliver minimal values of mechanical loads at a given shock wave Mach number.

Those angles of obstacle inclination corresponding to the pressure minima behind the reflected wave, in coordinates (M_S, θ) obey the equation

$$\sum_{n=0}^{3} Z_n z^n = 0, \tag{2.19}$$

where

$$z = \sin^2 \sigma_1 = \cos^2 \theta,\ Z_3 = (1-\varepsilon)^2\left(M_S^2 - 1\right)\cdot\left[(1+\varepsilon)M_S^4 - 2(1+\varepsilon)M_S^2 - (1-\varepsilon)\right],$$

$$Z_2 = -(1-\varepsilon)M_S^2 \cdot \left[3(1+\varepsilon)M_S^4 - 2(1+\varepsilon)M_S^2 + (1-\varepsilon)\right],$$

$$Z_1 = -(1-\varepsilon)\cdot\left[(3+2\varepsilon)M_S^2 + 1 - 2\varepsilon\right],\ \ Z_0 = (2\varepsilon - 1)M_S^6.$$

According to (2.19), in the limiting case of weak shock reflection ($M_S \to 1$), the minimum pressure behind the reflected wave is achieved at

$$z = \left(\sqrt{2-2\varepsilon} - 1\right)\Big/\sqrt{2-2\varepsilon} = 0.225,$$

which corresponds to $\theta_c = \arcsin(2-2\varepsilon)^{-1/4} = \arcsin[(\gamma+1)/4]^{1/4} = 61.656°$ (point c on curve 3). As $M_S = 2.175$, the minimum pressure corresponds to the von Neumann criterion for the transition from Mach reflection to regular one (point e of intersection of curves 2 and 3). Corresponding value ($\theta_e = 56.105°$) of the obstacle inclination angle obeys the relation

$$z_e = \cos^2 \theta_e = \frac{(1-\varepsilon)(3-\varepsilon)(1-2\varepsilon)^2 - \sqrt{3 - 20\varepsilon + 49\varepsilon^2 - 52\varepsilon^3 + 20\varepsilon^4}}{(1-\varepsilon)(3-2\varepsilon)\left(1 - 5\varepsilon + 2\varepsilon^2\right)} = 0.311.$$

At $M_S > 2.175$, the optimal (delivering minimum pressure on the target) wedge angle corresponds to the region of ambiguity in the type of reflection located between curves 1 and 2 (the “dual solution domain”). But, at those parameters of interaction of an unsteady shock wave with an inclined target (in contrast to the steady case), as a rule [17], it is a regular reflection that is implemented.

In another limiting case of reflection of strong shock waves ($M_S \to \infty$), the optimal angle of inclination of the obstacle is determined by the following equation for the asymptote of curve 3:

$$(1-\varepsilon)\left(1-\varepsilon^2\right)z^3 - 3\left(1-\varepsilon^2\right)z^2 + (1-\varepsilon)(3+2\varepsilon)z + 2\varepsilon - 1 = 0,$$

so $z = 0.367$, $\theta = 52.715°$. Curve 3 situiates between the horizontal asymptotes of curves 1 and 2, corresponding to different criteria for strong shock reflection oftransition. The horizontal asymptote of curve 1, which corresponds to the "detachment criterion", obeys the equation

$$\left(1-\varepsilon^2\right)z^3 - \left(1-\varepsilon^2\right)z^2 - (1+2\varepsilon)z + 1 = 0$$

($z = 0.413$, $\theta = 50.029°$), and the horizontal asymptote of curve 2, corresponding to the von Neumann "mechanical equilibrium" criterion, obeys the relation

$$z = \frac{1+\varepsilon-\varepsilon^2+\varepsilon^3-\sqrt{1-2\varepsilon+3\varepsilon^2+4\varepsilon^3-2\varepsilon^5+\varepsilon^6}}{2\left(1-\varepsilon^2\right)} = 0.138.$$

($\theta = 68.231°$). Thus, the angle of inclination of the target, corresponding to the minimum of mechanical and thermal loads, for strong shock waves shifts towards the lower boundary of the region of existence of regular reflection.

2.1.4. Numerical results and discussion

Figure 2.5a shows the change in the coefficient (2.11) of reflection of shock waves of various amplitudes (curves 1-10) depending on the angle of target inclination. The range of this angle variation extends from curve 11, corresponding to reflection transition according to criterion (2.7-2.8), to the value $\theta = 90°$, which corresponds to normal reflection as a limiting case of regular one. In the latter case, the values of the reflection coefficient correspond to the Izmailov-Crussard relation in the form (2.13).

As can be seen from Figure 2.5,a, the decrease in pressure on the reflected shock wave due to the optimal placement of the barrier can be significant. When weak shock waves reflects, the amplitude Δp_2 at the appropriate choice of angle θ is almost 50% less than on the left boundary of the region of existence of regular reflection. At $\Delta p_1 = 50$ kPa (amplitude of the incident wave corresponding to the

lower threshold of barotrauma according to [100, 105]) increase in the wedge angle from $\theta = 43.2°$ до $\theta = 60.1°$ leads to a decrease in pressure on the reflected wave with $\Delta p_2 = 102.5$ kPa to $\Delta p_2 = 67.7$ kPa, i.e. by 33.9% (curve 1). For stronger incident waves, the range of angles within which a decrease in the pressure of the reflected wave is observed gradually decreases. The relative drop in Δp_2 also decreases, however, it is still a noticeable value (17.4% at $\Delta p_1 = 400$ kPa or 12-15% at $\Delta p_1 = 700 - 4000$ kPa), which must be taken into account in engineering calculations of explosion-resistant structures.

a) b)

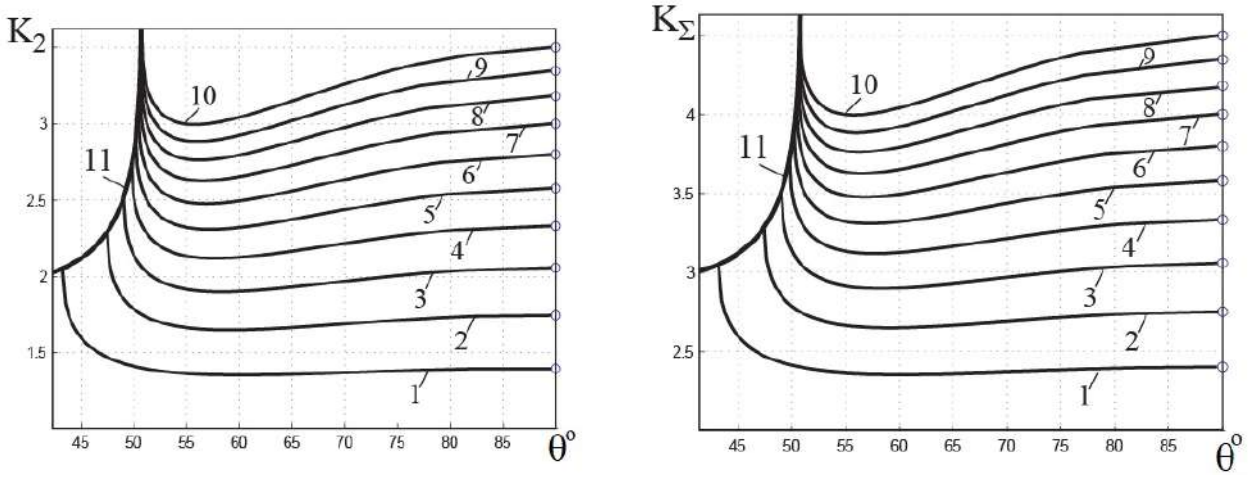

Figure 2.5 – Change in the reflection coefficient (a) and amplification factor (b) for a regularly reflecting wave depending on the angle of inclination of the target at different amplitudes of the incident shock wave: $\Delta p_1 = 50$ kPa (curves 1), 100 kPa (2), 150 kPa (3), 200 kPa (4), 250 kPa (5), 300 kPa (6), 350 kPa (7), 400 kPa (8), 450 kPa (9), 500 kPa (10). Curves 11 limit the region of existence of regular reflection according to the "detachment criterion"

According to Fig. 2.5a (see curve 1), the amplitude of the reflected shock at the point of the derived minimum is not much less than the amplitude of the normally reflected wave described by the Izmaylov-Crussard formula (rightmost points on curves 1-10). In the mentioned example ($\Delta p_1 = 50$ kPa, minimum reflected wave pressure $\Delta p_2 = 67.7$ kPa at $\theta = 60.1°$), normal reflection ($\theta = 90°$) leads to the formation of a reflected wave with an amplitude $\Delta p_2 = 69.7$ kPa. As the incident wave intensifies, the relative difference between the pressures of the optimally and

normally reflected waves becomes more noticeable (curves 2-10 in Figure 5,a). It is about 20-22% at $\Delta p_1 > 1000$ kPa.

The change in the amplification coefficient (2.12) of the incident wave under the same conditions is shown in Figure 2.5,b. On the right boundary of the computational domain ($\theta = 90°$), the amplification factors K_Σ correspond to the Izmailov-Crussard relation in the form (2.14). Maximum effect of this coefficient reduction in the interval from the left boundary of the computational domain (curve 11) to its minimum point is 30-32%. It is observed when weak shock waves reflect (at $\Delta p_1 < 10$ kPa). When sufficiently strong waves reflect (at $\Delta p_1 > 1000$ kPa), the effect of reducing the load on the obstacle is about 10%. The pressure on the target at normal reflection is greater than when it is optimally inclined: insignificantly for weak shock waves and by about 20% for strong waves ($\Delta p_1 > 1000$ kPa).

Thus, in a fairly wide range of problem parameters adjacent to the boundary of the region of existence of regular reflection, the pressure behind the reflected wave decreases as the angle of inclination of the target increases. In particular, when $\Delta p_1 = 100$ kPa (the amplitude of the incident wave corresponding to the lower threshold of lethal outcomes according to [100, 105]), the amplitude of the reflected wave and the overpressure behind the reflection point decrease from $\Delta p_2 = 228.8$ kPa ($\Delta p_\Sigma = 328.8$ kPa) at the point of its local maximum ($\theta = 47.5°$) to the value $\Delta p_2 = 165.1$ kPa ($\Delta p_\Sigma = 265.1$ kPa) at $\theta = 59.1°$. At the normal reflection of such a wave (at $\theta = 90°$), the overpressures are $\Delta p_2 = 174.0$ kPa and $\Delta p_\Sigma = 274.0$ kPa.

It should be noted that the pressure values behind the reflected wave on the left boundary of the considered computational domain at the incidence of shock waves of low and moderate intensity are some higher than on the right boundary (i.e., at their normal reflection).

a) b)

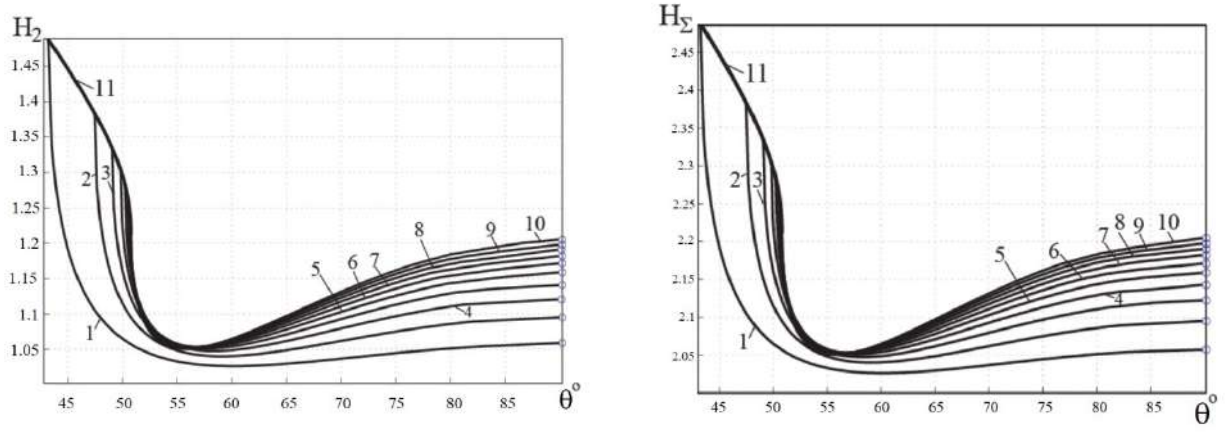

Figure 2.6. Change in the ratio of temperatures shocks on the reflected and incident shocks (a) and the coefficient of increase in thermal loads (b) depending on the angle of inclination of the obstacle at various amplitudes of the incident unsteady waves: $\Delta p_1 = 50$ kPa (curves 1), 100 kPa (2), 150 kPa (3), 200 kPa (4), 250 kPa (5), 300 kPa (6), 350 kPa (7), 400 kPa (8), 450 kPa (9), 500 kPa (10). Curves 11 limit the region of existence of regular reflection according to the "detachment criterion"

Ratio of temperature gaps H_2 (2.15) and coefficient of increase in thermal loads H_Σ (2.16) change similarly (see Figure 2.6,a-b). As it was shown earlier, the conditions for temperature extrema (minima) behind the reflected shock are also described by equation (2.19). However, the difference between the values of the temperature coefficients at the derived minimum points is slightly smaller in comparison with normal reflection or the limiting case of the transition of regulat reflection to Mach one. For example, the difference in values ΔT_2 at the normal reflection and at the derived minimum point it is 2.92% at $\Delta p_1 = 50$ kPa and 12.8% at $\Delta p_1 = 500$ kPa. Similarly, the difference in values ΔT_2 at the point of transition to the Mach reflection and at the found minimum point is equal to 31.0% at $\Delta p_1 = 50$ kPa and 14.3% at $\Delta p_1 = 500$ kPa. As the intensity (amplitude) of the incident wave increases, the temperature difference behind the reflected wave increases monotonically, but sometimes weaker than the temperature difference on the incident wave, which leads to the intersection of some curves in Figure 2.6,a-b.

Thus, the parameters of the incident steady shocks, which obtain the minimum static pressure and gas temperature behind the reflected one, are described by the cubic equation (2.15) or (2.16) in the variables "shock intensity – free-stream Mach

number". A similar cubic equation (2.17), first obtained in [93], analytically determines the obstacle inclination angles at which the static pressure behind the point of regular reflection of a propagating shock wave of a given amplitude is minimal. Those optimal angles of inclination of the reflecting surface exist for all theoretically possible parameters of the incident shock. In this case, the optimal reflection of the shock wave differs both from normal reflection and from another limiting case of transition from regular reflection to Mach one. Calculations show that geometric optimization of the interaction of shock (in particular, blast) waves with obstacles can significantly reduce mechanical and thermal loads on structural elements. For this reason, the obtained theoretical results can be used in the design of explosion-proof structures, in the development of blast protection means, in aircraft and rocket engineering, in supersonic aerodynamics and in many other applications.

2.2. Approximate analytical model of the shock-wave structure of the flow with Mach reflection of steady shocks

Gradually complicating the research problem, we consider a flow with Mach reflection of oblique steady shocks from the plane of symmetry in an inviscid supersonic flow of a perfect inviscid gas, which takes place in a narrowing channel between two wedges (Figure 2.7,a) or at the planar overexpanded jet flow from a supersonic nozzle (Figure 2.7, b). The first of the cases under consideration is a model example for the gas-dynamic design of supersonic air intakes, the second is fit for jet flows from jet engine nozzles, as well as in the development of jet technology devices.

a)

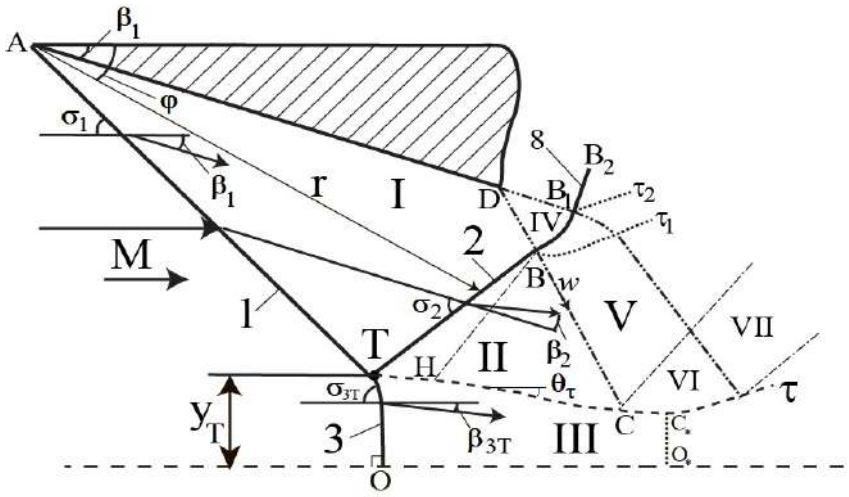

b)

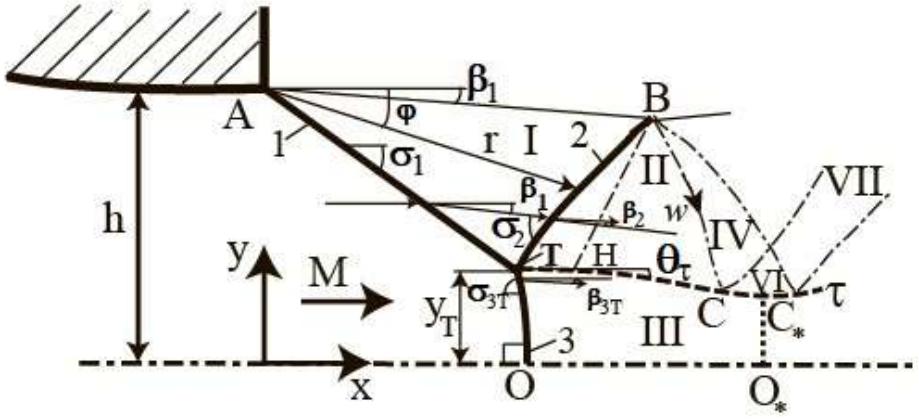

Figure 2.7. Flow patterns with Mach reflection: a) in a narrowing channel between two wedges; b) in an overexpanded gas jet

In Figure 2.7, the following notations are adopted: M is Mach number of the undisturbed flow; 1 (*AT*) is oblique shock wave which falls from the edge of the nozzle or the leading edge of the wedge; 2 (*TB*) is the reflected shock; 3 (*TO*) is the main shock (Mach stem); *T* is the triple point of Mach reflection, common to the incident, reflected and main shocks; τ is the slipstream which emanates from the triple point and separates the flows behind the reflected and Mach shocks (usually supersonic and subsonic ones, respectively); θ_τ is variable local slope angle of the sleepstream τ (which is curved in the general case) to the horizontal plane of flow symmetry; β_1 and β_2 are the angles of flow deflection at shocks 1 (incident) and 2 (reflected); $\beta_{3T} \equiv \theta_{3T}$ is the angle of flow deflection at the main shock 3 in the

vicinity of the triple point *T*, equal to the angle of inclination of the slipstreame manating from this point; σ_1 and σ_2 are the angles of slope of shocks 1 and 2 to the flow velocity vectors in front of them; σ_{3T} is the angle of inclination of the shock 3 at the triple point *T*; *h* is the width of the outlet section of the jet or channel between the wedges; y_T is the target size of the main shock (the height of the triple point); (r, φ) are the distance and the polar angle, measured from the horizontal direction, in a cylindrical coordinate system centered at point *A*; *HB* is the acoustic characteristic of the first family, which falls at point *B* of the exit of the reflected shock to the jet boundary or of the beginning of its interaction of the refelected shock with the tail rarefaction wave; I is the flow region behind the incident shock 1; II (*BTC*) is the flow region behind the reflected shock (as shown in [56, 62], it can be approximated as a simple Prandtl-Meyer expansion wave with straight acoustic characteristics of the first family); III is the flow region behind the Mach shock 3 ("virtual nozzle" with critical section C_*O_*, according to terminology [52]); IV is the fan of characteristics of an expansion wave descending from the jet boundary (from the point of its intersection with the reflected shock 2) or from the trailing edge of the streamlined wedge; V is the fan of characteristics of an expansion wave which forms as a result of wave IV interaction with curved shock wave BB_1; VI is the zone of reflection of the expansion wave IV or V from a slipstream τ, which turns due to this reflection in the horizontal direction and further; VII is the reflected Prandtl-Meyer wave (it is proven in [62] that this is a wave of compression); BC is the head acoustic characteristic of the first family of rarefaction waves IV or V; τ_1 and τ_2 (Figure 2.7, a) are the weak tangential discontinuities limiting the shear layer of variable entropy, formed as a result of the counter interaction of the reflected shock wave 2 with a centered expansion wave IV; 8 (B_1B_2, Figure 2.7,a) is the resulting shock wave after the interaction of the reflected shock with the expansion wave IV.

2.2.1 Local solution of the Mach reflection problem

It is assumed that the reflection of the shock 1 is the Mach one according to the von Neumann criterion. This means that the intensity J_1 of the incident shock (the ratio of static pressures behind the shock wave and in front of it) is in the range

$$J_N \le J_1 \le J_T . \qquad (2.20)$$

Intensity J_N, the minimal one for the implementation of the Mach reflection of shock 1, corresponds to the formation of the so-called "stationary Mach configuration" with a normal main shock. It is determined by equation (1.20). The highest permissible intensity $J_1 = J_T$ corresponds to a triple shock configuration with a normal reflected shock 2 (*TB*). This transition value satisfies the equation (1.21).

Shock-wave structures that arise when shocks with intensity $J_1 > J_T$ reflect, are known as Guderley and Vasiliev reflections [20, 104]; they usually not realize in steady flows, especially at moderate and high Mach numbers. As a rule, instead of them, flows with a detached bow shock (at the entrance to a supersonic air intake) or with a strong shock that blocks the flow through the nozzle (at excessive expansion regimes of the gas jet) arise. The problem of the ambiguity of realized shock-wave structures is discussed further in Subsection 2.3.

As inequality (2.20) is satisfied, a Mach reflection occurs at the triple point *T* with the formation of a triple configuration of the second type according to the classification [1, 10, 79]. The conditions of co-directionality of flows and equality of static pressures on both sides of the slipstream emanating from the triple point lead to the following system of equations that determines the parameters of the reflected shock 2 (*TB*) and the main (Mach) shock 3 (*TO*):

$$\beta_1 + \beta_{2T} = \beta_{3T}, \; J_1 J_{2T} = J_{3T}, \qquad (2.21)$$

Here J_{2T} and J_{3T} are the intensities of shocks 2 and 3 at point *T*. The following relations (1.4) determine the flow deflection angles β_{2T} и β_{3T} from the horizontal direction at the triple point:

$$\operatorname{tg}|\beta_{2T}| = \sqrt{\frac{(1+\varepsilon)M_1^2 - J_{2T} - \varepsilon}{J_{2T} + \varepsilon}} \frac{(1-\varepsilon)(J_{2T}-1)}{(1+\varepsilon)M_1^2 - (1-\varepsilon)(J_{2T}-1)},$$
$$\operatorname{tg}|\beta_{3T}| = \sqrt{\frac{(1+\varepsilon)M^2 - J_{3T} - \varepsilon}{J_{3T} + \varepsilon}} \frac{(1-\varepsilon)(J_{3T}-1)}{(1+\varepsilon)M^2 - (1-\varepsilon)(J_{3T}-1)}. \quad (2.22)$$

The flow deflection angles are considered positive, as the flow turns counterclockwise. Flow Mach numbers (M_1 is one after the incident shock 1, and also M_{2T} and M_{3T} are Mach numbers after corresponding shocks in the vicinity of the triple point) satisfy the formulas (1.6):

$$M_1 = \sqrt{\frac{(J_1+\varepsilon)M^2 - (1-\varepsilon)(J_1^2-1)}{J_1(1+\varepsilon J_1)}},$$
$$M_{2T} = \sqrt{\frac{(J_{2T}+\varepsilon)M_1^2 - (1-\varepsilon)(J_{2T}^2-1)}{J_{2T}(1+\varepsilon J_{2T})}}, \quad (2.23)$$
$$M_{3T} = \sqrt{\frac{(J_{3T}+\varepsilon)M^2 - (1-\varepsilon)(J_{3T}^2-1)}{J_{3T}(1+\varepsilon J_{3T})}}.$$

As usually at Mach reflection of oblique shocks in a steady supersonic flow, it is assumed that the flow behind the reflected shock 2 is supersonic (i.e. $M_2 \geq 1$). This leads to the following limitation for the intensity of the incident shock:

$$J_N \leq J_1 \leq J_S, \quad (2.24)$$

which is a little stricter than (2.20). The intensity J_S of the incident shock corresponds to the critical flow velocity behind the irregularly reflected one. Its value is determined by the 10th order algebraic equation with respect to M^2 and the 14th order equation with respect to J_S. Their numerical solution and analysis of which are given in studies [109, 145].

Angles σ_1, σ_{2T} and σ_{3T} of the inclination of the corresponding shocks to the direction of the flow in front of them relate to their intensities by formula (1.1):

$$J_1 = (1+\varepsilon)M^2 \sin^2\sigma_1 - \varepsilon,\ J_{2T} = (1+\varepsilon)M_1^2 \sin^2\sigma_{2T} - \varepsilon,$$
$$J_{3T} = (1+\varepsilon)M^2 \sin^2\sigma_{3T} - \varepsilon. \quad (2.25)$$

Since the reflected shock (2) and the main one (3) have non-zero geometric curvature, their intensities (J_2 and J_3) are the variable functions that change from the values J_{2T} and J_{3T} at the triple point to values J_{2B} and J_{3O} at points B and O, respectively. According to (1.4), angles β_2 and β_3 of flow turn at arbitrary points on shock fronts 2 and 3 saisfy the relations

$$\operatorname{tg}\beta_2 = \sqrt{\frac{(1+\varepsilon)M_1^2 - J_2 - \varepsilon}{J_2 + \varepsilon}}\,\frac{(1-\varepsilon)(J_2-1)}{(1+\varepsilon)M_1^2 - (1-\varepsilon)(J_2-1)},$$

$$\operatorname{tg}|\beta_3| = \sqrt{\frac{(1+\varepsilon)M^2 - J_3 - \varepsilon}{J_3 + \varepsilon}}\,\frac{(1-\varepsilon)(J_3-1)}{(1+\varepsilon)M^2 - (1-\varepsilon)(J_3-1)},$$

and the angles σ_2 and σ_3 of inclination of the shocks 2 and 3 towards the flow in front of them at arbitrary points of shocks obey the relations (1.1)

$$J_2 = (1+\varepsilon)M_1^2 \sin^2\sigma_2 - \varepsilon,\ J_3 = (1+\varepsilon)M^2 \sin^2\sigma_3 - \varepsilon,$$

Similarly to (1.6), Mach numbers M_{2T} and M_{3T} in regions II and III immediately after those curved shocks are also calculated:

$$M_2 = \sqrt{\frac{(J_2+\varepsilon)M_1^2 - (1-\varepsilon)(J_2^2-1)}{J_2(1+\varepsilon J_2)}},\ M_3 = \sqrt{\frac{(J_3+\varepsilon)M^2 - (1-\varepsilon)(J_3^2-1)}{J_3(1+\varepsilon J_3)}}.$$

Thus, relations (2.21-2.23) with additional restrictions (2.20) or (2.24) make it possible to calculate the parameters of all shocks and the flow behind them in the vicinity of the triple point of the Mach reflection. For given parameters of the oncoming flow and the intensity of the incident shock, the solution at the triple point is unique and accurate for the flow of an inviscid gas. It has been well studied parametrically [83, 107–109] and is often used in various analytical models [52, 53, 56–58, 66–68, 110]. At the same time, it does not determine the geometric size of the Mach shock and, accordingly, the shape of other resulting shocks and discontinuities. Consequently, the integral characteristics of the flow as a whole remain unknown. This problem has remained unresolved for quite some time (see [16]).

2.2.2. Analytical description and choice of initial approximation for the parameters of the flow along the "virtual nozzle" behind the main shock

Slipstream τ, inclined at an angle $\theta_{3T} = \beta_{3T} = \beta_1 + \beta_{2T}$ to the horizontal plane at the triple point T of Mach reflection, limits from above the flow region III behind a strong main (Mach) shock, which is initially (immediately behind the main shock) subsonic. According to the von Neumann criterion, Mach reflection exists when $\theta_{3T} < 0$. The so-called von Neumann reflection, which theoretically can occur at $\theta_{3T} > 0$, is unstable in real steady flows and does not form in practice [21, 45].

Due to the small transverse gradients of flow parameters in region III, this flow is usually considered as isentropic and quasi-one-dimensional one, similar to quasi-one-dimensional flow through a classical supersonic nozzle ("de Laval nozzle") with small surface inclination angles. The analogy with a supersonic nozzle is even more complete, since, under the influence of the fan characteristics of the expansion wave IV (Fig. 2.7, b) or V (Fig. 2.7, a), a slipstream τ turns upward, causing its angle of inclination β_τ becomes equal to zero at some point C_*. As evidenced in laboratory [21, 24, 36-38] and numerical [32, 34] research, flow velocity in the subsonic region TOO_*C_* downstream some line O_*C_* ("critical section") becomes supersonic. Thus, the term "virtual nozzle" is an adequate characteristic of the flow in region III after the main shock.

The coincidence of the slipstream turn and of the flow transition behind the Mach shock to supersonic speeds is a key condition in various analytical models [40, 52-58, 66-68, 110, 145] and numerical studies that allow estimating the height y_T of the Mach stem. If the expected height is too low, the gas flow in region III reaches the critical speed before the slipstream turns to the horizontal direction; otherwise, if the height estimation y_T is too large, the slipstream turns to a horizontal direction, but the flow velocity below it remains subsonic ($\beta_\tau = 0$ at $M_3 < 1$).

Within the framework of a quasi-one-dimensional model of flow in region III behind the Mach shock 3, width y of an arbitrary cross section of this flow region is

determined by the flow Mach number $M_{3\tau}$ in the corresponding section through the ratio of flow rate functions like (1.22):

$$y_*/y = q\left(M_{3\tau}\right), \tag{2.26}$$

so

$$y/y_T = q\left(M_3\right)/q\left(M_{3\tau}\right). \tag{2.27}$$

Here $q\left(M\right) = M \cdot \left[1+\varepsilon\left(M^2-1\right)\right]^{-1/2\varepsilon}$ is the dimensionless isentropic flow rate function, y_* in (2.26) is the width the "critical section" O_*C_* of region III, and M_3 is the averaged Mach number of the flow just downstream the curvilinear shock wave 3 (at a first approximation, $M_3 = M_{3T}$). Static pressure p, equal on both sides of the sleepstream, as well as other flow parameters on the lower side of this sleepstream, is determined by the isentropic flow formulas (1.23):

$$p/p_T = \pi\left(M_{3\tau}\right)/\pi\left(M_3\right) = \pi\left(M_{2\tau}\right)/\pi\left(M_{2T}\right). \tag{2.28}$$

Here $\pi\left(M\right) = \left(1+\dfrac{\gamma-1}{2}M^2\right)^{-\gamma/(\gamma-1)}$ is the isentropic pressure function, and $M_{2\tau}$ is the Mach number of the flow at the considered point, but on the upper side of the slipstream.

If the height of the Mach shock is sufficiently large compared to the cross-sectional size of the flow as a whole, and transverse flow gradients in region III cannot be neglected, then some methods for averaging flow parameters can be used [111]. First of all, instead of the Mach number M_{3T} behind the main shock in the vicinity of the triple point, the Mach number M_0 behind the direct main shock at point O can be used in (2.26-2.28). Similarly, some averaged (between M_0 and M_{3T}) values (for example, half the sum of these Mach numbers) can be used. However, since it is the Mach number M_{3T} in fact, accurately characterizes the initial (in the vicinity of the triple point) state of the flow at the lower side of the slipstream, the approximation $M_3 \equiv M_0$ is more controversial. As a compromise, the initial static pressure at the left boundary of subsonic zone III can be estimated as the averaged integral value according to [52]:

$$p_3 = \int_0^{y_T} p_3^l(y)\,dy \Big/ y_T\,, \tag{2.29}$$

supplemented with a parabolic approximation of the main shock shape.

An original method for averaging flow in the subsonic zone was proposed and applied in [58] and [67]. Based on a first-order approximation for the flow behind the main shock, the following relation is derived in [58, 67] to estimate the initial average Mach number in region III:

$$M_3 = \frac{2\left(\rho_{3T} u_{3T} \cos\sigma_{3T} + \rho_O u_O\right)}{\left(\rho_{3T} + \rho_O\right)\left(a_{3T} + a_O\right)}. \tag{2.30}$$

In (2.30), ρ_{3T}, u_{3T} and a_{3T} are gas density, flow velocity and sound speed in zone III immediately after the triple point; ρ_O, u_O and a_O are the same parameters behind the direct shock at point O; σ_{3T} is the slope angle of the Mach shock at the triple point.

2.2.3. Approximation of the flow behind a reflected shock

Already in the first work [52], devoted to an approximate analytical model of a flow with Mach reflection, it was assumed that the head acoustic characteristic BC of the second family of the expansion wave falls on a slipstream in the critical section of region III (i.e., $C \equiv C_*$ in Figure 2.7,a-b), but the sleepstream τ is geometrically straight and has the same angle of inclination as beyond the triple point. Provided that all the angles of inclination of all strong and weak discontinuities that form the triangle BTC are constant, it is easy to determine the length of the subsonic part of the "virtual nozzle" III and, therefore, the height of the triple point.

However, comparison with experimental results [21, 24] reveals large (up to 50–100%) errors in the estimates of the study [52]. The main reasons for unacceptable errors are as follows:

- the slipstream τ is actually curvilinear. Its angle of inclination is variable, and initially (at the triple point) it is quite small. Therefore, even a small quantitative error in estimating the angle of inclination of the slipstream significantly affects the estimation of the length and width of the subsonic zone. Imagine, for example, a variation in the inclination angle θ_τ from $\theta_{3T} = -2^\circ$ to $\theta_\tau = -10^\circ$ at point

C. If you consider the angle θ_τ constant, as in [52-55], it leads to error for length and width of the subsonic zone by several times. Thus, neglecting the change in the inclination angle leads to a very strong underestimation of the size of the Mach shock;

- the inverse turn of the slipstream τ under the influence of the incident rarefaction wave IV or V does not occur instantly, but along the finite sector CC_*. Neglecting the finite length of the sector CC_* also leads to significant discrepancies.

Approximation [53] of the flow in region II by the Grib-Ryabinin method [112] based on the Legendre tangent transformation significantly complicates the mathematical model, but the difference between the results of [52] and [53] is only 2-4%, as shown in [56], Therefore, the errors in determining the dimensions of the Mach stem remained.

It was first proposed in [56, 62] (subsequent applications in [57, 58, 68, 145]) to consider the flow in region II behind the reflected shock as a simple Prandtl-Meyer wave with straight acoustic characteristics of the first family. The proposed model resembles the “shock-expansion method” [113, 114], but is used not only to estimate pressure, but also to restore the shape and corresponding characteristics of all discontinuities in the flowfield. According to the Prandtl-Meyer invariant and the condition of equality of pressures across the slipstream τ, the following relations (1.35-1.38), proven in [62, 64, 65], can be used:

$$\frac{dy_\tau}{dx} = \tan\ \theta_\tau, \tag{2.31}$$

$$\frac{d\theta_\tau}{dx} = -\frac{\chi M_{3\tau}^2 \sqrt{M_{2\tau}^2 - 1}\ \tan\ \theta_\tau}{M_{2\tau}^2 \left(M_{3\tau}^2 - 1\right) y_\tau}, \tag{2.32}$$

$$\frac{dM_{2\tau}}{dx} = \frac{\mu\left(M_{2\tau}\right)\ \tan\ \theta_\tau}{\left(1-\varepsilon\right) M_{2\tau} \left(M_{3\tau}^2 - 1\right) y_\tau}, \tag{2.33}$$

$$\frac{dM_{3\tau}}{dx} = \frac{\mu\left(M_{3\tau}\right) M_{3\tau}^2 \tan\ \theta_\tau}{\left(1-\varepsilon\right)\left(M_{3\tau}^2 - 1\right) y_\tau}. \tag{2.34}$$

Here $M_{2\tau}$ and $M_{3\tau}$ are the local Mach numbers above and below the slipstream, respectively; $\mu(M)=1+\varepsilon(M^2-1)$; $y_\tau(x)$ is the slipstream shape equation; $\theta_\tau(x)$ is the local slipstream angle; $\chi=+1$ is the wave direction coefficient. Relations (2.31) and (2.34), describing the region of quasi-one-dimensional flow, are similar to equations (1.24) and (1.25), respectively.

Equations (2.31-2.34) should be integrated to the point of intersection of the slipstream with the incident characteristic BC. As it is shown in [65] and follows from equations (1.51-1.59), the shape of this curvilinear characteristic can be determined by the integration of the equations

$$\begin{aligned}
\frac{d\theta_w}{dw} &= \frac{2\sqrt{M_{2w}^2-1}}{M_{2w}^2}\cdot N_2,\\
\frac{dM_{2w}}{dw} &= -\frac{2\chi\left(1+\varepsilon\left(M_{2w}^2-1\right)\right)}{(1-\varepsilon)M_{2w}}\cdot N_2,\\
\frac{d\alpha_{2w}}{dw} &= \frac{2\chi\left(1+\varepsilon\left(M_{2w}^2-1\right)\right)}{(1-\varepsilon)M_{2w}^2\sqrt{M_{2w}^2-1}}
\end{aligned} \qquad (2.35)$$

in the direction w of its incidence (see Figure 2.7,a-b). Here β_w is local flow angle; M_{2w} is local Mach number; $\alpha_{2w}=\arcsin(1/M_{2w})$ is the Mach angle; N_2 is the local curvature of the streamline. The relation following from (1.54),

$$N_2=-\frac{\psi(1-\varepsilon)\left(M_{2w}^2-1\right)M_{3w}^2\sin(\theta_w+\chi\alpha_{2w})\sin\theta_w}{M_{2w}^2\left[M_{2w}M_{3w}^2\sin\theta_w\cdot\Omega+\chi\psi(1-\varepsilon)\sqrt{M_{2w}^2-1}\left(M_{3w}^2-1\right)\sin(\theta_w+\chi\alpha_{2w})\right]},$$

where $\Omega=y_{C_1}-y_T q(M_{3T})/q(M_{3w})$, determines the curvature of the streamline at some arbitrary point C_1 of the simple Prandtl-Meyer wave. Here $\psi=+1$, since flow region II is considered as a expansion wave (and not a compression wave, since it is adjacent to region III through a slipstream τ, and the static pressure in region III decreases downstream). Mach numbers M_{3w} depends on M_{2w} similarly as $M_{3\tau}$ depends on $M_{2\tau}$, see (2.26-2.28).

The results of integration of (2.31-2.34) show that the slipstreamis is always convex upward. Therefore, its inclination to the horizontal plane increases along the entire sector TC. The characteristic BC is a weak discontinuity, and therefore the instantaneous turn of the slipstream at the point C from the finite angle of inclination (in absolute value it is greater than at the triple point) to the zero value of this angle is impossible. As is known, the intersection of the slipstream and the weak discontinuity leads to a breakin the curvature of the slipstream, and not to its kink [1, 56].

2.2.4. Curvature of the reflected shock and approximation of its shape

Since the expanding flow in region II influences the previous reflected shock TB, the shape of this shock is curvilinear, and its intensity (J_2) and the angle of its slope to the oncoming flow (σ_2) are variable. But, as it is shown, for example, in [9, 112], the disturbances reflected during the interaction of an oblique shock with the subsequent overtaking expansion wave are very small (they have the third order compared to similar parameters of the expansion wave, which itself is rather weak in the considered case), and their influence can be neglected. Consequently, the shape of the reflected shock can be restored as follows: the direction of the flow at any point behind the shock must correspond to the flowfield in the downstream overtaking expansion wave II. The basics of this method and the corresponding relationships can be found in [9, 62].

In most practically important cases, variation of the slope angle of the reflected shock *TB* does not exceed 1°. For example, when $M = 5$, $\sigma_{1T} = 36^\circ$ and $\gamma = 1.4$ in the problem of jet outflow (dimensionless height of the Mach shock $y_T/h = 0.390$ according to calculations of the supersonic part of the flowfield by the method of characteristics [115]), angle of inclination of the reflected shock at the triple point $\sigma_{2T} = 40.857^\circ$, and the angle of inclination of the same shock at point B of its exit to the jet boundary $\sigma_{2B} = 40.395^\circ$. At $M = 5$ and $\sigma_{1T} = 40^\circ$, when $y_T/h = 0.589$, the corresponding angles of inclination of the shocks are equal $\sigma_{2T} = 47.492^\circ$ and $\sigma_{2B} = 47.043^\circ$. For this reason, if we consider the reflected shock wave *TB* as a

surface with a constant angle of inclination equal to the angle of inclination at the triple point, as is customary in numerous studies [52-55, 57, 58, 66-68], it does not lead to a significant error in determining the size of the Mach stem and in estimating other flow parameters.

If we do not neglect the curvature of the reflected oblique shock, we can propose a method for its conjugation with a subsequent overtaking expansion wave, which was discussed in [62, 145]. The shape of the shock 2 is determined in the polar coordinate system (r,φ), associated with a point *A*, by solving equations:

$$\frac{dr}{d\varphi} = r \cdot \cot\left(\sigma_2 + \beta_1 - \varphi\right), \tag{2.36}$$

$$\frac{d\sigma_2}{d\varphi} = \frac{r}{\sin\left(\sigma_2 + \beta_1 - \varphi\right)} \cdot \Theta \cdot \frac{\partial \sigma_2}{\partial \beta_2}. \tag{2.37}$$

Here r is the distance from point *A* to the considered point on the shock surface; σ_2 is shock slope angle to the flow in front of it at this point; $\Theta = M_2 \cdot K_S \cdot \sin\left(\alpha_2 - \sigma_2 + \beta_2\right)$; $\alpha_2 = \arcsin\left(1/M_2\right)$; M_2 is local Mach number behind the shock; β_2 is the angle of flow deflection on shock surface; K_S is the curvature of the streamline at the point under consideration behind the shock which corresponds to (1.56):

$$K_S = -\frac{\left(1-\varepsilon\right)\left(M_2^2 - 1\right)M_3^2 \sin\left(\theta + \alpha_2\right)\sin\theta}{M_2^2\left[M_2 M_3^2 \sin\theta \cdot \Omega + \left(1-\varepsilon\right)\sqrt{M_2^2 - 1}\left(M_3^2 - 1\right)\sin\left(\theta + \alpha_2\right)\right]};$$

where

$$\frac{\partial \sigma_2}{\partial \theta_2} = \frac{M_1^4\left(\left(1-\varepsilon\right)\cos^4\sigma_2 - \left(1-2\varepsilon^2\right)\cos^2\sigma_2 - \varepsilon^2\right) - 2\varepsilon\left(1-\varepsilon\right)M_1^2\sin^2\sigma_2 - \left(1-\varepsilon\right)^2}{\left(1-\varepsilon\right)\left[M_1^4\left(\left(1+\varepsilon\right)\cos^4\sigma_2 - \left(1+2\varepsilon\right)\cos^2\sigma_2 + \varepsilon\right) - M_1^2\left(2\left(1-\varepsilon\right)\cos^2\sigma_2 - \left(1-2\varepsilon\right)\right) - \left(1-\varepsilon\right)\right]},$$

$\theta = \beta_1 + \beta_2$ is flow angle behind the shock at a considered point, $q\left(M_3\right)$ is flow rate function, M_3 depends on M_2 according to the relations (2.26-2.28), $\Omega = y - y_T\, q\left(M_{3T}\right)/q\left(M_3\right)$, and M_{3T} is flow Mach number behind the main shock in the vicinity of the triple point.

Equations (2.36-2.37) are to be integrated from the value $\varphi_T = -\sigma_1$ at the triple point T (other initial conditions also correspond to the triple point) to a negative value $\varphi_B = \theta_1$, corresponding to the point B.

The results achieved by integrating equations (2.36) and (2.37) differ insignificantly (usually by 0,01-0,02° for value of angle σ_{2B}) from the results of calculations of the supersonic part of the flow by the method of characteristics, asymptotically obtained at the maximum refinement of the computational grid. All other flow parameters behind the reflected shock (for example, flow angle θ_{2B} and Mach number M_{2B}) are determined simultaneously throughout its entire length.

2.2.5. Interaction of a reflected shock with an oncoming expansion wave

There are at least two ways to construct the shape of a reflected shock wave in the region of its interaction with a expansion wave IV of the opposite direction (see Figures 2.7a and 2.8; the latter one considers this type of interaction separately). The first of that methods was proposed in [60, 61] and applied in [54-56] and further studies. It assumes equality of static pressure and co-directionality of flow velocity vectors behind the outgoing shock B_1B_2 and a refracted expansion wave V, which then influences the sleepstream τ. The second way [61, 63] assumes that the outgoing shock B_1B_2 behind the point B_2 is geometrically straight (i.e., it has zero geometric curvature). Both methods lead to a second-order ordinary differential equation for determining the shock shape BB_1 in the interaction region. In addition, they make it possible to determine the flow parameters in a expansion wave V.

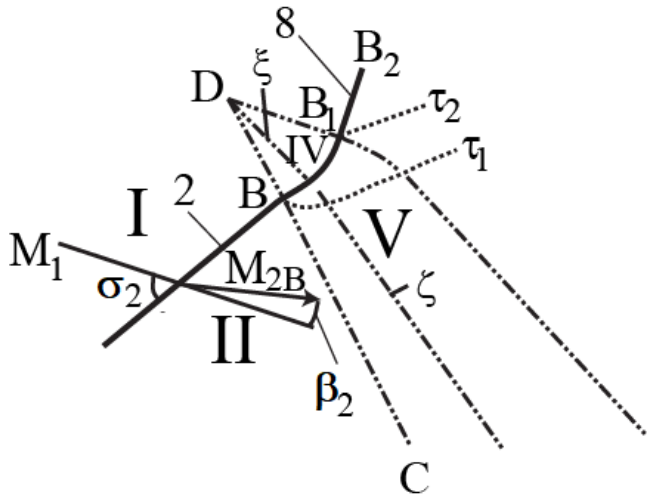

Figure 2.8. Interaction of an oblique shock with a fan of characteristics of the expansion wave (fragment of Fig. 2.7a with additional notations)

The implementation of the first method [60, 61] is as follows. The so-called shear layer, limited by weak tangential discontinuities τ_1 and τ_2, separates the flows that have passed through: on one side of the layer – a centered expansion wave IV and the resulting (outgoing) shock 8 (B_1B_2); on the other side of the shear layer – reflected shock 2 (TB) and the refracted wave V, which is also considered as a Prandtl-Meyer flow with straight acoustic characteristics of the second family. The conditions for equality of pressures and co-directionality of flows behind the resulting shocks and waves are written in the form

$$J_{2B}J_5 = J_4J_8, \tag{2.38}$$

$$\beta_{2B} + \beta_5 = \beta_4 + \beta_8 \tag{2.39}$$

The deflection angles on the shocks considered in (2.38-2.39) depend on their strength as it follows (1.4):

$$\tan|\beta_{2B}| = \sqrt{\frac{(1+\varepsilon)M_1^2 - J_{2B} - \varepsilon}{J_{2B} + \varepsilon}} \frac{(1-\varepsilon)(J_{2B}-1)}{(1+\varepsilon)M_1^2 - (1-\varepsilon)(J_{2B}-1)}, \tag{2.40}$$

$$\tan|\beta_8| = \sqrt{\frac{(1+\varepsilon)M_4^2 - J_8 - \varepsilon}{J_8 + \varepsilon}} \frac{(1-\varepsilon)(J_8-1)}{(1+\varepsilon)M_4^2 - (1-\varepsilon)(J_8-1)}. \tag{2.41}$$

In Prandtl-Meyer waves IV and V, they obey the relations in the form (1.30) и (1.32):

$$\beta_4 = \nu(M_4) - \nu(M_1),\ \beta_5 = \nu(M_2) - \nu(M_{2B}), \tag{2.42}$$

$$J_4 = \pi(M_4)/\pi(M_1),\ J_5 = \pi(M_2)/\pi(M_{2B}).$$

Here $\nu(M) = 1/\sqrt{\varepsilon}\arctan\sqrt{\varepsilon(M^2-1)} - \arctan\sqrt{M^2-1}$ is the Prandtl-Meyer function.

In the relations (2.38-2.42), M_4 and M_5 are the Mach numbers of flows after the waves IV and V; J_8 and β_8 are the intensity of the outgoing shock 8 at the point B_1 and corresponding flow deflection angle on its surface. As a result of solving (2.38-2.42), the intensity J_8 of the resulting shock wave and its angle of inclination are determined, as well as the intensity J_5 of the reflected wave V, flow Mach number M_5 downstream it and the angle of inclination of its tail straight acoustic characteristic, since it is inclined at a Mach angle to the flow velocity vector.

In Figure 2.8, which illustrates the counter interaction of an oblique shock with a Prandtl-Meyer wave, I is the flow region behind the incident shock wave (M_1 is the Mach number of the flow in this zone); II is flow region behind the reflected shock 2 incoming to the interaction region; IV is the fan of characteristics of an expansion wave coming from the trailing edge of a streamlined wedge (*D* is its center; ξ is its arbitrary straight characteristic of the second family); V is the fan of characteristics of the outgoing expansion wave (ζ is its arbitrary characteristic of the second family); BB_1 is the curved shock under the influence of a wave IV; 8 (B_1B_2) is the outgoing shock resulting from this ineraction; τ_1 and τ_2 are the weak tangential discontinuities limiting the shear layer of variable entropy between them; σ_2 and β_2 are, respectively, the angle of shock slope and the angle of flow deflection at the shock 2; M_{2B} is flow Mach number at point B immediately after that shock.

Without additional reservations, we can consider the interaction of the shock wave not with the entire expansion wave of the opposite direction (so-called counter wave), but with part of it up to an arbitrary straight characteristic ξ. This characteristic with local Mach number M_ξ is directed at an angle $\beta_1 + \nu(M_\xi) - \nu(M_1) - \alpha(M_\xi)$ to the horizontal.

Solving a system completely analogous to expressions (2.38-2.42), up to the characteristic ξ, one can obtain: the Mach numbers of the flow on both sides of the interacting shock BB_1 at an arbitrary point; the angle of inclination which leads to the equation for $y'_{BB_1}(x)$, determining the shape of the shock; angle of inclination of an arbitrary characteristic ς of reflected wave V (see Figure 2.8); flow direction and flow Mach number on this characteristic. As it is shown in [61-63], the obtained solutions are almost indistinguishably close to the exact one.

The second method of analysis [61-63] is based on the assumption that the outgoing oblique shock wave is almost straight (has zero curvature) immediately before the entry point B into the fan of characteristics (shock 2) and immediately after the point B_1 of the exit from that fan (shock 8). Differential conditions of the dynamic compatibility [1, 63], together with an exact solution to the problem of the interaction of an oblique shock with a weak discontinuity [1], make it possible to estimate the geometric curvature of the shock BB_1 at its arbitrary point accurately. This leads to a second-order ordinary differential equation that determines the shock shape, variable shock intensity, Mach numbers and other flow variables on both sides of the interacting and outgoing shocks with, as it is shown in [62, 63], with almost the same or slightly better accuracy.

2.2.6. Reflection of a fan of characteristics of the expansion wave, which leads to a reverse turn of the slipstream

Opposite rotation of a slipstream τ to the horizontal direction at a point C_* (see Fig. 2.7, a-b) occurs under the influence of an expansion wave IV (Figure 2.7,b) or a refracted expansion wave V (Figure 2.7,a).

An analytical method for study the reflection of a expansion wave from a slipstream is discussed in [56, 62, 145]. Limiting ourselves to the reflection of a centered wave and maintaining the nomenclature of notations shown in Figure 2.9, we discuss below an analytical method that can be generalized to the reflection of an uncentered (“simple”) refracted wave in a flow between two wedges.

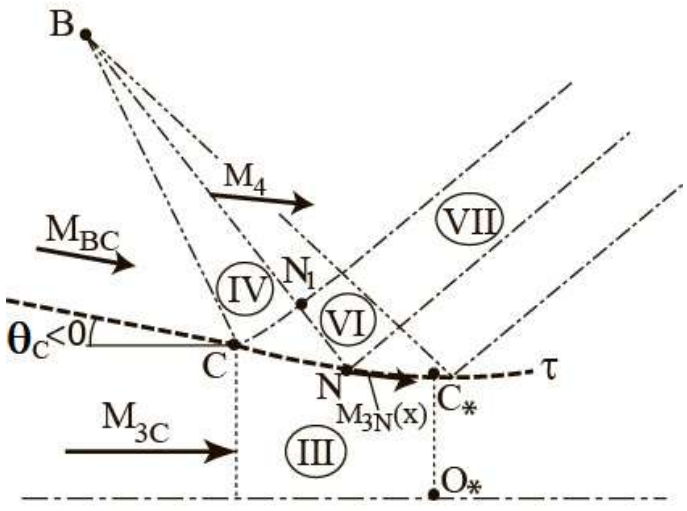

Figure 2.9. Incidence of the expansion wave IV on a slipstream which borders quasi-one-dimensional flow region III (fragment of Fig. 2.7b with additional notations)

Here τ is the slipstream (θ_C is its angle of inclination at point C of the incidence of the head characteristic of the expansion wave); III is the «virtual nozzle» (C_*O_* is its «critical section»; M_{3C} is flow Mach number just below the point C; M_{3N} is flow Mach number at an arbitrary point N just below the slipstream); IV is the incident expansion wave (BC is its head characteristic of the second family; M_{BC} is the Mach number on the characteristic BC; M_4 is flow Mach number on an arbitrary incident characteristic BN_1); VI is the interaction area; VII is the reflected wave.

Calculations of the supersonic part of the flow demonstrate that the gradients of gas-dynamic variables in the region behind the reflected shock are small compared to the intense variation of flow parameters in the region IV (see Figure 2.7). For example, a sector *TC* of slow flow deflection at a slipstream is several times longer than the sector CC_* of its reversal in the opposite direction to a slightly larger (in absolute value) angle. Thus, it is permissible to consider the flow parameters on the characteristic *BC* as averaged and identical. Then, the characteristic *BC* itself should be considered as the straight one, and the flow in the region IV – as a centered Prandtl-Meyer wave with straight characteristics of the second family.

Boundary characteristic *BC* is also a weak discontinuity: the streamlines undergo a finite break in curvature when crossing that line. In particular, the

curvature of the slipstream τ changes sharply and, as a rule, abruptly becomes positive at the point *C*. Thus, the slipstream τ becomes convex downwards.

Average flow Mach number M_{BC} on the characteristic *BC* is defined as follows:

$$M_{BC} = 1 \Big/ \sin\left(\theta_C + \arctan\Delta_{xy} + n\pi\right). \tag{2.43}$$

Here $n = 0$ at $x_C > x_B$; $n = 1$ otherwise; $\Delta_{xy} = \left(y_C - y_B\right)\Big/\left(x_C - x_B\right)$; θ_C is flow angle at a point *C*.

The following relation is valid for an arbitrary internal straight characteristic BN_1 of the expansion wave IV:

$$\left(y_{N_1} - y_B\right)\Big/\left(x_{N_1} - x_B\right) = \tan\left(\theta_C + \nu\left(M_4\right) - \nu\left(M_{BC}\right) - \alpha\left(M_4\right)\right). \tag{2.44}$$

Here $\nu\left(M\right)$ is the Prandtl-Meyer function.

Expression (2.44) determines the flow Mach number M_4 on this arbitrary characteristic, as well as the angle of its inclination and flow parameters on it not only in region IV, but also in the section N_1N inside zone VI. By relating the angles of flow deflection in the incident (IV) and reflected (VII) Prandtl-Meyer waves, it is easy to obtain the equation for the shape of the sector *DC* of the slipstream τ:

$$y'_\tau\left(x_\tau\right) = \tan\left(\theta_C + 2\nu\left(M_4\right) - \nu\left(M_{BC}\right) - \nu\left(M_N\right)\right), \tag{2.45}$$

while an equation similar (2.45),

$$\left(y_\tau - y_B\right)\Big/\left(x_\tau - x_B\right) = \tan\left(\theta_C + \nu\left(M_4\right) - \nu\left(M_{BC}\right) - \alpha\left(M_4\right)\right), \tag{2.46}$$

determines the flow Mach number M_4 in an incident wave. Mach number M_N on the upper side of the slipstream obeys the condition of equality of static pressures which is similar to (2.28):

$$\pi\left(M_N\right)\Big/\pi\left(M_{BC}\right) = \pi\left(M_{3N}\right)\Big/\pi\left(M_{3C}\right), \tag{2.47}$$

and the Mach number M_{3N} on its lower side is determined by the law of mass conservation in the form analogous to (1.22):

$$y_N / y_C = q\left(M_{3N}\right)\Big/q\left(M_{3C}\right). \tag{2.48}$$

Equation (2.45) with restrictions (2.43, 2.44, 2.46-2.48) allows us to construct a shape of the slipstream τ after the point *C* at least until the flow below it reaches a critical speed (i.e., until we meet the condition $M_{3N}=1$).

Applying the solution for the interaction of an oblique shock with the fan of characteristics of the oncoming expansion wave, it is easy to generalize equations (2.43-2.48) to the case of the interaction with a refracted uncentered wave.

2.2.7. General algorithm for calculating the shock-wave structure of a flow with Mach reflection

The equations discussed above make it possible to calculate and to analyze the shock-wave structure of the entire flow under study if the defining conditions are specified (i.e., Mach number M of the undisturbed flow, slope angle σ_1 of the incident shock and the ratio of gas specific heats). One unknown quantity (height y_T of the main shock) can be assigned quite arbitrarily in a first approximation. It is to be refined iteratively. To estimate the height of the Mach stem in jet [56, 62, 145] and internal (nozzle, channel) [62, 145] flows most accurately, the following algorithm was proposed:

1. Values M, σ_1 and γ, corresponding to the case under consideration, are set. The problem of local calculation of the triple configuration arising at Mach reflection of shock 1 is solved. The resulting solution determines the intensities J_2 and J_3 of the reflected shock and the main one in the vicinity of the triple point, as well as the Mach numbers M_{2T} and M_{3T} behind those shocks and the initial angle θ_{3T} of inclination of the slipstream τ.

2. Some initial estimated value of y_T (height of the triple point, also known as the size of the Mach stem) is assigned at the first iteration.

3. Shape of the reflected shock 2 in the section *TB* is determined by equations (2.36) and (2.37). Those equations must be integrated up to the boundary of the overexpanded jet or the point of shock intersection with the first characteristic of the oncoming expansion wave (i.e., to point B). Thus, the Mach number of the flow M_{2B} and flow rotation angle β_{2B} at shock wave 2 at point *B* are determined.

4. Equations (2.31-2.34), which determine the shape of the slipstream τ in the sector TC (as well as flow parameters on both sides), are to be integrated. At the same time, equations (2.35) are to be solved, which determine the shape of the first incident characteristic BC (and flow parameters along it) up to the point C of its intersection with the slipstream.

5. When analyzing the Mach reflection in a narrowing channel between the wedges, the problem of the interaction of an oblique shock wave with the fan of expansion wave characteristics is also to be solved. Using methods developed by ie and Ben-Dor [60], or Meshkov and Omelchenko [61], we determine the shape of the interacting shock BB_1 and flow parameters in the outgoing refracted expansion wave V.

6. The flow parameters at the first boundary characteristic of the expansion wave incident on the sleepstream are averaged. Equations (2.43-2.48) determine the shape of the sector CC_*. of the slipstream. Those equations are to be integrated until one of the following two conditions is met: complete horizontal rotation of the sleepstream τ (expressed by condition $\theta_\tau = 0$) or increasing the flow velocity at its lower side to a critical value $(M_{3\tau} = 1)$. In the first case, the height y_T of the triple point considered at this iteration is too large, in the second case it is too small.

7. Based on the above conclusion about the value of the triple point height, we adjust the value of the height y_T of the Mach shock and return to the step 3. The result of the last iteration (if sufficient accuracy is achieved) is considered the final one.

Thus, the problem of calculating the height of the triple point (with the corresponding analysis of the entire flowfield and its shock-wave structure) is reduced to a boundary value problem for several ordinary differential equations.

The calculation have shown the absence of numerical instabilities for reasonably specified flow parameters, at least in a supersonic jet flow with Mach number $M > 2$, when the strength of the incident shock satisfies the inequality (2.20). Iterative calculation of Mach stem size using a conventional PC and selected widely

available software (MATLAB 2017) takes about ten second, while solving a similar problem when calculating the supersonic part of the flow using the method of characteristics of second-order accuracy takes several minutes at each iteration (in total, at least several hours). Direct calculation of the flowfield by CFD methods using well-known codes (for example, ANSYS Fluent, applied in [150, 151, 152] to similar problems) takes about two hours on one computer, but does not allow one to estimate the size of the Mach shock and the shape of other gas-dynamic discontinuities due to their insufficient resolution, as well as to apply differential shock wave analyzers [116] to the resulting flowfields.

2.2.8. Results of application of the proposed analytical model and its experimental verification

Calculation results for triple point height y_T (referred to half the width of the nozzle exit section h) in an overexpanded jet flow are presented in Table 2.1 (see also Figure 2.10) for the flow Mach number $M = 5$ and different angles σ_1 of shock incidence [145]. The results obtained by the method of characteristics applied to the entire supersonic part of the flowfield [115] are presented in the last row of Table 2.1. Analytical and numerical data differ by approximately 0.5-1%; the results of their comparison are presented in Figure 2.10. Consequently, the proposed approximate analytical method has very high accuracy, quite sufficient for quickly solving relevant problems arising in aircraft and rocket engine building. Calculation of similar characteristics of the shock-wave structure at Mach numbers $M = 3$ and $M = 4$ demonstrated even greater accuracy than presented in Table 2.1.

As shown in Fig. 2.10, the size of the main (Mach) shock is a continuous function of the angle σ_1, starting from value $y_T = 0$ at $\sigma_1 = 30.796^\circ$ (that corresponds to the von Neumann criterion).

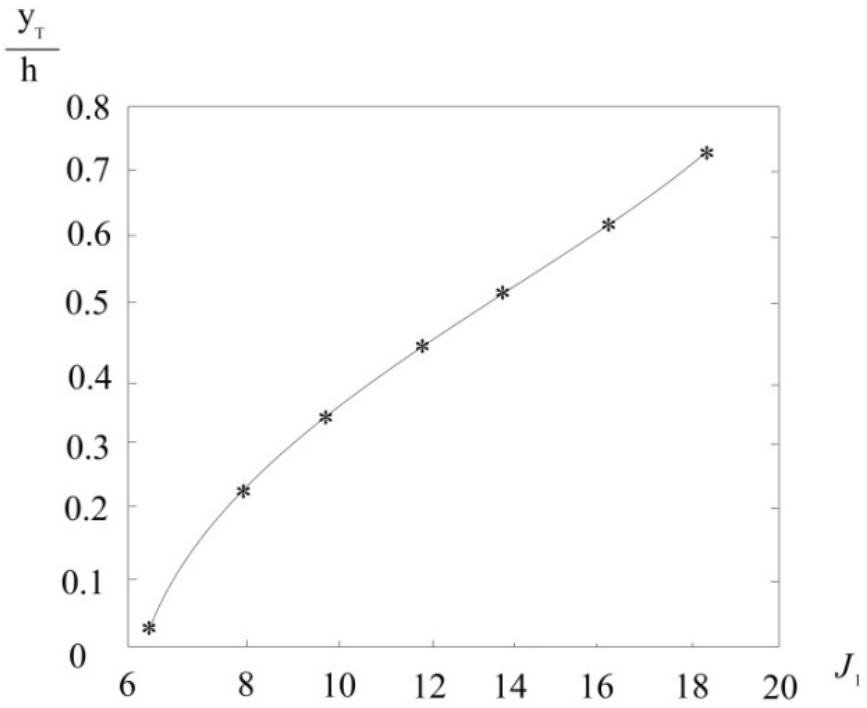

Figure 2.10. Values of the dimensionless height of the triple point (y_T/h), determined analytically (solid line) and numerically (asterisks) depending on the intensity J_1 of incident shock

Table 2.1

Results of calculating the size of the Mach shock y_T/h, obtained by two methods

$\sigma_1,^\circ$	31	35	39	43	47	51	55	59
y_T/h, the proposed method	0.046	0.243	0.363	0.455	0.532	0.602	0.673	0.753
y_T/h, the method of characteristics	0.046	0.245	0.364	0.457	0.536	0.607	0.677	0.756

We should note that, at large strengths of the incident shock (at $\sigma_1 = 57^\circ$ and more), the fan of characteristics of the expansion wave IV does not completely turn the flow in the horizontal direction with the simultaneous transition of the flow in region III through the critical speed. The presented solutions are based on artificially lengthening the fan of characteristics of the expansion wave. It is assumed that the gas flow through the "virtual nozzle" can remain subsonic at such a deep overexpansion (the separation of the flow inside the nozzle, as well as the occurrence of a detached shock upon entering the supersonic air intake, are not studied here, but have their chance to be realized in engineering practice).

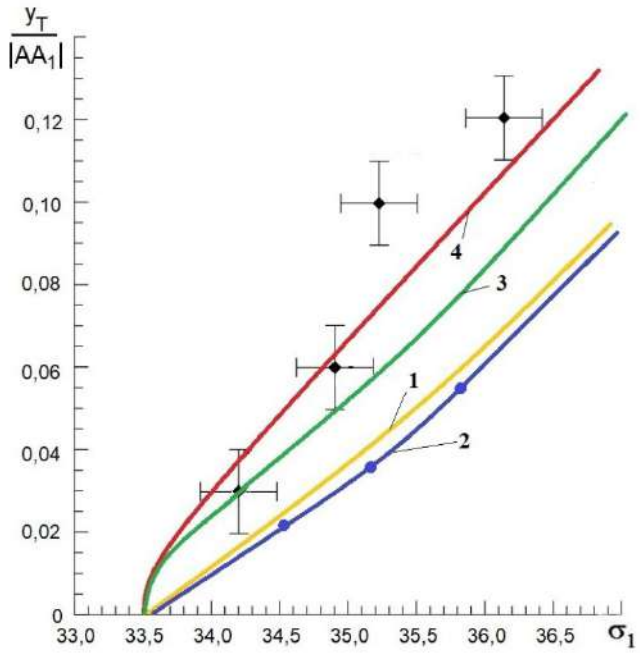

Figure 2.11. Values of the dimensionless height of the main shock wave ($y_T/|AD|$) at Mach reflection in a narrowing channel depending on the slope angle σ_1 of the incident shock

The values of the dimensionless height of the Mach shock that occurs in the narrowing channel (model of the supersonic air intake) are shown in Figure 2.11 depending on the angle σ_1 of slope of the incident shock at flow Mach number $M = 3.98$. The results shown in Figure 2.11, are within the measurement errors of experimental data [21], while the results of the analytical model [58] differ from them by 20-25%, and the approximate model [52] – even to a greater extent (40-90%).

In Figure 2.11, flow Mach number $M = 3.98$; large crosses correspond to experimental data [21]; curve 1 was obtained using the engineering approach [52]; circles and approximating curve 2 –to the method [53]; curve 3 –to the method [58]; 4 to the data [145], obtained by applying the proposed analytical method.

Thus, based on the previously obtained results of solving local problems of the interaction of gas-dynamic discontinuities and waves, including the solution for the triple configuration of Mach reflection, the conjugation of a Prandtl-Meyer wave with a previous overtaking shock, with a counter shock and with a quasi-one-dimensional flow, the interaction of an incident centered or simple expansion wave with a slipstream, etc., a new complex analytical model of the shock-wave structure of a supersonic flow with Mach reflection has been developed. Based on the results

obtained for a supersonic overexpanded jet flow or flow in a narrowing channel, its high accuracy is demonstrated, especially when determining the size of the main shock (Mach stem).

The next necessary step to adapt this analytical model to real flows is to take into account the possible pulsed heat supply at the Mach shock, as well as the effects of real gas, which are significant for irregular reflection in flows with high Mach numbers.

2.3. Ambiguity of solutions for shock-wave structures forming in high-speed gas flows with a low adiabatic index

The analytical model presented in the Subsection 2.2 allows us to estimate the height of the triple point, other parameters of the shock-wave structure and the flowfield with Mach reflection as a whole with high accuracy. As numerous experimental and numerical data show [25-29, 32-37, 40-44], those parameters (including the size of the main shock) are the only ones that can be realized if Mach reflection actually occurs.

At the same time, the solution with the Mach reflection of an incident shock of a given strength, as is known, is not unique. For example, in a wide domain of problem parameters (“dual solution domain”), solutions for both steady regular and Mach oblique shock reflection coexist [1, 17-20, 44]. According to modern concepts of hysteresis, the Mach reflection is preserved within this region, for example, during the jet outflow of an overexpanded jet from the supersonic nozzle of an taking off rocket or upon entering the supersonic air intake of an accelerating aircraft, but not in reverse directed processes.

As it is shown below, solutions for the flowfield with a separated (bow) shock or for a triple configuration of overtaking shocks (see, for example, [144]) can coexist with the solution for the Mach reflection of a steady shock of a given intensity.

Problems of stability and ambiguity of solutions for Mach reflection of shock waves are especially relevant due to the development of aerospace technologies for high supersonic speeds; in this case, strong shocks form, which are more adequately described by mathematical models of gas flows with a reduced (compared to diatomic gas) “effective” adiabatic index. For such high-speed gas flows with a reduced ratio of specific heat capacities, the triple configurations of Mach reflection with a negative (relative to the oncoming flow) slope angle of the reflected shock were found [69] and theoretically studied [70-77]. The possibility of realizing such (“negative”) triple configurations, their stability and the uniqueness of the corresponding solutions traditionally seem doubtful. Solutions corresponding to the formation of “negative” configurations are usually always very ambiguous [144], and it is necessary to confirm their realization (as well as the stability of the emerging shock wave structures) in each individual practically important case.

Thus, for the theory of interaction of gas-dynamic discontinuities and its practical applications, it is important to determine the areas of ambiguity in the solution for shock-wave structures that can arise under the same parameters of a supersonic steady flow and of a branching shock [144, 166].

Unless otherwise indicated, gas flows with the adiabatic index $\gamma = 1.2$ are considered in all calculation examples given in the Subsection 2.3,.

2.3.1. Mathematical apparatus for studying triple configurations of steady shocks

Triple configurations are the shock-wave systems consisting of three shocks and a slipstream emanating from their common (triple) point (*T* in Fig. 1.3,a-f). Such configurations arise in many supersonic flows: in nozzles, jets and air intakes, in supersonic flow around bodies, at the interaction of supersonic jets with obstacles, in jet technologies and other applications of supersonic aerodynamics and gas dynamics.

Steady shocks j_i ($i = 1..3$, Fig. 1.3,a-f), which form a triple configuration, can be straight or oblique ones; in the latter case, they deflect the supersonic flow opstream them by a non-zero angle β_i. Depending on the mutual ratio of the angles

of flow deflection at the shocks, the configurations of the first type (TC-1, $\beta_1\beta_2<0$, $\beta_1\beta_3<0$, Figure 1.3,a), the second one (TC-2, $\beta_1\beta_2<0$, $\beta_1\beta_3>0$, Figure 1.3,c) and the third one (TC-3, $\beta_1\beta_2>0$, $\beta_1\beta_3>0$, Figure 1.3,e) are distinguished. Stationary Mach configuration (SMC) with a normal main ("Mach") shock j_3 ($\beta_3=0$, Figure 1.3,b) is the transitional one between structures of the first and second types; in also corresponds to the well-known von Neumann criterion of "mechanical equilibrium" [8, 16] of changing the type of reflection of the shock j_1 from a plane of symmetry or a solid surface. Configuration TC-2-3 with normal shock j_2 ($\beta_2=0$, Figure 1.3,d) occupies an intermediate position between TC-2 and TC-3.

It is generally accepted that the configurations of the second type form at irregular (Mach) shock reflection, and TC-1 and TC-3 occur in special cases of regular interaction of counter and overtaking shocks. Types of Mach shock reflection with the formation of TC-1 and TC-3, named after Guderley, von Neumann, Vasiliev, realize in steady flows with high supersonic speeds extremely rarely [20, 44]. However, the formation of branched shock-wave structures with several triple configurations of all three types is possible [1, 18, 20] at any irregular interactions between overtaking and counter shocks,.

The compatibility conditions at the slipstream τ make it possible to relate the intensities J_i of individual shocks and the angles β_i of flow deflection by equations (1.18). In this case, the expression $J_1J_2=J_3$ can be written in the form (1.19)

$$\Lambda_1+\Lambda_2=\Lambda_3, \tag{2.49}$$

here $\Lambda_i=\ln J_i$ ($i=1..3$);angles β_i of flow deflection and Mach numbers M_i behind the shocks are associated with shock intensities J_i and Mach numbers M_{i-1} after them by the formulas similar to (1.4) и (1.6):

$$\operatorname{tg}|\beta_i|=\sqrt{\frac{(1+\varepsilon)M_{i-1}^2-J_i-\varepsilon}{J_i+\varepsilon}}\,\frac{(1-\varepsilon)(J_i-1)}{(1+\varepsilon)M_{i-1}^2-(1-\varepsilon)(J_i-1)}. \tag{2.50}$$

$$M_i=\sqrt{\left[(J_i+\varepsilon)M_{i-1}^2-(1-\varepsilon)(J_i^2-1)\right]/\left[J_i(1+\varepsilon J_i)\right]} \tag{2.51}$$

($M_{i-1} \equiv M$ for shocks j_1 and j_3).

To calculate the triple configuration, the parameters of the undisturbed flow must be specified (its Mach number and adiabatic exponent γ), as well as some parameter of the branching shock j_1 (for example, its intensity). The resulting solution is clearly represented on the plane of shock polars $(\beta;\Lambda)$, shown in Figure 2.12. Heart-shaped curve (polars) I in Figure 2.12,a-f represents the set of shock waves that can form in a flow with a Mach number M, polar II corresponds to the similar set of shocks in flow with Mach number M_1, pre-rotated at an angle β_1 on the surface of the shock j_1. Point a on polar I corresponds to the given parameters of the first shock, point b of the intersection of the polars determines the parameters of other shocks. The possible presence of several points of intersection of shock polars (points b, b', b'' in Figure 2.12, b-c) indicates the solution ambiguity of the system (2.21, 2.49-2.51) for given M, J_1 и γ.

Among the many points on shock polars corresponding to the special properties of shocks and flows behind them, the following ones are the most significant in this case:

- point m, corresponding to the formation of a normal shock j_i with zero deflection angle ($\beta_i = 0$) and intensity $J_m = (1+\varepsilon)M_{i-1}^2 - \varepsilon$;

- point l, corresponding to an oblique shock with a deflection angle $\beta_l(M_{i-1},\gamma)$, whickh is maximal for a single shock (the total deflection angle of on several oblique shocks, according to [62, 118-120], can be significantly greater). Intensity $J_l(M_{i-1},\gamma)$ of such a shock is determined by the expression (1.5):

$$J_l = \frac{M^2-2}{2} + \sqrt{\left(\frac{M^2-2}{2}\right)^2 + (1+2\varepsilon)(M^2-1) + 2};$$

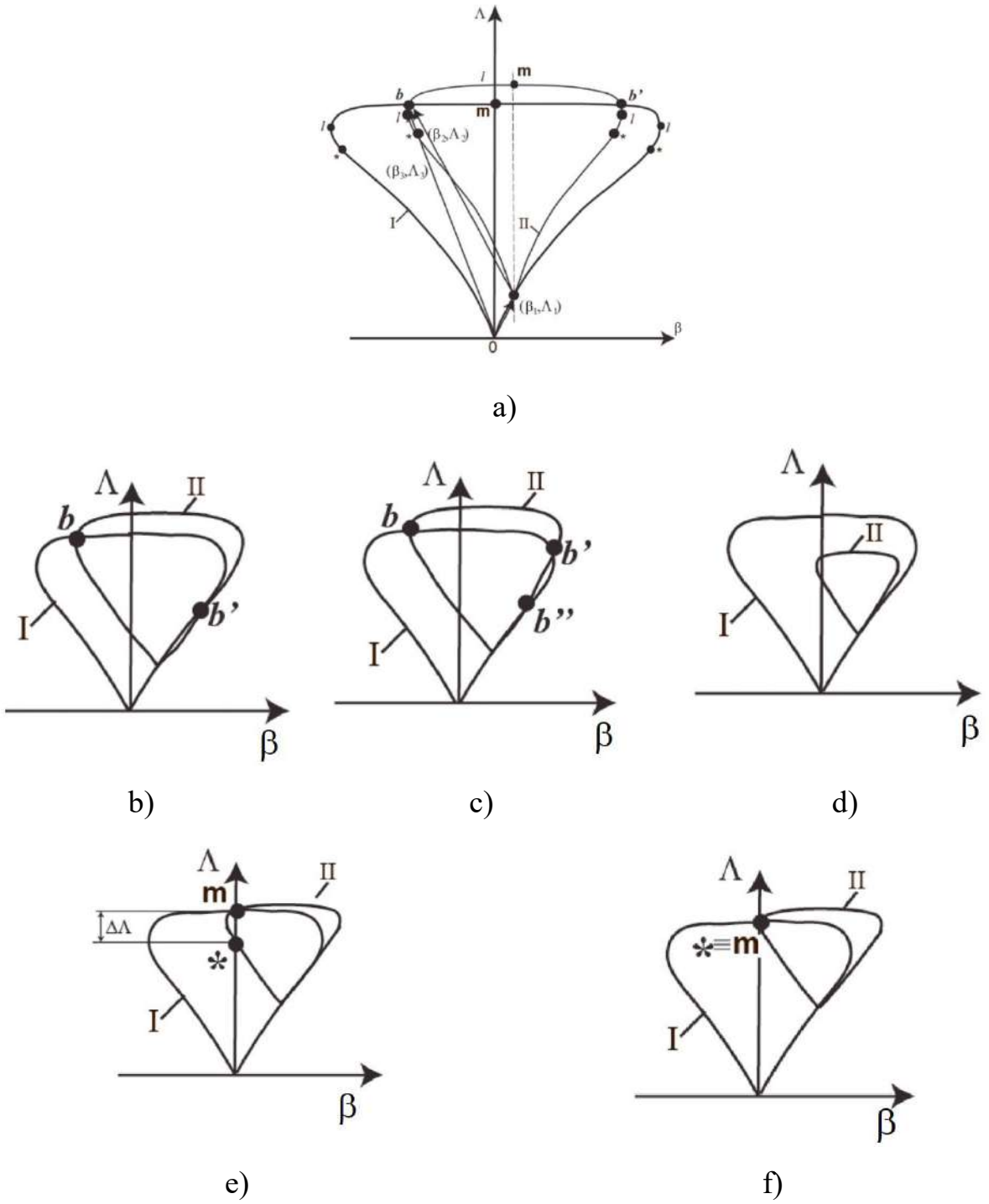

Figure 2.12. Graphical solution for the triple configurations on the plane of shock polars: a) main solution; b) "main" solution and "alternative" one; c) a "main" solution and two "alternative" ones; d) absence of solution; e) dualism of regular/Mach reflection at $M = M_{h2}$; f) dualism of regular/Mach reflection at $M = M_{h1}$

- point "*", which corresponds to an oblique shock j_i with a critical flow velocity behind it $\left(M_i = 1\right)$. Dependence (1.7) in the form

$$J_*\left(M\right) = \frac{M^2 - 1}{2} + \sqrt{\left(\frac{M^2 - 1}{2}\right)^2 + \varepsilon\left(M^2 - 1\right) + 1}$$

defines the “critical” intensity $J_*\left(M_{i-1},\gamma\right)$ of such a shock.

2.3.2. Existence conditions and ambiguity of solutions for the triple configurations

The need to implement supersonic flow behind the shock j_1 limits from above the area of flow deflection angles β_1 by the curve 1 (Figure 2.13), which corresponds to the condition $\beta_1=\beta_*\left(M_{i-1},\gamma\right)$. At high Mach numbers ($M\to\infty$), deflection angle on the shock with critical flow velocity after it strives to a finite limit:

$$\left|\beta_1\right|=\arctan\left[\left(1-\varepsilon\right)/2\sqrt{\varepsilon}\right]=56.443^\circ. \tag{2.52}$$

Parametric analysis of shock-wave structures is traditionally performed on a plane $\left(M;\sigma_1\right)$, shown in Figure 2.14. The slope angle σ_i $(i=1..3)$ of the shock j_i to the velocity vector of the oncoming flow in front of it relates to the shock intensity by (1.1):

$$\left|\sigma_i\right|=\arcsin\sqrt{\left(J_i+\varepsilon\right)/\left[\left(1+\varepsilon\right)M_{i-1}^2\right]}.$$

Curve 1 in Figure 2.14 corresponds to shocks with “critical” intensity and limits the region of existence of triple configurations from above. Coordinates of the bottom point c on this curve correspond to the following branching shock parameters:

$$M_c=\sqrt{\frac{5-4\varepsilon}{2\left(1-2\varepsilon\right)}}=1.683,\ \sigma_c=\arcsin\sqrt{\frac{4\left(1-\varepsilon\right)}{5-4\varepsilon}}=62.327^\circ,$$

and the horizontal asymptote of curve 1 obeys the relation

$$\sigma_1=\arcsin\left(1/\sqrt{1+\varepsilon}\right)=73.221^\circ. \tag{2.53}$$

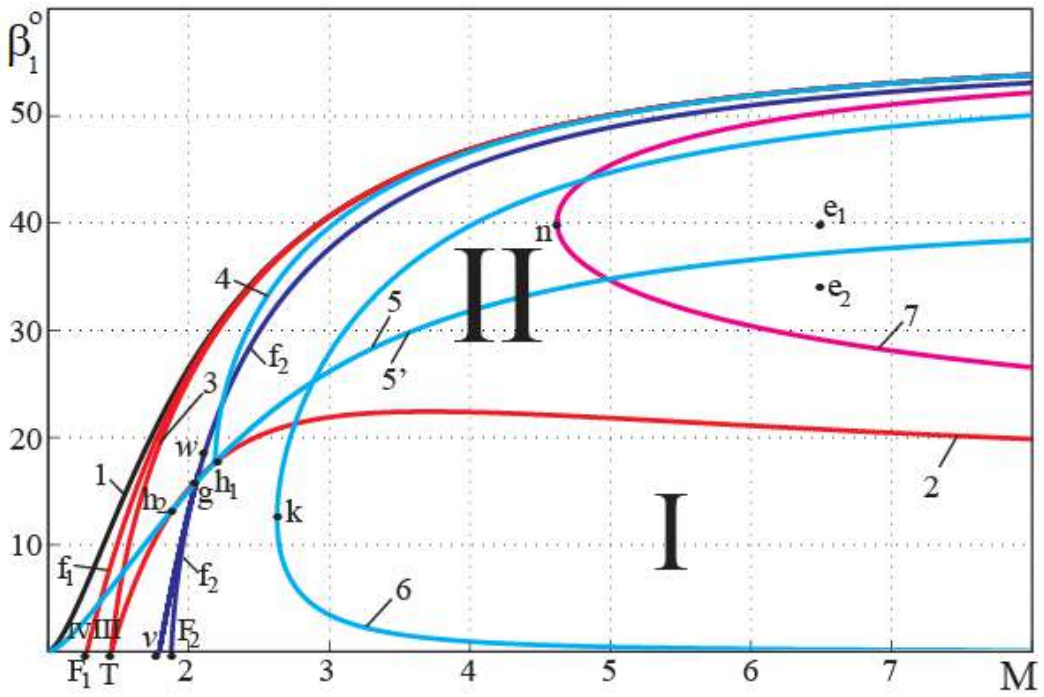

Figure 2.13. Areas of the solution ambiguity on the plane "Mach number of undisturbed flow – angle of flow deflection on the incident shock"

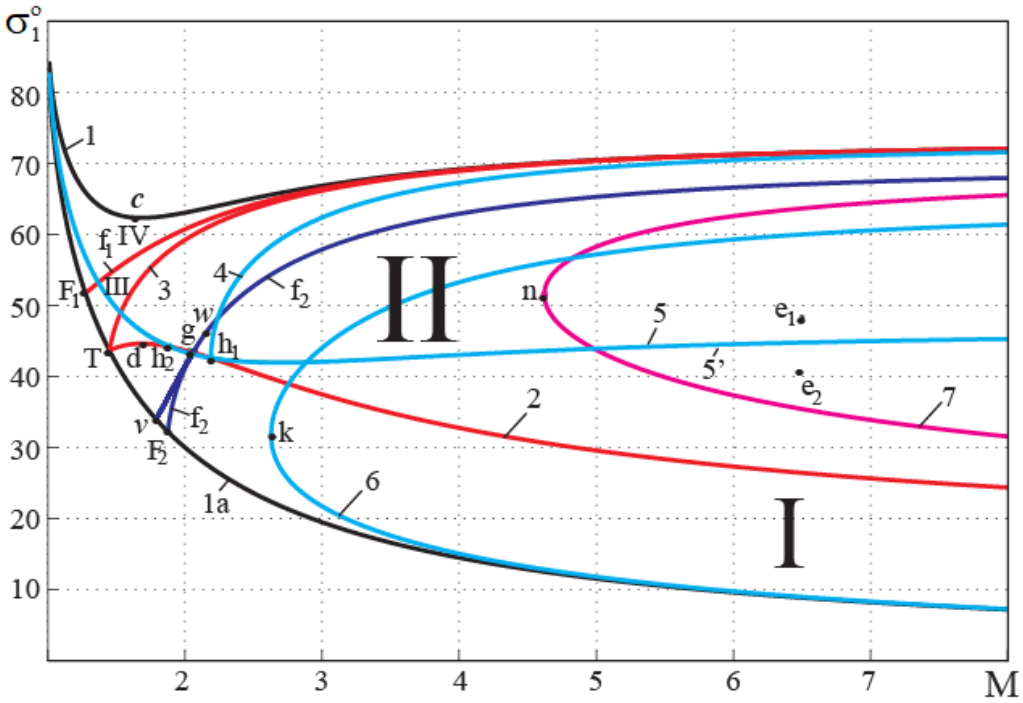

Figure 2.14. Areas of solution ambiguity on the plane "Mach number of the unperturbed flow – slope angle of the incident shock"

Curve 2, defined by the relation $\sigma_1 = \arcsin(1/M) = \alpha(M)$, where $\alpha(M)$ is the Mach angle, is shown in Figure 2.14 as the lower boundary of the region of existence of triple configurations. Intensities $J_2 = J_3 = J$ of the shocks j_2 and j_3 in this extreme $(J_1 \to 1)$ case can be determined from the solution of the problem of the

interaction of an oblique shock with a previous weak disturbance (which coincides ewith the overtaking or counter acoustic characteristic). They obey the following relation [62, 63, 121]:

$$\sum_{i=0}^{3} A_i M^{2i} = 0,$$

$$A_3 = J^2\left(1+\varepsilon\right)^2 - 4\varepsilon\left(J+\varepsilon\right)^2,$$

$$A_2 = 4\varepsilon\left(1-\varepsilon\right)\left(J+\varepsilon\right)\left(J^2-1\right) - 2\left(1-\varepsilon^2\right)J^2\left(J-1\right) - 4\left(1-2\varepsilon\right)\left(J+\varepsilon\right)^2, \qquad (2.54)$$

$$A_1 = \left(1-\varepsilon\right)\cdot\left[4\left(1-2\varepsilon\right)\left(J^2-1\right)\left(J+\varepsilon\right) + 4\left(J+\varepsilon\right)^2 + \left(1-\varepsilon\right)J^2\left(J-1\right)^2\right],$$

$$A_0 = -4\left(1-\varepsilon\right)^2\left(J+\varepsilon\right)\left(J^2-1\right).$$

Implementation of supersonic flow behind a shock j_1 is not enough for the existence of a triple configuration at given values M, J_1 and γ. Triple configurations form only at shock parameters j_1 which correspond to areas I-III in Figures 2.13 and 2.14 (there is no solution in region IV). One ("main") of the solutions of the system (2.21, 2.49-2.51) is continuous throughout the entire zone I-III. It corresponds to configurations of the first type in region I, of the second type – in region II, of the third type – in region III.

Curve 2, which separates regions I and II, corresponds to stationary Mach configurations and is described by a relation in the form (1.20). The beginning of this curve corresponds to the Mach number $M_T = \sqrt{\left(2-\varepsilon\right)/\left(1-\varepsilon\right)} = 1.449$, its highest point d – to the parameters ($M_d = 1.687$, $\sigma_{1d} = 44.684^\circ$), which can be determined from relation (1.20) and the equation

$$\sum_{i=0}^{5} D_i M_d^{2i} = 0,$$

$$D_5 = \left(1-\varepsilon\right)\cdot\left(2-2\varepsilon^2+\varepsilon^3+2\varepsilon^4+2\varepsilon^5+3\varepsilon^6+\varepsilon^7\right),$$

$$D_4 = -\left(1-\varepsilon\right)\left(10+12\varepsilon-17\varepsilon^2-9\varepsilon^3+12\varepsilon^4+17\varepsilon^5-18\varepsilon^6+5\varepsilon^7\right),$$

$$D_3 = 12+37\varepsilon-65\varepsilon^2-49\varepsilon^3+74\varepsilon^4+40\varepsilon^5-97\varepsilon^6+52\varepsilon^7-10\varepsilon^8,$$

$$D_2 = 1-46\varepsilon-4\varepsilon^2+139\varepsilon^3-64\varepsilon^4-103\varepsilon^5+131\varepsilon^6-28\varepsilon^7+10\varepsilon^8,$$

$$D_1 = -\varepsilon(1-\varepsilon)\left(4 - 50\varepsilon + 20\varepsilon^2 + 47\varepsilon^3 - 59\varepsilon^4 + 27\varepsilon^5 - 5\varepsilon^6\right),$$

$$D_0 = \varepsilon^2(1-\varepsilon)^4\left(4 - 3\varepsilon + \varepsilon^2\right).$$

The horizontal asymptote of curve 2 corresponds to the value

$$\sigma_1 = \arcsin\sqrt{\frac{2\varepsilon(1-\varepsilon)}{1+\varepsilon-\varepsilon^2+\varepsilon^3+\sqrt{(1+\varepsilon)^2-\varepsilon(1-\varepsilon)\left[2(1+\varepsilon)(2-\varepsilon)-\varepsilon^3(1-\varepsilon)\right]}}} = 16.694^\circ.$$

Region II between curves 2 and 3 corresponds to triple configurations of the second type, which form at Mach reflection (Figure 1.3c). Flow behind the resulting (Mach) shock j_3 in such configurations is subsonic; flow behind the reflected shock j_2 can be either subsonic or (in the vast majority of cases) supersonic one. Curve 4 in Figures 2.13 and 2.14 divides region II into subregions corresponding to Mach reflection with subsonic (below curve 4) or supersonic (above it) flow behind the reflected shock. Curve 4 starts at point h_1, which corresponds to stationary Mach configuration with a critical flow velocity after the reflected shock. Point h_1 ($M_{h1} = 2.188$, $\sigma_{1h1} = 42.593^\circ$, $\beta_{1h1} = 17.664^\circ$) can be determined from the equations for the SMC and the following relation:

$$\sum_{i=0}^{3} H_i M_{h1}^{2i} = 0,$$

$$H_3 = (1-\varepsilon)\left(1 - \varepsilon - 2\varepsilon^2 + \varepsilon^4\right), \quad H_2 = -\left(4 - 6\varepsilon^2 + 2\varepsilon^3 + 5\varepsilon^4 - 3\varepsilon^5\right),$$

$$H_1 = \varepsilon\left(4 - 4\varepsilon - 3\varepsilon^2 + 7\varepsilon^3 - 3\varepsilon^4\right), \quad H_0 = -\varepsilon^2(1-\varepsilon)^3.$$

Horizontal asymptotes of the curve 4 ($\sigma_1 \to 72.937^\circ$, $\beta_1 \to 56.439^\circ$) are analytically described by cumbersome algebraic equations of high degrees and do not coincide with the asymptotes of other curves.

The formation of an SMC, which corresponds to curve 2, satisfies the von Neumann criterion of a transition in the type (regular or Mach) of reflection of the shock j_1. The von Neumann criterion is most often used for steady flows, especially at moderate and high Mach numbers. When analyzing unsteady flows and steady supersonic flows with low Mach numbers, the maximum flow deflection angle

("detachment criterion") criterion is widely used. According to this criterion, the regular reflection of the shock j_1 persists as long as there is a solution to the equation

$$\beta_1(M, J_1) + \beta_2(M_1, J_2) = 0, \qquad (2.55)$$

here M_1 is the Mach number behind the incident shock, determined by relation (2.51). Solution of equation (2.55) at $J_2 = J_l(M_1)$ defines curve 5 in Figures 2.13 and 2.14; in the region above which there is no solution for regular reflection. Curves 2 and 5, which describe two criteria of reflection transition, do not intersect, but have a single point of tangency g ($M_g = 2.030$, $\sigma_{1g} = 43.516^\circ$, $\beta_{1g} = 15.683^\circ$), determined by the equations

$$\sum_{n=0}^{4} G_n M_g^{2n} = 0,$$

$$G_4 = (1-\varepsilon)(2 - 4\varepsilon + 2\varepsilon^3 - \varepsilon^4),$$

$$G_3 = -10 + 20\varepsilon - 10\varepsilon^2 - 10\varepsilon^3 + 12\varepsilon^4 - 4\varepsilon^5,$$

$$G_2 = 12 - 24\varepsilon + 10\varepsilon^2 + 16\varepsilon^3 - 18\varepsilon^4 + 6\varepsilon^5,$$

$$G_1 = -2(1+\varepsilon)(3 - 4\varepsilon + 2\varepsilon^2)(1-\varepsilon)^2,\ G_0 = (1+\varepsilon)(1-\varepsilon)^4.$$

The horizontal asymptote of curve 5 obeys the same relations (2.52) and (2.53) as the asymptote of curve 1.

In the wide region between curves 2 and 5 ("dual solution domain") with the same shock parameters j_1 solutions that describe both its regular and Mach reflections coexist. The type of shock reflection in each specific case may depend on many factors, including the flow prehistory (have a hysteretic character).

If regular reflection of the shock j_1 implements, then the flow behind the reflected shock j_2 is usually supersonic, except for the thin region between curves 5 and 5'. Curve 5' is determined from equation (2.55) at $J_2 = J_*(M_1)$ and corresponds to the critical flow velocity behind a regularly reflected shock.

Curves 2 and 5’ have two intersection points (h_1 и h_2). Point h_1, such that $M_{h1}=2.188$, $\sigma_{1h1}=44.183^\circ$, $\beta_{1h1}=13.299^\circ$, is determined by the equation for the corresponding Mach number:

$$\sum_{i=0}^{6} H_i M_{h1}^{2i}=0,$$

$$H_6=-(1-\varepsilon)(1-6\varepsilon+3\varepsilon^2+8\varepsilon^3-\varepsilon^4-2\varepsilon^5+\varepsilon^6),$$

$$H_5=10-44\varepsilon+26\varepsilon^2+42\varepsilon^3-42\varepsilon^4-12\varepsilon^5+18\varepsilon^6-6\varepsilon^7,$$

$$H_4=-31+85\varepsilon-16\varepsilon^2-113\varepsilon^3+78\varepsilon^4+39\varepsilon^5-45\varepsilon^6+15\varepsilon^7,$$

$$H_3=(1-\varepsilon)(36-44\varepsilon-55\varepsilon^2+93\varepsilon^3+16\varepsilon^4-40\varepsilon^5+20\varepsilon^6),$$

$$H_2=-(1-\varepsilon)(23-29\varepsilon-48\varepsilon^2+57\varepsilon^3+9\varepsilon^4-30\varepsilon^5+15\varepsilon^6),$$

$$H_1=(1-\varepsilon)(1-\varepsilon^2)(11-9\varepsilon-6\varepsilon^2+12\varepsilon^3-6\varepsilon^4),\ H_0=-(1-\varepsilon)^5\cdot(1+\varepsilon)^2.$$

At the parameters of the incident shock corresponding to the points h_1 and h_2, both a stationary Mach configuration and a regular reflection with a critical flow velocity behind the reflected shock can occur. If the reflection transition corresponds to the point h_2, there is an abrupt change in the parameters of the reflected shock, corresponding to the value $\Delta\Lambda$ (see Figure 2.12,e). If it takes place at the parameters of the incident shock corresponding to the point h_1, shock j_2 does not change its intensity (Figure 2.12,f).

The horizontal asymptotes of closely spaced curves 5 and 5’ coincide.

Curve 3, which corresponds to the transition configurations TC-2-3, obeys the equation (1.21). It starts at a point T, and has horizontal asymptotes which obey the equations (2.52), (2.53) and coincide with the asymptotes of curve 1.

Curve f_1, which limits the region of existence of triple configurations from above, is determined from the solution of the problem of interaction of a shock with a subsequent overtaking weak discontinuity without formation of reflected disturbances. It is characterized by the following dependence, common to curves f_1 and f_2 [62, 79, 120, 122]:

$$M=\sqrt{\left[A\left(B\mp C\right)-1+\varepsilon\right]/\varepsilon},$$

$$A=\left(1+\varepsilon J_1\right)/\left[\left(1+\varepsilon\right)\left(J_1\left(1-3\varepsilon\right)-4\varepsilon^2\right)\right],\ B=J_1\left(1-2\varepsilon-\varepsilon^2\right)-2\varepsilon^2, \quad (2.56)$$

$$C=2\varepsilon\sqrt{\varepsilon\left(1+\varepsilon J_1\right)\left(J_1+\varepsilon\right)}.$$

Points F_1 and F_2, serving as the beginnings of the corresponding curves, obeys the relation $M_{F_{1,2}}=\sqrt{2\left(1\pm\sqrt{\varepsilon}\right)/\left(1\pm2\sqrt{\varepsilon}\right)}$ ($M_{F1}=1.274$, $M_{F2}=1.876$). Asymptotes of curves 1, 3 and f_1 coincide at high Mach numbers.

In a number of cases, the same parameters of the problem (values of M, J_1 and γ) corresponds not only to the above-described "basic" solution (point b in Figure 2.12,b-d), but also to "alternative" solutions (points b' and b''), describing a triple configuration of the third type. At the parameters corresponding to the area between the curves 2 and f_2 in Figure 2.14 (as well as to the area under the curve f_2 in Figure 2.13), there is a single solution for the "alternative" TC-3, and in a curvilinear triangle F_2vw there are two such solutions which appear on the curve vw from the point of contact of the shock polars. Triple configuration parameters corresponding to point v, can be determined by equations (2.56) for the Mach number ($M_v=1.790$) and the following equation for strengths of the shocks j_2 and j_3 ($J_2=J_3=J$):

$$\sum_{i=0}^{8}V_iJ^i=0,$$

$$V_8=(1-\varepsilon)^4,\ V_7=-2(1-\varepsilon)^2(1-3\varepsilon+11\varepsilon^2-\varepsilon^3),$$

$$V_6=-2\varepsilon(9-44\varepsilon+72\varepsilon^2-64\varepsilon^3+35\varepsilon^4),$$

$$V_5=4\varepsilon(7-26\varepsilon+62\varepsilon^2-78\varepsilon^3+31\varepsilon^4-20\varepsilon^5),$$

$$V_4=3-18\varepsilon+114\varepsilon^2-304\varepsilon^3+275\varepsilon^4-326\varepsilon^5+48\varepsilon^6-32\varepsilon^7),$$

$$V_3=-2+14\varepsilon-100\varepsilon^2+156\varepsilon^3-378\varepsilon^4+118\varepsilon^5-128\varepsilon^6,$$

$$V_2=-4\varepsilon(3-6\varepsilon+41\varepsilon^2-20\varepsilon^3+42\varepsilon^4),$$

$$V_1=-8\varepsilon^2(3-2\varepsilon+11\varepsilon^2),\ V_0=-16\varepsilon^3.$$

Coordinates of the point w satisfies the equation

$$\sum_{i=0}^{5} W_i M_w^{2i} = 0,$$

$$W_5 = 4\varepsilon^2(1-3\varepsilon-6\varepsilon^2),$$

$$W_4 = -(1-7\varepsilon+18\varepsilon^2+14\varepsilon^3+53\varepsilon^4+113\varepsilon^5-64\varepsilon^6),$$

$$W_3 = 2(1-\varepsilon)(2-4\varepsilon+\varepsilon^2-83\varepsilon^3-115\varepsilon^4-13\varepsilon^5-172\varepsilon^6),$$

$$W_2 = -(1-\varepsilon)^2(5-13\varepsilon+113\varepsilon^2+249\varepsilon^3+230\varepsilon^4+824\varepsilon^5+256\varepsilon^6),$$

$$W_1 = 4(1-\varepsilon)^3(1-6\varepsilon-41\varepsilon^2-56\varepsilon^3-154\varepsilon^4-128\varepsilon^5),$$

$$W_0 = -4(1-\varepsilon)^4(1+8\varepsilon+21\varepsilon^2+34\varepsilon^3+64\varepsilon^4)$$

for the corresponding Mach number ($M_w = 2.074$) and the expression (2.56), which relates the parameters of the triple configuration on the curve f_2.

At $\gamma \geq 1.25$, the curve f_2, limiting the area of existence of the "alternative" TC-3, has the leftmost point u ($M_u = 2.462$, $J_u = 1.515$ при $\gamma = 1.4$), determined by the equations

$$\sum_{i=0}^{3} U_i M_u^{2i} = 0,$$

$$U_3 = (1-3\varepsilon)^2,\ U_2 = -(3-7\varepsilon)(1-2\varepsilon+5\varepsilon^2),$$

$$U_1 = (1-\varepsilon)(3-23\varepsilon+25\varepsilon^2+27\varepsilon^3),\ U_0 = -(1-\varepsilon)^2(1+10\varepsilon-27\varepsilon^2),$$

$$\sum_{i=0}^{3} u_i J_u^i = 0,$$

$$u_3 = 1-3\varepsilon,\ u_2 = \varepsilon(1-11\varepsilon),\ u_1 = -\varepsilon(4+\varepsilon+9\varepsilon^2),\ u_0 = -\varepsilon(1+5\varepsilon).$$

At $\gamma < 1.25$, the leftmost point is absent, and the curve f_2 corresponds to a unique solution for any Mach number which exceeds M_{F2}. Horizontal asymptote of the curve f_2 is described as follows:

$$\sigma_1 = \arcsin\frac{\sqrt{1-3\varepsilon}}{1-\varepsilon} = 69.732^\circ,\quad \beta_1 = \arctan\sqrt{\frac{(1+\varepsilon)(1-3\varepsilon)}{4\varepsilon}} = 55.902^\circ.$$

The flow behind the shock j_1 and j_2, arriving to the triple point of an "alternative" configuration, is supersonic. Flow behind the resultant shock j_3 is subsonic at the parameters of the shock j_1, which correspond to the area to the right of curve 6 in Figures 2.13 and 2.14. The leftmost point k in curve 6 corresponds to the values $M_k = 2.628$, $\sigma_{1k} = 31.772^\circ$, $\beta_{1k} = 12.463^\circ$. The upper branch of the curve 6 has a horizontal asymptote, determined from the condition $J_1/M^2 \to C$. Here, the value C is the root of the equation

$$\sum_{i=0}^{3} E_i C^i = 0,$$

$$E_3 = (1-\varepsilon)^2(1-2\varepsilon+9\varepsilon^2),\ E_2 = -(1-\varepsilon)(3-7\varepsilon+19\varepsilon^2+11\varepsilon^3+6\varepsilon^4),$$

$$E_1 = (1+\varepsilon)(3-11\varepsilon+22\varepsilon^2-6\varepsilon^3+7\varepsilon^4+\varepsilon^5),\ E_0 = -(1+\varepsilon)^2(1-\varepsilon)^4,$$

and

$$\sigma_1 = \arcsin\sqrt{C/(1+\varepsilon)} = 64.109^\circ \text{ and } \beta_1 = \operatorname{arctg}\left[\sqrt{C(1+\varepsilon-C)}/(\gamma-C)\right] = 53.501^\circ.$$

The lower branch of the curve 6 at high Mach numbers corresponds to a rather weak shock j_1 ($J_1 \to 1$, $\beta_1 \to 0$, $\sigma_1 \to \alpha(M)$).

Thus, there is a wide range of parameters of the problem, within which the followins flow structures can coexist for the same branching shock j_1:

- Mach reflection with subsonic flow behind the main shock; the flow after the reflected shock can be either supersonic or subsonic;

- regular reflection (usually, one with supersonic flow downstream the reflected shock);

- the "alternative" triple configuration of the third type. In this case, the flow behind the resulting shock j_3 is subsonic in most cases.

The subsonic nature of the flow behind outgoing shocks and the the ambiguity of the solution indicates possible instability and dependence of the type of the resulting shock-wave structure on external disturbances located downstream, as well as on the initial conditions of flowfield formation.

2.3.3. Ambiguity of the solution for triple configurations of the second type with a negative slope angle of the reflected shock

At high flow Mach numbers and reduced (compared to $\gamma = 1.4$) gas adiabatic indices, the formation of triple configurations with a negative (relative to the free stream) slope angle of the reflected shock j_2 is possible (see Figure 1.3,f). Flights at high supersonic speeds, usage of polyatomic hydrocarbon fuels, as well as a decrease in the "effective" gas adiabatic index at strong steady and unsteady shocks [8, 17-19] make the analysis of the realizability and stability of such ("negative") triple configurations (NTCs) especially relevant.

The "negative" triple configurations have been theoretically and numerically studied in [69-77, 92, 123, 124]. An analytical description of the area of existence of the NTCs was first given in [75]. According to the results of [75], the NTC always belongs to the second type (TC-2) and forms at the Mach reflection of the shocks, the parameters of which correspond to the region to the right of curve 7 in Figures 2.13 and 2.14, in gases with reduced adiabatic indices ($\gamma < 1.392$). Mach number, starting from which the formation of NTC is possible (points n in Figures 2.13 and 2.14), grows from rather moderate values ($M_n = 3.064$ при $\gamma \to 1$) to large ones ($M_k = 4.621$, $\sigma_{1k} = 51.486^\circ$, $\beta_{1k} = 40.087^\circ$ at $\gamma = 1.2$) and infinitely large ones (at $\gamma \to 1.392$). The dependence of this, as well as other characteristic values of Mach numbers, on gas adiabatic index is presented in Figure 2.15. It shows that the overlappng of the regions of existence of various shock-wave structures noted here occurs at all small adiabatic indices.

The upper and lower branches of the curve 7, which limits the region of existence of the NTCs, have horizontal asymptotes described by the relations

$$\sigma_1 = \arcsin\sqrt{S_1} = 76.562^\circ,\ \beta_1 = \arctan\frac{(1-\varepsilon)\sqrt{S_1(1-S_1)}}{1-(1-\varepsilon)S_1} = 55.731^\circ$$

for the upper branch, and

$$\sigma_1 = \arcsin\sqrt{S_2} = 21.901^\circ,\ \beta_1 = \arctan\frac{(1-\varepsilon)\sqrt{S_2(1-S_2)}}{1-(1-\varepsilon)S_2} = 19.808^\circ$$

for the lower one. Here S_1 and S_2 are, respectively, the larger and smaller of the roots of the equation

$$(1-\varepsilon)^3 S^5 - (1-\varepsilon^2)(4-5\varepsilon)S^4 + (1+\varepsilon)(6-2\varepsilon-7\varepsilon^2)S^3 - 2\gamma^2(2-2\varepsilon-\varepsilon^2)S^2 + \\ +\gamma^3(1+\varepsilon-\varepsilon^2-3\varepsilon^3)S - \varepsilon\gamma^4(1-\varepsilon+2\varepsilon^2) = 0,$$

which belong to the interval $(0;1)$.

Many flow parameters (stagnation pressure, temperature, flow velocity, dynamic pressure) across of the sleepstream τ, emanating from the triple point of the OTC, the more different as the closer the parameters of the incident shock are to the lower branch of curve 7. For example, according to [76], the ratios of stagnation pressures (I_{p0}) and flow dynamical pressures (I_d) at the utmost ($M \to \infty$) case tend to the values

$$I_{p_0} = \left[\frac{1+\varepsilon-S_1}{\varepsilon(2\gamma-S_1)}\right]^{\frac{1+\varepsilon}{2\varepsilon}} = 1.736,\ \ I_d = P_1 / \left[(2\gamma-S_1)R_1\right] = 3.430,$$

on the upper branch of curve 7, and to the values

$$I_{p_0} = \left[\frac{1+\varepsilon-S_2}{\varepsilon(2\gamma-S_2)}\right]^{\frac{1+\varepsilon}{2\varepsilon}} = 9861.0,\ \ I_d = P_2 / \left[(2\gamma-S_2)R_2\right] = 437.447.$$

on the lower branch of this boundary of the domain of existence of the NTCs. Here

$$P_{1,2} = \gamma(1+\varepsilon) - \gamma(3-2\varepsilon-4\varepsilon^2)S_{1,2} + (1+\varepsilon)(3-4\varepsilon)S_{1,2}^2 - (1-\varepsilon)^2 S_{1,2}^3,$$

$$R_{1,2} = \gamma\varepsilon - (1+\varepsilon)(1-2\varepsilon)S_{1.2} + (1-\varepsilon)^2 S_{1,2}^2.$$

Thus, a flow with a large difference in the mechanical properties in its various parts forms behind the “negative” configuration. The problem of the stability of such a flow requires additional research, especially for the parameters of the NTCs corresponding to the lower part of its region of existence in Figures 2.13 and 2.14. In this case, the differences in flow parameters across the slipstream are especially large

and, in addition, there is a “dualism” of solutions for the Mach (with formation of NTC) reflection and the regular one.

The flow behind the main (Mach) shock of the NTC is subsonic. Curve 4, which separates the subregions of existence of the Mach reflection with subsonic and supersonic flow behind the reflected shock, passes above the region of existence of the NTCs. Thus, the gas flow behind the reflected shock at the NTC is always supersonic.

The region of existence of the NTC is embedded in the region under the curve f_2 for any value of the adiabatic index. This means that any shock j_1, reflected with the formation of the NTC, can also form an “alternative” triple configuration of the third type (i.e., the configuration of overtaking shocks) with supersonic (in the region above the upper branch of curve 6) or subsonic (in the opposite case) flow behind the resulting shock j_3. At the same time, the coexistence of the NTC with the “alternative” TC-3, the flow behind the resulting shock of which is subsonic, takes place in most of the region of existence of the NTC.

Curve 5, corresponding to the well-known “detachment criterion” of steady and unsteady shock reflection transition, divides the region of existence of the NTCs into two subregions. In the lower of them (shaded in Figures 2.13 and 2.14) there is a dualism of regular and Mach reflection: a shock j_1 can be reflected both irregularly (with a negative angle of inclination of the reflected shock) and regularly. In the upper subdomain, there is no solution for regular reflection of the shock with corresponding parameters.

The dualism of Mach reflection with the formation of OTC and regular reflection was numerically demonstrated in [77]. Oblique shock with parameters corresponding to the point p_1 in Figures 2.13 and 2.14 ($M = 6.5$, $\beta_1 = 40^\circ$), could not reflect regularly. However, its weakening under the influence of the subsequent Prandtl-Meyer expansion wave to an intensity that, according to calculations, corresponded to $\beta_1 = 35.519^\circ$ (point p_2), made such a reflection possible and implementable at a computational experiment.

In addition to the three indicated solutions (Mach reflection with a negative angle of inclination of the reflected shock; regular reflection; formation of a triple configuration of the overtaking shocks), the others are possible at the interaction of a high-speed gas flow with streamlined bodies, associated with a crucial restructuring of the flowfield. For example, our calculations show that a change in flow deflection angle β_1 in a system of two symmetrical wedges described in [77], from 43° to 45° at $M = 6.5$ leads to the formation of a separated bow shock, although a solution with a "negative" TC theoretically exists in both cases. Sometimes (with the same parameters of the problem), it is not possible during a numerical experiment to establish a flow with the formation of NTC (in those cases, the implementation of a non-stationary (possibly self-oscillating) regime is assumed [70]). In some cases [71], calculations show the existence of more complex, branched configurations reminiscent of double Mach reflection in unsteady flows.

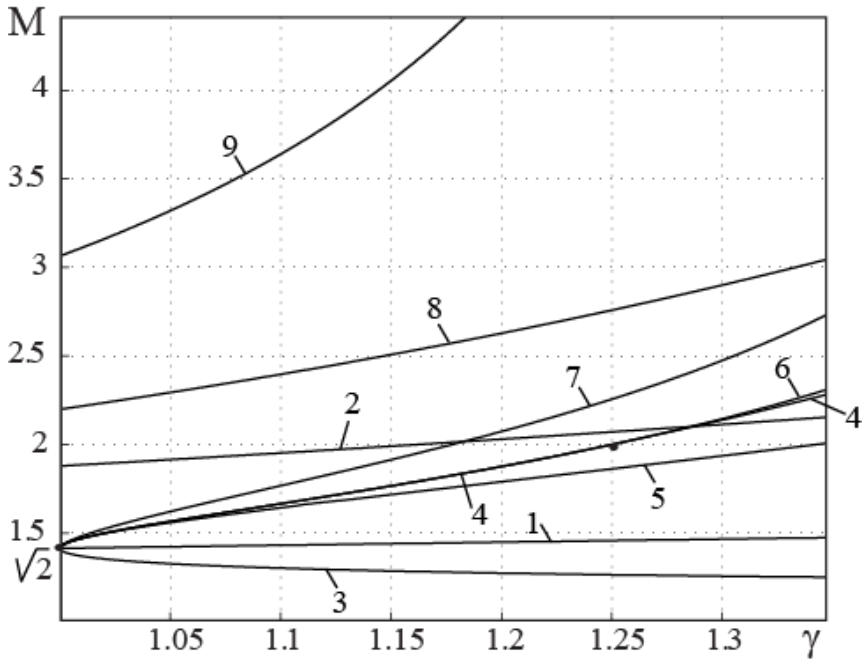

Figure 2.15. Dependence of some Mach numbers important for the problem under consideration on the value of the gas adiabatic index: 1) $M_T(\gamma)$; 2) $M_g(\gamma)$; 3) $M_{F_1}(\gamma)$; 4) $M_{F_2}(\gamma)$; 5) $M_v(\gamma)$; 6) $M_u(\gamma)$; 7) $M_w(\gamma)$; 8) $M_k(\gamma)$; 9) $M_n(\gamma)$

The overlapping of the regions of existence of various shock-wave structures, noted in this subsection, occurs at all small adiabatic indices. For example, all special Mach numbers found analytically in this study exist at all ratios of specific heat capacities of the gas (see Figure 2.15).

Thus, for all parameters of the branching shock and the oncoming flow, which correspond to “negative” configurations, triple configurations of overtaking shocks (in most cases, with a subsonic flow behind the main (resulting) shock) can also occur. In many cases, the same parameters of the incident shock also correspond to its regular reflection (dualism of the solution), as a rule, with a supersonic flow behind the reflected shock. In addition, with similar problem parameters in real gas-dynamic devices (for example, during flow around supersonic air intakes), the formation of separated shocks, unsteady flows, as well as more complex and branched configurations cannot be excluded. Thus, the solutions corresponding to the formation of “negative” configurations are always highly ambiguous, and their realization (as well as the stability of the resulting shock-wave structures) must be confirmed in each individual practically important case.

2.4. Conclusions to the Chapter 2

Study of shock-wave systems and structures using the mathematical apparatus developed in the works of V.N. Uskov, A.V. Omelchenko, M.V. Chernyshov, P.V. Bulat, P.S. Mostovykh and other authors, allows one to obtain theoretically important and practically valuable analytical results.

In particular, in the Section 2 of this study, the parameters of incident shock waves are determined, providing a minimum of static pressure and gas temperature of behind the reflected shock. They were described by a cubic equation in the variables “incident shock intensity – free-stream Mach number”. A similar cubic equation analytically determines the angles of inclination of the obstacle at which the static pressure and temperature behind the point of regular reflection of an unsteady shock wave of a given amplitude are minimal. Those optimal angles of inclination of the reflecting surface exist for all theoretically possible parameters of the incident shock. In this case, the optimal reflection of the shock wave differs both from normal reflection and from another limiting case of transition from regular reflection to Mach one. Calculations show that geometric optimization of the interaction of shock (in particular, blast) waves with obstacles can significantly reduce mechanical and

thermal loads on structural elements. For this reason, the obtained theoretical results can be used in the design of blast-resistant structures, the development of blast protection equipment, in aircraft and rocket engineering, in supersonic aerodynamics and many other applications.

In addition, based on the previously obtained results of solving individual problems of the interaction of gas-dynamic discontinuities and waves, including the solution for the triple configuration of Mach reflection, the conjugation of a Prandtl-Meyer wave with a previous overtaking shock, with a counter shock and with a quasi-one-dimensional flow, the interaction of an incident centered or simple expansion wave with sleepstream, a new analytical model of the shock wave structure of a supersonic flow with Mach reflection has been developed in the Chapter 2. Based on the results obtained for a supersonic overexpanded jet flow or a flow in a narrowing channel, its high accuracy is shown, especially when determining the size of the main (Mach) shock.

When analyzing shock-wave structures that arise under the same parameters of an oncoming supersonic flow and a branching shock, it was established that there is a wide range of problem parameters, within which the following shock-wave structures can coexist for the same branching shock j_1:

- Mach reflection with subsonic flow after the main shock; the flow downstream the reflected shock can be either supersonic or subsonic;

- regular reflection (usually with supersonic flow behind the reflected shock);

- the “alternative” triple configuration of the third type which consists of the overtaking shocks. In this case, the flow behind the resulting shock j_3 is subsonic in most cases.

The subsonic nature of the flow behind the outgoing shocks and the discussed ambiguity of the solution indicates possible instability and dependence of the type of the resulting shock-wave structure on external disturbances located downstream, as well as on the initial conditions of its formation.

For all parameters of the branching shock and the free-stream flow, which correspond to “negative” triple-shock configurations (i.e. triple configurations of Mach reflection with a negative slope angle of the reflected shock), triple configurations of the overtaking shocks can also form (in most cases, with a subsonic flow behind the main (resulting) shock) . In many cases, the same parameters of the incident shock also correspond to its regular reflection (“dualism” of the solution), as a rule, with a supersonic flow behind the reflected shock. In addition, at similar problem parameters in real gas-dynamic devices (for example, in a flow around supersonic air intakes), the formation of separated bow shocks, the formation of unsteady flows, as well as more complex and branched configurations are not excluded. Thus, the solutions corresponding to the formation of “negative” configurations are always ambiguous, and their feasibility (as well as the stability of the emerging shock-wave structures) must be confirmed in each individual practically important case.

The next necessary step is to adapt the obtained theoretical results to the needs of engineering practice is to take into account the possible pulsed energy release at the Mach shock, as well as the effects of real gas, which are significant for irregular reflection in flows with high Mach numbers.

Chapter 3. Analysis of Mach reflection in supersonic gas flows with the possibility of pulsed energy release at the main shock

3.1. Stationary Mach configurations with pulsed energy release and changes in the chemical composition of the gas at the main shock

3.1.1. Preliminaries for the study of a stationary Mach configuration with energy release at the main shock

The theory of triple configurations of shock waves formed in supersonic flows of a perfect gas should now be considered as almost complete [92]. A classification of triple configurations was developed in detail [1, 10], their parametric analysis was obtained [1, 79, 106-108], configurations with special properties of individual shocks were identified [79] as well as the extreme ratios of parameters across the outgoing sleepstream [76, 79]; the solutions obtained are generalized for triple configurations of propagating shock waves [125]. Possible additional research in this field in the future may be related to the problems of the realizibility of triple configurations of Mach reflection with a negative slope angle of the reflected shock [69-71, 76] or to the analysis of the differential characteristics of the flowfield using dynamic compatibility conditions [1, 126].

It was shown in [76, 79, 127] that the gas temperature behind the main (Mach) shock j_3 of the triple configuration (in region III in Figure 3.1) can many times exceed the temperature of the flow that has passed through the sequence from the incident (j_1) and reflected (j_2) shocks, namely in region II on the other side of the slipstream τ. Temperature ratio acrodd the sleepstream $I_T = T_{\text{III}}/T_{\text{II}}$ is especially significant at high Mach numbers M of the oncoming flow. In particular, in extreme triple configurations (providing a maximum of this ratio for fixed values of M), this relation tends to the limit

$$I_T = 1/\varepsilon = 6. \tag{3.1}$$

at $M \to \infty$. In stationary Mach configurations SMC (configurations with a normal main shock j_3, Figure 3.1) it strives to the value [79, 127]

$$I_T = \frac{1+2\varepsilon-2\varepsilon^3+\varepsilon^4+(1-\varepsilon)D}{2\varepsilon(2-\varepsilon)} = 3.363, \qquad (3.2)$$

here

$$D = \sqrt{(1+\varepsilon)^2 - \varepsilon(1-\varepsilon)\left[2(1+\varepsilon)(2-\varepsilon) - \varepsilon^3(1-\varepsilon)\right]}.$$

(hereinafter it is assumed by default that $\gamma = 1.4$). Real gas effects inherent in motion at high supersonic speeds and temperatures usually lead to a decrease in the "effective" adiabatic index of the flow passing through the main shock and a further increase in the values of I_T.

A sharp temperature increase in a supersonic flow of a combustible gas mixture, occurring primarily at the main (Mach) shock, can initiate combustion or detonation with a corresponding pulsed energy release. As relations (3.1) and (3.2) show, in particular, the excitation of detonation at the main shock (and not behind the system of incident and reflected ones) is most effective when flying at high supersonic speeds, which corresponds to modern trends in the development of aerospace technology. Flow in region II after the reflected shock j_2 (on the other side of the slipstream), has a significantly lower temperature, but its total pressure can be many times larger. Relation $I_{p_0} = p_{0\text{II}}/p_{0\text{III}}$ of the stagnation pressures across the sleepstream behind "extreme" configurations [79] at high Mach numbers tends to the limit

$$I_{p_0} = \varepsilon^{-\frac{1+\varepsilon}{2\varepsilon}} = 529.1, \qquad (3.3)$$

and for the SMCs it strives to the value

$$I_{p_0} = \left[\frac{1+2\varepsilon-2\varepsilon^3+\varepsilon^4+(1-\varepsilon)D}{2\varepsilon(2-\varepsilon)}\right]^{\frac{1+\varepsilon}{2\varepsilon}} = 69.72. \qquad (3.4)$$

Relations (3.1-3.4) show the applicability of combustible gas flow behind the main (Mach) shock according to the scheme of detonation engines (in the Fickett-Jacobs thermodynamic cycle, including ramjet engines). The peripheral flow behind the reflected shock is more convenient to use according to the scheme of the

"classical" ramjet t engine (in the Brayton thermodynamic cycle) with flow deceleration without energy release and its subsequent supply to the combustion chamber [86, 150, 152].

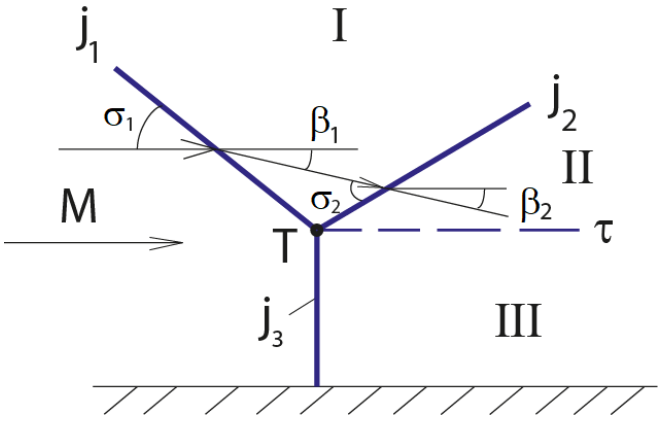

Figure 3.1. Stationary Mach configuration. Here M is the Mach number of undisturbed flow, j_1 is the incident shock, j_2 is the reflected one, j_3 is the main (Mach) shock, I, II and III are the flow regions behind the corresponding shocks, T is the triple point, τ is the slipstream, σ_1 and σ_2 are the slope angles of of incident and reflected shocks, β_1 and β_2 are the angles of flow deflection on the incident and reflected shocks

For further attempts to the practical implementation of that combined-type jet engines proposed in [86, 150, 152], a theoretical analysis of the conditions of existence, stability and flow parameters behind triple configurations that arise during irregular (Mach) shock reflection with pulsed energy release at the Mach stem is necessary. A model example of such a structure, the simplest one and the most accessible one to theoretical analysis, is an SMC with a normal main shock (Figure 3.1). The formation of SMC corresponds to the well-known von Neumann criterion ("mechanical equilibrium criterion") of the transition from Mach reflection to regular reflection [44] and, thus, it corresponds to the minimum intensity of the incident shock j_1, at which the Mach reflection occurs (the lower boundary of the region of existence of the Mach reflection), including in the presence of pulsed energy release and "real gas effects" at the main shock j_3.

3.1.2. Basic relations for the stationary Mach configuration

Compatibility conditions at a slipstream τ, that goes out from the triple point T (Figure 3.1), lead to a system of equations (1.18) relating the parameters of the shocks j_1, j_2 and j_3:

$$\beta_1 + \beta_2 = \beta_3, \tag{3.5}$$

$$J_1 J_2 = J_3, \tag{3.6}$$

which is to be solved at $\beta_3 = 0$ for SMC with normal main shock j_3.

Angles β_1 and β_2 of flow deflection on the incident and reflected shocks is related to their intensities by the expressions (1.4):

$$\tan|\beta_1| = \sqrt{\frac{(1+\varepsilon_{12})M^2 - \varepsilon_{12} - J_1}{J_1 + \varepsilon_{12}}} \cdot \frac{(1-\varepsilon_{12})(J_1 - 1)}{(1+\varepsilon_{12})M^2 - (1-\varepsilon_{12})(J_1 - 1)}, \tag{3.7}$$

$$\tan|\beta_2| = \sqrt{\frac{(1+\varepsilon_{12})M_{\text{I}}^2 - \varepsilon_{12} - J_2}{J_2 + \varepsilon_{12}}} \cdot \frac{(1-\varepsilon_{12})(J_2 - 1)}{(1+\varepsilon_{12})M_{\text{I}}^2 - (1-\varepsilon_{12})(J_2 - 1)}. \tag{3.8}$$

Here M is flow Mach number before the triple configuration, M_{I} is Mach number in the region I behind the shock j_1 (in the future, the subscripts "I-III" correspond to various flow parameters in flow zones I-III behind the shocks j_1 - j_3), $\varepsilon_{12} = (\gamma_{12} - 1)/(\gamma_{12} + 1)$, and γ_{12} is gas adiabatic index in the upper part of the flow (above the slipstream). Values of Mach number M_{I} and M_{II} behind the shocks j_1 and j_2 are determined by the relations (1.6):

$$M_{\text{I}} = \sqrt{\frac{(J_1 + \varepsilon_{12})M^2 - (1-\varepsilon_{12})(J_1^2 - 1)}{J_1(1 + \varepsilon_{12}J_1)}}, \quad M_{\text{II}} = \sqrt{\frac{(J_2 + \varepsilon_{12})M_{\text{I}}^2 - (1-\varepsilon_{12})(J_2^2 - 1)}{J_2(1 + \varepsilon_{12}J_2)}}. \tag{3.9}$$

Expresions (3.7) and (3.8) can be displayed on the plane ($\beta; \Lambda = \ln J$, Figure 3.2,a-c) by the shock polars (I and II), which are divided into two parts ("strong" and "weak" ones) by the points l, corresponding to the maximum deflection angles of the shock. According to (1.5), intensity J_l of such a shock with a maximum angle of flow turn is determined by the Mach number M of the in front of it:

$$J_l(\mathrm{M}) = \frac{\mathrm{M}^2 - 2}{2} + \sqrt{\left(\frac{\mathrm{M}^2 - 2}{2}\right)^2 + (1 + 2\varepsilon_{12})(\mathrm{M}^2 - 1) + 2}$$

(curve 1 in Figure 3.3), or

$$J_l(M_\mathrm{I}) = \frac{M_\mathrm{I}^2 - 2}{2} + \sqrt{\left(\frac{M_\mathrm{I}^2 - 2}{2}\right)^2 + (1 + 2\varepsilon_{12})(M_\mathrm{I}^2 - 1) + 2}\,.$$

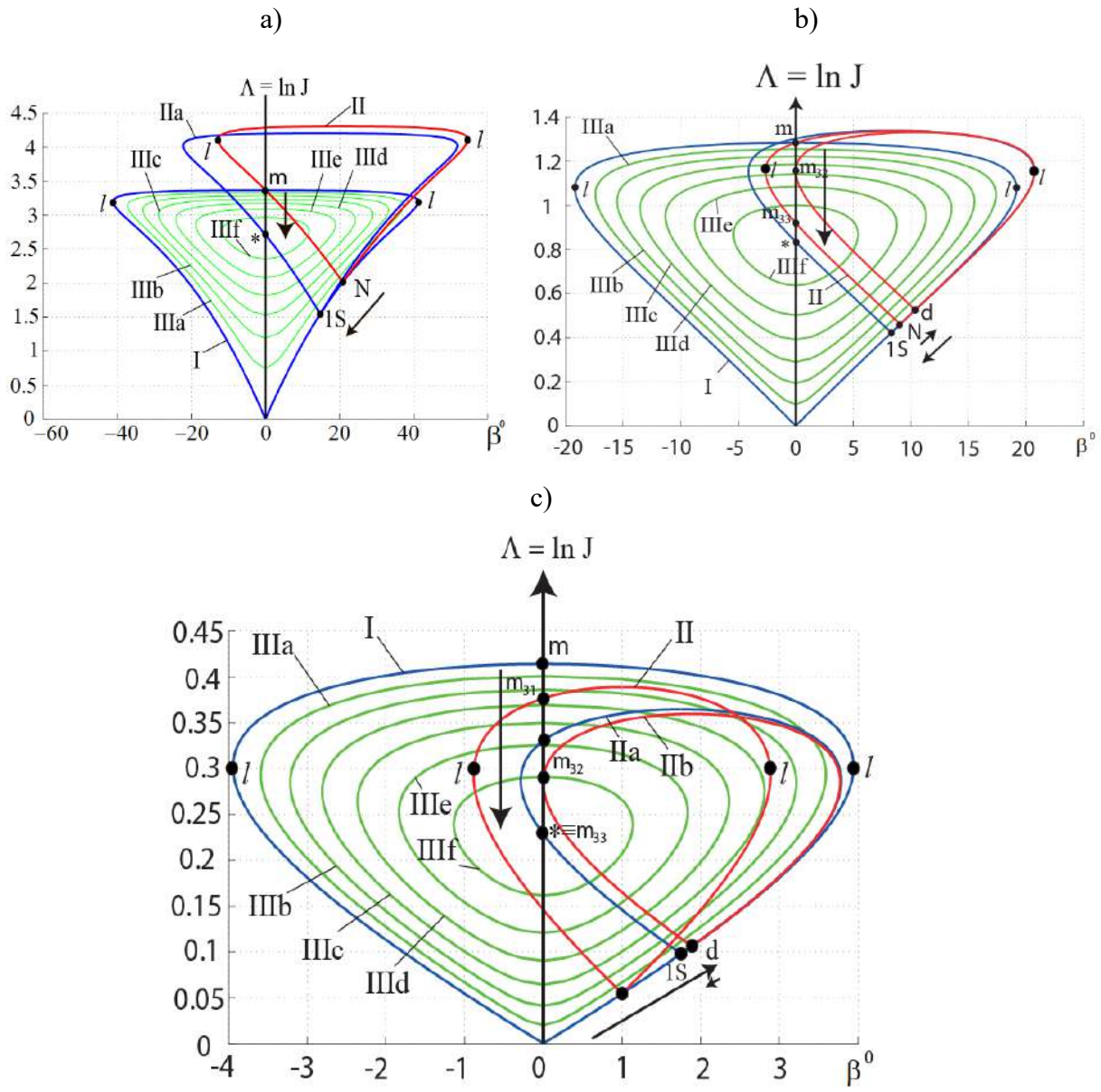

Figure 3.2. Graphic solution on the plane of shock polars: a) at $M > M_b$ ($M = 5$ in this case); b) at $M_a < M < M_b$ (here $M = 1.8$); c) at $M < M_a$ (here $M = 1.2$). Polars IIIa-IIIf correspond to the energy release behind the main shock, equal to, respectively, 15, 30, 45, 60, 75 and 90% of the maximum value ϕ_*; point "*" corresponds to this maximum value. Vertical arrows show changes in the intensity of the main shock (it decreases with increasing energy release). Oblique arrows show the change in the intensity of the incident shock in the SMC with increasing energy release (it decreases monotonically at $\mathrm{M} > \mathrm{M}_b$, but at $\mathrm{M} < \mathrm{M}_b$ it initially increases, and decreases only with

further increase of the energy release). Points *l* correspond to shocks with maximum flow deflection, point *N* points to von Neumann criterion, point *d* corresponds to the "detachment criterion", point 1*s* corresponds to the incident shock, that forming the SMC at maximum theoretically possible energy release

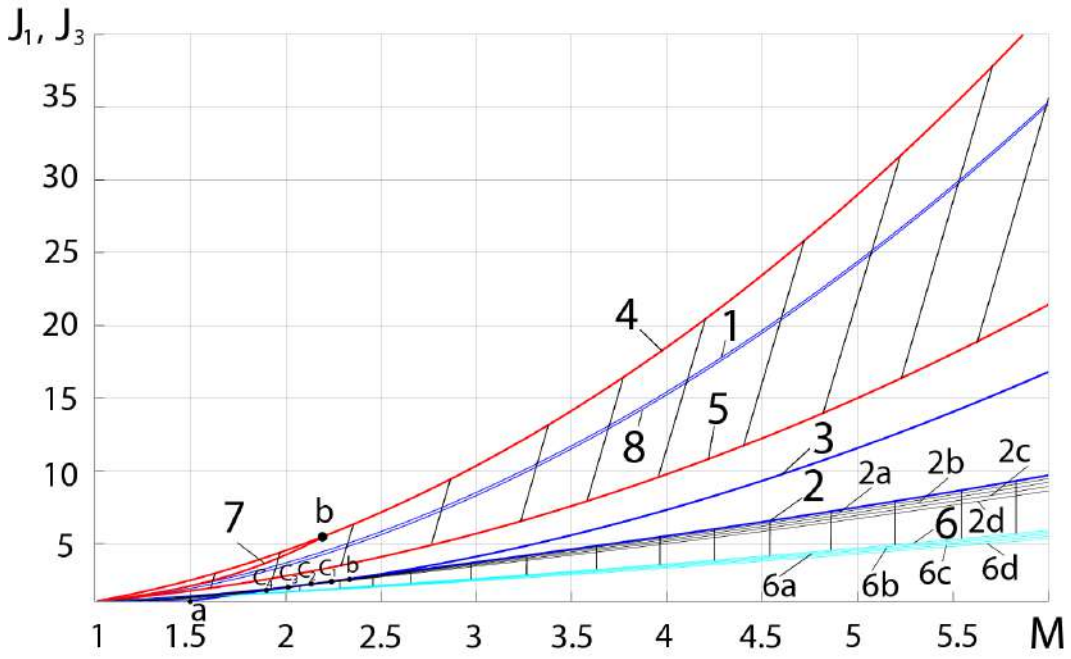

Figure 3.3. Special intensities of the shocks. Curve 1 corresponds to the shocks with maximum flow rotation: $J_1 = J_l(M)$, curve 2 – to the von Neumann criterion: $J_1 = J_N(M)$, curve 3 – to the "detachment criterion": $J_1 = J_d(M)$, curve 4 – to the normal shocks without energy release: $J_3 = J_m(M)$, curve 5 – to normal shocks with the maximum possible energy release: $J_3 = J_*(M)$, curve 6 – to incident shocks that form the SMC at maximum possible energy release: $J_1 = J_{1S}(M)$, curve 7 – to the main shocks in the SMC, when the intensity of the incident shock is maximum, curve 8 – to the incident shocks with a critical flow velocity behind them. Curves 2a-2d and 6a-6d correspond to the maximum and minimum intensity values of the incident shock in the SMC with energy release at different values of the "effective" adiabatic index on the main shock. Points c_1-c_4 show the change in Mach number M_b, in which two main criteria of shock reflection transition coincide, at various adiabatic indices on the main shock.

Gas flow behind shocks which correspond to the upper branch of the polar (at $J_l \le J < J_m$, where $J_m = (1+\varepsilon_{12})\mathrm{M}^2 - \varepsilon_{12}$ is the intensity of the normal shock), is subsonic, and gas stream after the shocks, corresponding to the weak branch (at $1 < J < J_l$), is usually supersonic.

Classical relations describing the thermodynamic parameters of a perfect gas at shock waves determine gas density, temperature, stagnation pressure, speed of sound, acoustic impedance in region II downstream the reflected shock:

$$\rho_{\mathrm{II}} = \rho / (E_1 E_2),\ T_{\mathrm{II}} = E_1 E_2 J_1 J_2 T,\ \ p_{0\mathrm{II}} = \left(J_1 J_2 E_1^{\gamma_{12}} E_2^{\gamma_{12}}\right)^{-\frac{1-\varepsilon_{12}}{2\varepsilon_{12}}} p_0,$$

$$a_{\text{II}} = a \cdot \sqrt{E_1 E_2 J_1 J_2}\ ,\ z_{\text{II}} = \rho_{\text{II}} a_{\text{II}} = z \cdot \sqrt{J_1 J_2 / (E_1 E_2)}\ .$$

Here $E_i = (1 + \varepsilon_{12} J_i)/(J_i + \varepsilon_{12})$ is the inverse ratio of gas densities on the sides of the incident or reflected shock. The flow velocity in region II and other parameters dependent on it, such as specific flow rate per unit cross-sectional area $q = \rho v$, velocity head (dynamic pressure) $d = \rho v^2/2$, flow impulse, are determined similarly:

$$f = p + \rho v^2 :$$

$$v_{\text{II}} = M_{\text{II}} a_{\text{II}} = M_{\text{II}} a \sqrt{E_1 E_2 J_1 J_2}\ ,\ \ q_{\text{II}} = \rho_{\text{II}} v_{\text{II}} = \rho a \cdot M_{\text{II}} \sqrt{J_1 J_2 / (E_1 E_2)}\ ,$$

$$d_{\text{II}} = \rho_{\text{II}} v_{\text{II}}^2/2 = \gamma_{12} J_1 J_2 M_{\text{II}}^2 p/2\ ,\ \ f_{\text{II}} = p_{\text{II}} + \rho_{\text{II}} v_{\text{II}}^2 = J_1 J_2 p\left(1 + \gamma_{12} M_{\text{II}}^2\right).$$

Ecxpressions relating the pulsed energy release on a shock to its shape, changes in flow properties, and flow deflection its surface are given in [87, 88, 91, 128, 129]. In particular, according to [88], the angle β_3 of flow deflection depends on the intensity J_3 of that shock (the ratio of the static pressures on its sides) as it follows (1.12):

$$\tan|\beta_3| = \frac{(J_3 - 1)\sqrt{F - 1}}{\gamma_{\text{III}} M^2 - (J_3 - 1)}, \tag{3.10}$$

where

$$F = \frac{2\gamma M^2}{(\gamma - 1)(J_3 - 1)} \frac{(\gamma - \gamma_{\text{III}}) + (\gamma - 1)\left[(J_3 - 1) - (\gamma_{\text{III}} - 1)\bar{\phi}\right]}{(\gamma_{\text{III}} + 1)(J_3 - 1) + 2\gamma_{\text{III}}}.$$

Here $\bar{\phi} = \phi\rho/p = \gamma\phi/(\gamma - 1)c_p T$, according to (1.11); ϕ is the specific pulse energy release at the shock. Values c_p, p, ρ, T, γ and M characterize, respectively, the specific isobaric heat capacity, the static pressure, gas density, temperature, adiabatic index and Mach number of the gas flow before the shock; γ_{III} is the adiabatic index corresponding to the thermodynamic properties of gas in the flow behind the surface of a strong shock.

The ratio of gas densities on both shock sides with energy release is written in the form (1.17)

$$E_3 = \frac{\rho}{\rho_{\text{III}}} = 1 - 2\frac{J_3 - 1 + (\gamma - \gamma_{\text{III}})/(\gamma - 1) - (\gamma_{\text{III}} - 1)\bar{\phi}}{2\gamma_{\text{III}} + (\gamma_{\text{III}} + 1)(J_3 - 1)}, \qquad (3.11)$$

and the temperature ratio has the form [88]

$$T_{\text{III}}/T = M_{\text{III}}^2\left(\cos^2\sigma_3 + E_3^2\sin^2\sigma_3\right)/M^2 . \qquad (3.12)$$

In this case, the angle σ_3 of the shock slope to the flow velocity vector in front of it is determined by the relation (1.16):

$$\cot\sigma_3 = \left[\gamma M^2 - (J_3 - 1)\right]\tan|\beta_3|/(J_3 - 1), \qquad (3.13)$$

and the flow speed v_{III} in region III behind the main shock obeys the dependence [88]

$$v_{III} = v\cdot\sqrt{E_3^2\sin^2\sigma_3 + \cos^2\sigma_3} . \qquad (3.14)$$

When introducing the average (between γ and γ_{III}), "effective" adiabatic exponent γ_3, in the first approximation describing the properties of gas at a shock with energy release when "real gas effects" manifest themselves, relations (3.10-3.14) and similar ones are noticeably simplified:

$$\tan|\beta_3| = \sqrt{\frac{J_{m3} - J_3 - \xi}{J_3 + \varepsilon_3}}\cdot\frac{(1-\varepsilon_3)(J_3 - 1)}{(1+\varepsilon_3)M^2 - (1-\varepsilon_3)(J_3 - 1)}, \qquad (3.15)$$

$$\xi = \frac{2\varepsilon_3\gamma_3 M^2\bar{\phi}}{J_3 - 1},\ J_{m3} = (1+\varepsilon_3)M^2 - \varepsilon_3,$$

$$E_3 = \rho/\rho_{\text{III}} = \left(1 + \varepsilon_3 J_3 + 2\varepsilon_3\bar{\phi}\right)/(J_3 + \varepsilon_3),$$

$$a_{\text{III}}/a = \sqrt{\gamma_{\text{III}}/\gamma}\cdot\sqrt{J_3\cdot\left(1 + \varepsilon_3 J_3 + 2\varepsilon_3\bar{\phi}\right)/(J_3 + \varepsilon_3)},$$

$$\cot\sigma_3 = \sqrt{(J_m - J_3 - \xi)/(J_3 + \varepsilon_3)},$$

$$v_{\text{III}} = a\sqrt{\frac{(J_3 + \varepsilon_3)M^2 - (1-\varepsilon_3)(J_3^2 - 1) - 2\varepsilon_3(J_3 - 1)\bar{\phi}/\gamma_3}{J_3 + \varepsilon_3}},$$

$$M_{\text{III}} = \sqrt{\frac{\gamma}{\gamma_{\text{III}}}}\cdot\sqrt{\frac{(J_3 + \varepsilon_3)M^2 - (1-\varepsilon_3)(J_3^2 - 1) - 2\varepsilon_3(J_3 - 1)\bar{\phi}/\gamma_3}{J_3\left(1 + \varepsilon_3 J_3 + 2\varepsilon_3\bar{\phi}\right)}}.$$

(here $\varepsilon_3 = (\gamma_3 - 1)/(\gamma_3 + 1)$).

Relation (3.15) describes the detonation shock polar, the name of which suggests that the pulsed energy release at the shock or in the immediate vicinity of it occurs as a result of detonation initiated by an increase in temperature on the shock surface. Figure 3.2,a-c shows the family of detonation polars IIIa-IIIf, corresponding to the effective adiabatic index $\gamma_3 = \gamma_{12} = 1.4$ and various energy release values. In the following calculation examples, the default assumption is that $\gamma_3 = \gamma_{12} = 1.4$.

The intensity J_3 of the chock j_3 with positive pulse energy release ($\overline{\phi} > 0$) at a fixed value of the Mach number before the shock belongs to the range

$$J_{\min} \le J_3 \le J_{\max}, \tag{3.16}$$

here

$$J_{\min} = 1 + \delta, \quad J_{\max} = J_{m3} - \delta, \quad \delta = \frac{(1+\varepsilon_3)(M^2-1)}{2}\left[1 - \sqrt{1 - \frac{8\varepsilon_3 M^2 \overline{\phi}}{(1-\varepsilon_3^2)(M^2-1)^2}}\right]. \tag{3.17}$$

As it is obvious from relations (3.17), the range (3.16) is narrower than the interval $1 \le J_3 \le J_{\text{m}}$ of possible change in shock intensity in the absence of energy release. This is confirmed by a visual comparison of the shock polars I (with $\overline{\phi} = 0$) and detonation polars IIIa-IIIf (at $\overline{\phi} > 0$), corresponding to the same flow Mach number before the shock. Dependencies $J_{\min}(\overline{\phi})$ and $J_{\max}(\overline{\phi})$ for various Mach numbers are given in Figure 4, respectively, as the lower and upper branches of curves 1-5.

At the limiting dimensionless value of energy release

$$\overline{\phi}_* = (1-\varepsilon_3^2)(M^2-1)^2 \Big/ (8\varepsilon_3 M^2), \tag{3.18}$$

which corresponds to the dimensional value

$$\phi_* = (1-\varepsilon_3)(M^2-1)^2 c_p T \Big/ (4M^2),$$

values $J_{\min}$ and $J_{\max}$ are equal:

$$J_* = J_{\min} = J_{\max} = (1+J_m)/2. \tag{3.19}$$

In this case, the detonation polar (3.15) degenerates into the single point "*" (see Figure 3.2,a-c, and also Figure 3.4), which corresponds to a critical flow velocity behind the normal stationary detonation wave ($M_{III}=1$). A further increase in energy release leads to a loss of stability of shock j_3 and the triple configuration in general.

Thus, the system of equations (3.5-3.9, 3.15), solved at $\beta_3 = 0$ and $J_3 = J_{max}$, allows one to find the flow deflection angles and the intensities of the shocks that composethe SMC. The parameters of flows beyond the triple point, determined by the relations for shock and detonation waves [1, 88], should be compared in future studies in order to optimize various gas-dynamic devices, including detonation engines [130-133].

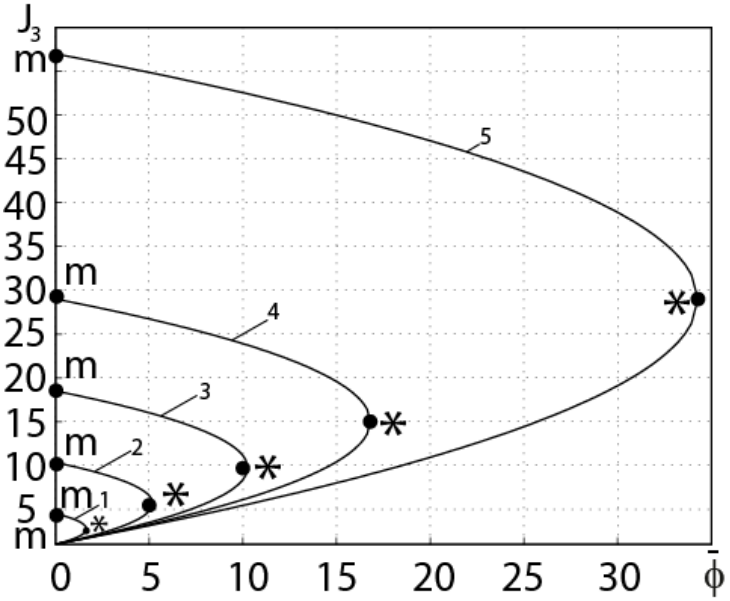

Figure 3.4. Minimum (shown by the lower branches of curves 1-5) and maximum (shown by their upper branches) values of the shock intensities at different flow Mach numbers (curves 1-5 correspond to the values *M*=2, 3, 4, 5 and 7) depending on the amount of energy release. The "*" points correspond to the maximum energy release with degeneration of the shock polar into a single point (see also Figure 3.2)

3.1.3. Analytical description of the domain of existence of a stationary Mach configuration

Three main parameters (free-stream Mach number, pulsed heat release ϕ and change in adiabatic index γ_3 on the main shock compared to that value γ in the flow before the triple point) affect the region of existence of the SMCs. The method and degree of influence of the last two factors is studied in detail in the work [146].

The conditions for the existence of a stationary Mach configuration in a gas flow with a constant adiabatic index without physical and chemical transformations have been studied in detail in [1, 79, 144]. A stationary Mach configuration exists if $M > M_a$, here $M_a = \sqrt{(2-\varepsilon)/(1-\varepsilon)} = 1.483$. In this case, the parameters of the the reflected shock at $M > M_b$ ($M_b = 2.202$ at $\gamma = 1.4$) correspond to the lower (weak) branch of shock polar II (Figure 3.2,a), and at $M_a < M < M_b$ it corresponds to its upper (strong) branch (Figure 3.2,b). Parameters of the main (normal) shock j_3 correspond to the point m in Fig. 3.2,a-b. At $M < M_a$, there are no solutions describing the SMC without energy release at its jumps (see Figure 3.2c).

Intensity $J_1 = J_N$ of the incident shock that forms the SMC at $M > M_a$ is determined by equation (1.20) and corresponds to the well-known von Neumann criterion of oblique shock reflection transition (see curve 2 in Figure 3.3). Another well-known criterion for changing the reflection type (the "detachment criterion") corresponds to the following equation for intensity $J_1 = J_d$ of the incident shock at all $M > 1$:

$$\sum_{n=0}^{5} D_n J_d^n = 0, \tag{3.20}$$

$$D_5 = (1-\varepsilon)^2, \quad D_4 = -(1-\varepsilon)\cdot\left[\left(3+4\varepsilon-\varepsilon^2\right)M^2 + \left(4-5\varepsilon+\varepsilon^2\right)\right],$$

$$D_3 = \left(3+4\varepsilon+2\varepsilon^2\right)M^4 + 4(1-\varepsilon)\left(1+2\varepsilon-\varepsilon^2\right)M^2 + 2(3-2\varepsilon)(1-\varepsilon)^2,$$

$$D_2 = -(1+\varepsilon)M^6 + \varepsilon\left(1+2\varepsilon^2\right)M^4 - 4\varepsilon(1-\varepsilon)(1-2\varepsilon)M^2 - 2(2-3\varepsilon)(1-\varepsilon)^2,$$

$$D_1 = -\left[1+\varepsilon\left(M^2-1\right)\right]\cdot\left[2(1+\varepsilon)M^4 + \varepsilon(1+4\varepsilon)M^2 - \left(1-5\varepsilon+4\varepsilon^2\right)\right],$$

$$D_0 = -\left[(1+\varepsilon)M^2 - \varepsilon\right]\cdot\left[1+\varepsilon\left(M^2-1\right)\right]^2$$

(curve 3 in Figure 3.3). Single point b of tangency of curves 1 and 2, which corresponds to the Mach number $M = M_b$, is defined by the equation

$$\sum_{n=0}^{4} F_n M_b^{2n} = 0, \tag{3.21}$$

$$F_4=(1-\varepsilon)\left(2-4\varepsilon+2\varepsilon^3-\varepsilon^4\right),\ F_3=-10+20\varepsilon-10\varepsilon^2-10\varepsilon^3+12\varepsilon^4-4\varepsilon^5,$$

$$F_2=12-24\varepsilon+10\varepsilon^2+16\varepsilon^3-18\varepsilon^4+6\varepsilon^5,\ F_1=-2(1+\varepsilon)\left(3-4\varepsilon+2\varepsilon^2\right)(1-\varepsilon)^2,$$

$$F_0=(1+\varepsilon)(1-\varepsilon)^4.$$

For all other Mach numbers, the inequality $J_N<J_d$ defines dualism (the existence of solutions that describe both regular and Mach reflection for the same parameters of the incident shock) in the region between curves 2 and 3 in Figure 3.4.

The influence of energy release on the region of existence of a stationary Mach configuration manifests as it follows. According to relations (3.16) and (3.17), the increase in energy release at the main shock from zero to the limiting value $\overline{\phi}=\overline{\phi}_*$ (3.18) leads to a monotonic decrease in intensity $J_3=J_{\max}$ of the main shock in the SMC from the value $J_m(M)$ at $\overline{\phi}=0$ (curve 4 in Figure 3.3) to the value $J_*(M)$, defined by expression (3.19), at $\overline{\phi}=\overline{\phi}_*$ (curve 5). If the flow Mach number is moderate or high ($M\geq M_b$), the intensity J_1 of the incident shock also decreases monotonically. In the limiting case ($\overline{\phi}=\overline{\phi}_*$), the minimum intensity $J_1=J_{1s}$ of the incident shock forming the SMC, at $\gamma_3=\gamma$ obeys the equation

$$\sum_{k=0}^{5}S_kJ_{1s}^k=0, \tag{3.22}$$

$$S_5=4(1-\varepsilon),\ \ S_4=\left(8+6\varepsilon-8\varepsilon^2+2\varepsilon^3\right)M^2+2(4-\varepsilon)(1-\varepsilon)^2,$$

$$S_3=-2(1+\varepsilon)\left(2+4\varepsilon-2\varepsilon^2+\varepsilon^3\right)M^4-\left(10-4\varepsilon-28\varepsilon^2+14\varepsilon^3-4\varepsilon^4\right)M^2-2(1-\varepsilon)\left(3-11\varepsilon+5\varepsilon^2-\varepsilon^3\right),$$

$$S_2=(J_m+1)\left[\varepsilon(1+\varepsilon)(2-\varepsilon)M^4+\varepsilon\left(4-15\varepsilon+5\varepsilon^2\right)M^2+4(1-\varepsilon)\left(1-3\varepsilon+\varepsilon^2\right)\right],$$

$$S_1=y_3M^6+y_2M^4+y_1M^2+y_0,\ y_3=2\left(1-\varepsilon+\varepsilon^2\right)(1+\varepsilon)^2,$$

$$y_2=2(1+\varepsilon)\left(1-4\varepsilon+7\varepsilon^2-3\varepsilon^3\right),$$

$$y_1=-2+4\varepsilon+10\varepsilon^2-22\varepsilon^3+6\varepsilon^4,\ y_0=-2(1-\varepsilon)\left(1-3\varepsilon+5\varepsilon^2-\varepsilon^3\right),$$

$$S_0=-\left(M^2-1\right)(J_m+1)\left[(1+\varepsilon)(1-2\varepsilon)M^2-2\varepsilon(1-\varepsilon)\right].$$

The solution of (3.22) corresponds to curve 6 in Figure 3.4. At $M \geq M_b$, the reflected shock in the SMC with energy release always corresponds to the weak branch of the shock polar (for example, on curve IIa, see Figure 3.2a), and the flow behind it is, as a rule, supersonic.

At low Mach numbers ($M < M_b$) a small pulsed energy release at the main shock leads to the appearance of an SMC with a strong reflected shock (see, for example, polars IIa in Figures 3.2, b and 3.2,c, polar IIa in Figure 3.2,c and the solution corresponding to the point m_{31} in the same Figure). With a gradual increase in energy release, the intensity of the main shock decreases from $J_m(M)$ (curve 4 in Figure 3) to the values corresponding to curve 6; the intensity of the incident shock increases from the unity (at $M \leq M_a$) or from $J_N(M)$ (curve 2 in Figure 3.3, at $M_a < M < M_b$) to $J_d(M)$ (curve 3). With a further increase in energy release, the reflected shock in the SMC becomes weak (solutions corresponding to the point m_{33} in Figure 3.2, b-c). Intensity J_3 of the Mach stem continues to decrease (from curve 4 in Figure 3.3 to the values $J_*(\mathrm{M})$, shown by curve 5), and the intensity J_1 decreases from $J_d(\mathrm{M})$ (curve 3 in Figure 3.3) to its minimum value $J_1 = J_{1S}$ at $\bar{\phi} = \bar{\phi}_*$ (curve 6).

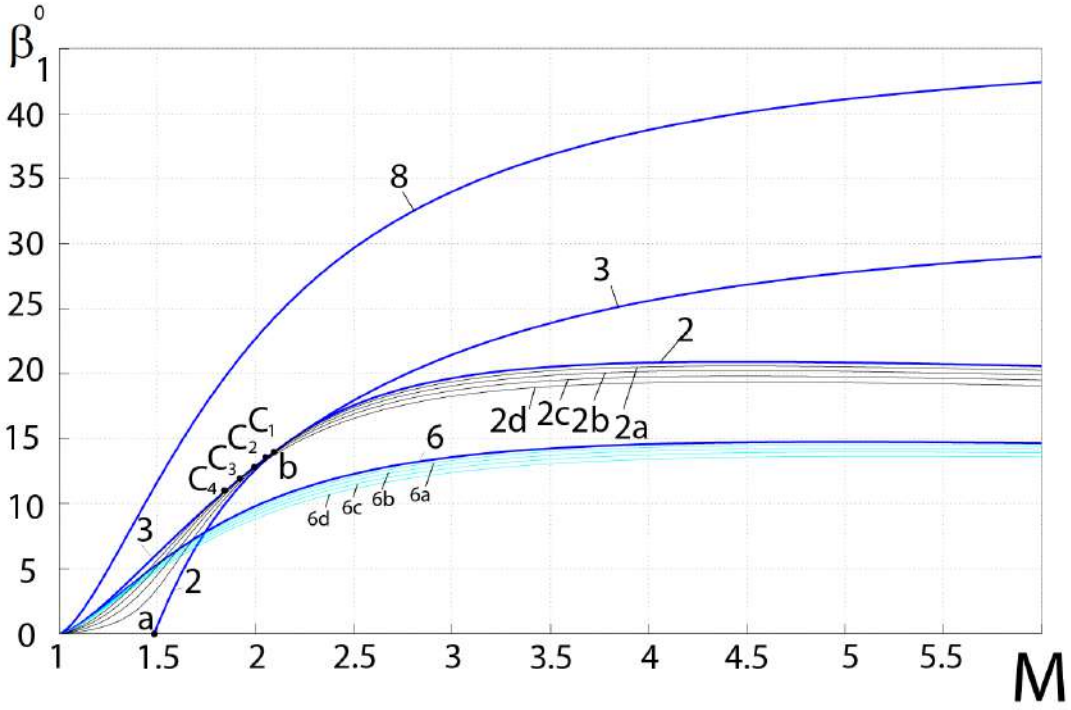

Figure 3.5. Angles of flow deflection at some special incident shocks. As in Figure 3.3, curve 2 corresponds to the von Neumann criterion, curve 3 – to the "detachment criterion", curve 6 – to the incident shocks that form the SMC at maximum energy release, curve 8 – to shocks with a critical flow velocity behind them. Curves 2a-2d and 6a-6d describe the change in the properties of the incident shock as the "effective" adiabatic index on the main shock decreases. Points c_1-c_4 show a shift in the point of coincidence of two reflection transition criteria at a decrease in the "effective" adiabatic index

Thus, the occurrence of energy release behind the main (Mach) shock leads to an expansion of the region of existence of SMC, which occur at all Mach numbers of the supersonic flow in a wide range of parameters of the incident and main shocks (they are marked with straight and oblique shading, respectively, in Figure 3).

Slope angles (σ_1) and flow deflection (β_1) on incident shocks, the intensities of which correspond to curves 1, 2 and 5 in Figure 3.3, are also shown by the corresponding curves in Figures 3.5 and 3.6 (in addition, curve 8 shows the parameters of the incident shock with the critical flow velocity behind it, and curve 9 in Figure 3.6 shows the slope angles of the shock degenerating into a weak discontinuity, i.e. the Mach angles). At high flow Mach numbers ($M \to \infty$), values corresponding to the von Neumann criterion of shock j_1 reflectuion transition, strive for the following limits [76]:

$$\sigma_{1N} \to \arcsin\sqrt{\frac{2\varepsilon(1-\varepsilon)}{1+\varepsilon-\varepsilon^2+\varepsilon^3+\sqrt{1-2\varepsilon+3\varepsilon^2+4\varepsilon^3-\varepsilon^4-2\varepsilon^5+\varepsilon^6}}} = 21.769^\circ,$$

$$\beta_{1N} \to \arctan\frac{\sqrt{2\varepsilon(1-\varepsilon)^3\left(1-\varepsilon+\varepsilon^2+\varepsilon^3+\sqrt{1-2\varepsilon+3\varepsilon^2+4\varepsilon^3-\varepsilon^4-2\varepsilon^5+\varepsilon^6}\right)}}{1-\varepsilon+3\varepsilon^2-\varepsilon^3+\sqrt{1-2\varepsilon+3\varepsilon^2+4\varepsilon^3-\varepsilon^4-2\varepsilon^5+\varepsilon^6}} = 17.961^\circ$$

The values corresponding to the "detachment criterion" are determined by following the relations at large Mach numbers:

$$\left(1-\varepsilon^2\right)\sin^3\sigma_{1d} - \left(1-\varepsilon^2\right)\sin^2\sigma_{1d} - (1+2\varepsilon)\sin\sigma_{1d} + 1 = 0,$$

$$\operatorname{tg}|\beta_{1d}| = (1-\varepsilon)\sin\sigma_{1d}\cos\sigma_{1d} \Big/ \left[1-(1-\varepsilon)\sin^2\sigma_{1d}\right],$$

here $\sigma_{1d} = 39.971^\circ$, $|\beta_{1d}| = 32.018^\circ$. The smallest values of the parameters of the incident shock at which the formation of SMC with energy release is possible, at $M \to \infty$ are described by limits

$$J_{1s}/M^2 \to C,\ \ \sigma_{1s} \to \arcsin\left(\sqrt{C/(1+\varepsilon)}\right) = 14.815^\circ,$$

$$|\beta_{1s}| \to \arctan\left(\sqrt{C(1+\varepsilon-C)}\Big/(\gamma-C)\right) = 12.291^\circ,$$

where is the coefficient C=0.076 is defined as the positive real root of the equation

$$4(1-\varepsilon)C^3 - 2\left(4+3\varepsilon-4\varepsilon^2+\varepsilon^3\right)C^2 + 2(1-\varepsilon)\left(2+4\varepsilon-2\varepsilon^2+\varepsilon^3\right)C - \varepsilon(2-\varepsilon)(1+\varepsilon)^2 = 0.$$

Pulsed energy release and other physical and chemical phenomena, as a rule, lead to a decrease in the "effective" adiabatic index, which describes the change in flow parameters at a strong main shock.

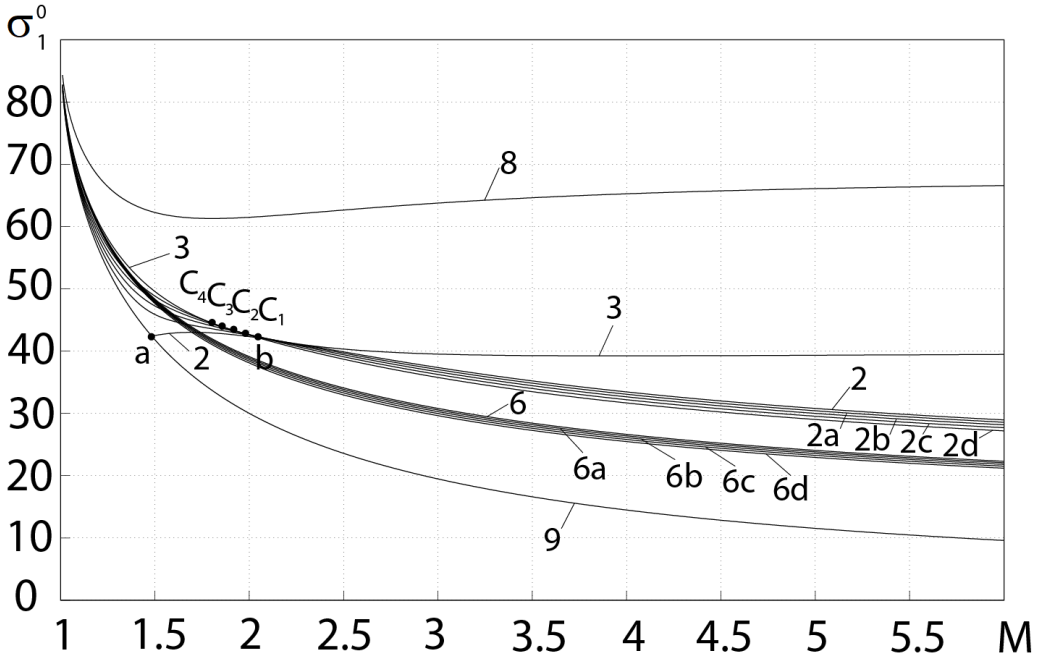

Figure 3.6. Slope angles of the incident shocks. As in Figures 3.3 and 3.5, curve 2 corresponds to the von Neumann criterion, curve 3 – to the "detachment criterion", curve 6 – to incident shocks that form the SMC at maximum energy release at the main shock, curve 8 – to shocks with a critical flow velocity behind them. Curve 9 shows the Mach angles, curves 2a-2d and 6a-6d illustrate changes in the properties of the incident shock with a decrease in the adiabatic index on the main shock, points c_1-c_4 demonstrate the shift of the point of coincidence of two major reflection transition criteria

The influence of the adiabatic index on the region of SMC existence is as follows. According to relation (3.17), a decrease in the adiabatic index γ_3 and, accordingly, in the values $\varepsilon_3 = (\gamma_3 - 1)/(\gamma_3 + 1)$ leads to a decrease in intensity $J_{\max}$, which corresponds to the maximum possible pulse energy release. At the same time, the minimum intensity J_{1s} of incident shock forming the SMC (defined by relation (3.22) at $\gamma_3 = \gamma$) decreases. In Figures 3.3, 3.5 and 3.6, the curves 6a-6d show,

respectively, the minimum intensities, slope angles of incident shocks and angles of flow deflection on their surface as the value γ_3 decreases from $\gamma_3=\gamma=1.4$ (curves 6) to $\gamma_3=1.3$ (curves 6a), $\gamma_3=1.2$ (6b), $\gamma_3=1.1$ (6c), $\gamma_3\to 1$ (6d). In the limiting case ($\gamma_3\to 1$),the minimum asymptotic (at $M\to\infty$) parameters of an incident shock obey the relations

$$J_{1s}/M^2\to C_1,\ \ \sigma_{1s}\to \arcsin\left(\sqrt{C_1/(1+\varepsilon)}\right)=13.646^\circ,$$

$$|\beta_{1s}|\to \arctan\left(\sqrt{C_1(1+\varepsilon-C_1)}/(\gamma-C_1)\right)=11.329^\circ,$$

here the coefficient C_1=0.065 can be determined from the equation

$$4(1-\varepsilon)C_1^3-2\left(4+3\varepsilon-3\varepsilon^2\right)C_1^2+2\left(2+6\varepsilon+2\varepsilon^2+\varepsilon^3\right)C_1-\varepsilon(2-\varepsilon)=0.$$

Parameters J_1, σ_1 and $|\beta_1|$ of the incident shock forming the SMC in the absence of energy release, also change with a decrease of γ_3 from the values corresponding to the von Neumann criterion (curves 2 in Figures 3, 5 and 6) to the values shown by curves 2a-2d for $\gamma_3=1.3$, $\gamma_3=1.2$, $\gamma_3=1.1$ and $\gamma_3\to 1$, respectively. In particular, the intensity J_1 of the shock j_1 and the Mach number of the flow in this case are related by the equation

$$\begin{gathered}
\sum_{k=0}^{3}N_kM^{2k}=0,\\
N_3=(1+\varepsilon_3)(1+\varepsilon J_1)\left[J_1(1-\varepsilon\varepsilon_3)-1+\varepsilon+\varepsilon^2-\varepsilon_3\right],\ \ N_2=\sum_{l=0}^{3}x_lJ_1^l,\\
N_1=\sum_{l=0}^{4}y_lJ_1^l,\\
N_0=-(1-\varepsilon)(J_1+\varepsilon)(J_1-1)^2\left[J_1^2+\varepsilon J_1(1-\varepsilon_3)-\varepsilon_3\right],\\
x_3=-1-3\varepsilon+\varepsilon^2(2\varepsilon_3-\varepsilon-\varepsilon\varepsilon_3),\ \ x_2=\varepsilon\left[2+\varepsilon_3-5\varepsilon+\varepsilon_3+2\varepsilon\varepsilon_3(\varepsilon+\varepsilon_3)\right],\\
x_1=-\varepsilon-\varepsilon_3+3\varepsilon^2+2\varepsilon\varepsilon_3-\varepsilon^3+4\varepsilon\varepsilon_3^2+\varepsilon^2\varepsilon_3(1-3\varepsilon),\\
x_0=1+3\varepsilon_3-2\varepsilon^2-\varepsilon\varepsilon_3+2\varepsilon_3^2-3\varepsilon^2\varepsilon_3,\\
y_4=2+\varepsilon(1-\varepsilon-\varepsilon_3+\varepsilon\varepsilon_3),\ \ y_3=-3+3\varepsilon-\varepsilon_3+\varepsilon(3\varepsilon+\varepsilon_3-5\varepsilon\varepsilon_3+2\varepsilon^2\varepsilon_3),\\
y_2=2-6\varepsilon+2\varepsilon_3+2\varepsilon^2-6\varepsilon\varepsilon_3+2\varepsilon^3+7\varepsilon^2\varepsilon_3-\varepsilon^2\varepsilon_3(\varepsilon_3+4\varepsilon),\\
y_1=-1+4\varepsilon-\varepsilon_3-3\varepsilon^2+4\varepsilon\varepsilon_3-\varepsilon^3-2\varepsilon\varepsilon_3^2-5\varepsilon^2\varepsilon_3+3\varepsilon^3\varepsilon_3,
\end{gathered}\qquad (3.23)$$

$$y_0 = -\varepsilon - \varepsilon_3 + \varepsilon^2 - \varepsilon\varepsilon_3 - \varepsilon_3 - \varepsilon_3\left(\varepsilon + \varepsilon_3\right).$$

At $\gamma_3 = \gamma$, the equation (3.23) transforms to the ratio (1.20), which describes the von Neumann criterion. The intensities of the shocks corresponding to the equation (3.23), decrease monotonically with decreasing adiabatic index, if $M > M_b$ (i.e. at moderate and high flow Mach numbers). In the limiting case ($\gamma_3 \to 1$), equation (3.23) transforms as it follows:

$$\sum_{k=0}^{3} Z_k M^{2k} = 0,$$

$$Z_3 = \left(1 + \varepsilon J_1\right)\left(J_1 - 1 + \varepsilon + \varepsilon^2\right),$$

$$Z_2 = -\left(1 + 3\varepsilon + \varepsilon^3\right)J_1^3 + \varepsilon\left(2 - 5\varepsilon\right)J_1^2 - \varepsilon\left(1 - 3\varepsilon + \varepsilon^2\right)J_1 + 1 - 2\varepsilon^2,$$

$$Z_1 = \left(1+\varepsilon\right)\left(2-\varepsilon\right)J_1^4 - 3\left(1-\varepsilon-\varepsilon^2\right)J_1^3 + 2\left(1-\varepsilon\right)\left(1-2\varepsilon-\varepsilon^2\right)J_1^2 - \left(1-4\varepsilon+3\varepsilon^2+\varepsilon^3\right)J_1 - \varepsilon\left(1-\varepsilon\right),$$

$$Z_0 = -\left(1-\varepsilon\right)J_1\left(J_1-1\right)^2\left(J_1+\varepsilon\right)^2,$$

and the asymptotic parameters of the shock j_1 corresponding to this solution (for $M \to \infty$) obey the relations

$$J_1/M^2 \to C_2, \quad \sigma_{1s} \to \arcsin\left(\sqrt{C/\left(1+\varepsilon\right)}\right) = 19.682^\circ,$$

$$\left|\beta_{1s}\right| \to \arctan\left(\sqrt{C\left(1+\varepsilon-C\right)}/\left(\gamma - C\right)\right) = 16.271^\circ.$$

Here, the coefficient C_2=0.132 is determined from the equation

$$\left(1-\varepsilon\right)C_2^3 - \left(1+\varepsilon\right)\left(2-\varepsilon\right)C_2^2 + \left(1+3\varepsilon+\varepsilon^3\right)C_2 - \varepsilon = 0.$$

A decrease in the “equilibrium” adiabatic index in a high-speed flow without energy release can be associated, for example, with ionization and recombination, the excitation of additional degrees of freedom of gas molecules.

At small supersonic Mach numbers (ar $M < M_b$), parameters of the incident shock, determined by equation (3.23) at $\gamma_3 < \gamma$, are greater than those corresponding to the von Neumann criterion (1.20). The resulting solution corresponds to a strong reflected shock j_2 at $1 < M \le M_c$ or to a weak shock j_2 at $M_c < M \le M_b$. Here M_c is the Mach number corresponding to the coincidence of the solution of (2.21) with the

"detachment criterion" (2.20) (see points c_1, c_2, c_3, c_4 in Figures 3.3, 3.5 and 3.6). It is determined by an algebraic equation of the fifth degree with respect to M_c^2 with coefficients depending on γ и γ_3. At $\gamma_3 = \gamma$, this equation can be reduced to the form (3.21), and $M_c = M_b$. At $\gamma_3 \to 1$, that equation determining the special Mach number M_c reduces to form

$$\sum_{k=0}^{5} A_k M_c^{2k} = 0,$$

$$A_5 = (1-\varepsilon)\left(4 - 4\varepsilon + 2\varepsilon^2 - \varepsilon^4\right), \quad A_4 = -(1-\varepsilon)\left(20 - 22\varepsilon + 5\varepsilon^3 - 11\varepsilon^4 - 4\varepsilon^5\right),$$

$$A_3 = 24 - 58\varepsilon + 36\varepsilon^2 + 18\varepsilon^3 - 37\varepsilon^4 + \varepsilon^5 + 16\varepsilon^6 + 4\varepsilon^7,$$

$$A_2 = -12 + 30\varepsilon - 16\varepsilon^2 - 23\varepsilon^3 + 22\varepsilon^4 + 23\varepsilon^5 - 16\varepsilon^6 - 12\varepsilon^7$$

$$A_1 = (1-\varepsilon)\left(2 - 2\varepsilon - 5\varepsilon^2 + 8\varepsilon^3 + 13\varepsilon^4 - 12\varepsilon^5 - 12\varepsilon^6\right), \quad A_0 = -\varepsilon\left[\left(1-\varepsilon^2\right)(1-2\varepsilon)\right]^2,$$

(in particular, $M_{c_4} = 1.861$ at $\gamma = 1.4$). Mach number M_c corresponds to the coincidence of two main criteria of shock reflection transition as the adiabatic index changes at the main shock.

Comparison of the numerical data shown in Figures 3.3, 3.5 and 3.6, leads to the conclusion that the decrease in the adiabatic exponent at the main shock is a factor that acts in the same direction as the pulsed energy release, but it is an order of magnitude weaker. Due to the decrease in the adiabatic index, Mach reflection of oblique shocks, that are weaker than shocks corresponding to the von Neumann criterion, becomes theoretically possible at moderate and high Mach numbers. At low Mach numbers ($1 < M < M_c$), a decrease in the adiabatic index leads to solutions that describe Mach reflection with weak incident shock and strong reflected one.

An increase in the adiabatic index at the main shock compared to its value in the oncoming flow (theoretically possible, for example, during the dissociation of gas molecules) leads to the opposite effect: to an expansion of the range of Mach numbers of the flow, in which the formation of SMCs is impossible (compared to the interval $1 < M < M_a$ at $\gamma_3 = \gamma$), as well as of the range of Mach numbers

$M_a \le M < M_b$, which corresponds to the formation of SMCs with weak incident shock and strong reflected one.

Thus [146], the pulsed energy release behind the main (Mach) shock, as well as, to a much lesser extent, the decrease in the "effective" adiabatic index caused by physical and chemical effects, lead to an expansion of the region of existence of stationary Mach configurations, which, in the presence of energy release and real gas effects, can form at all Mach numbers of supersonic flow. The possibility of energy release behind the main shock contributes to the Mach reflection of relatively weak incident shocks, which, in the absence of combustion, detonation and other physicochemical effects, reflect only regularly.

A complete parametric analysis of all types of triple shock-wave configurations with the possibility of pulsed energy release, which is planned to be obtained in the future, may be of interest in the analysis and design of gas-dynamic pulse devices and aerospace propulsion systems. In particular, a theoretical analysis of the relationship between the parameters of flows formed behind the triple point and separated by slipstream, and the identification of triple configurations that are optimal for solving the assigned engineering problems are necessary. Of no less interest is the analysis of flowfield gradients in the vicinity of the triple point using differential conditions of dynamic compatibility.

In further studies of triple configurations with energy release and significant changes in the physicochemical properties of the gas, one should take into account:

- the existence of modern models of detonation transformations, replacing the Chapman–Jouguet model;

- a more complex nature of physical and chemical transformations at strong shock waves, which is not always described by the one-parameter model of the "effective adiabatic index" with a sufficient degree of accuracy and reliability;

- the ambiguity of the solution discussed in the Subsection 2.3 for triple-shock configurations forming at high Mach numbers of gas flow with a reduced adiabatic index.

3.2. Analytical model of the shock-wave structure of a supersonic flow with Mach reflection and pulsed energy release at the main shock

Analysis of flows with irregular (Mach) reflection of oblique shocks is important in the gas-dynamic design and optimization of supersonic air intakes [134, 135], nozzle blocks, jet technology devices, launch complexes, as well as in the development of blast technologies and means of suppressing the damaging effects of an explosion [92]. According to [76, 79, 92], various flow parameters (stagnation pressures, velocities, dynamic pressures, etc.) can vary significantly (at high supersonic speeds – in tens of times) in flows separated by slipstream behind the triple point of Mach reflection, which can determine the design of gas-dynamic devices. For example, the idea of a new combined ramjet engine was proposed and theoretically substantiated in studies [86, 150, 152]. According to this concept, the gas flow after the reflected shock j_2 (in region 2 in Figure 3.7,a-b), which has a significantly higher full pressure than the flow behind the main (Mach) shock j_3 (in region 3), can be used in the thermodynamic cycle of a classic ramjet engine. At the same time, the flow behind the main shock has a significantly higher static temperature, especially when flying at high supersonic speeds; it can promote detonation of the gas mixture, due to which this flow can be used in the thermodynamic cycle of a detonation engine. To successfully separate two flows beyond the triple point T of the Mach reflection, it is necessary to determine the height y_T of the triple point and shape $y(x)$ of the slipstream τ emanating from it, and to assess the integral characteristics of a prospective combined engine, as well as shape and size of all other gas-dynamic discontinuities.

One of the first approximate analytical models of planar supersonic flow with Mach reflection was formulated in [52]. Within the framework of this model, it was quite reasonably assumed [136] that the flow in region 3 forms the so-called “virtual convergent-divergent (de Laval) nozzle” with the acceleration of the subsonic flow behind the shock j_3 up to critical speed ($M_3 = 1$) in the narrowest section (CC' in Figure 3.7,b). Reaching the critical speed of sound coincides with the reversal of the

slipstream τ in the horizontal direction (flow angle $\theta = 0$ at the point *C*) under the influence of an expansion wave ψ_4, which falls from the trailing edge of the wedge (Figura 3.7,a), or from the boundary of the jet (Figure 3.7,b), or forms in another way. However, as discussed in Subsection 2.3, it was unreasonably assumed in [52] that theslipstream τ is straight, and the critical section of the "virtual nozzle" 3 corresponds to the point of incidence of the first characteristic *BD* of the expansion wave ψ_4. This assumpsion led to large (50-90%) errors in determining the height of the triple point and other flow parameters. The application of the Grib-Ryabinin transformation [112] to region 2 of supersonic flow, carried out in [53], led to a slight refinement of the results while simultaneously complicating the mathematical model.

a)

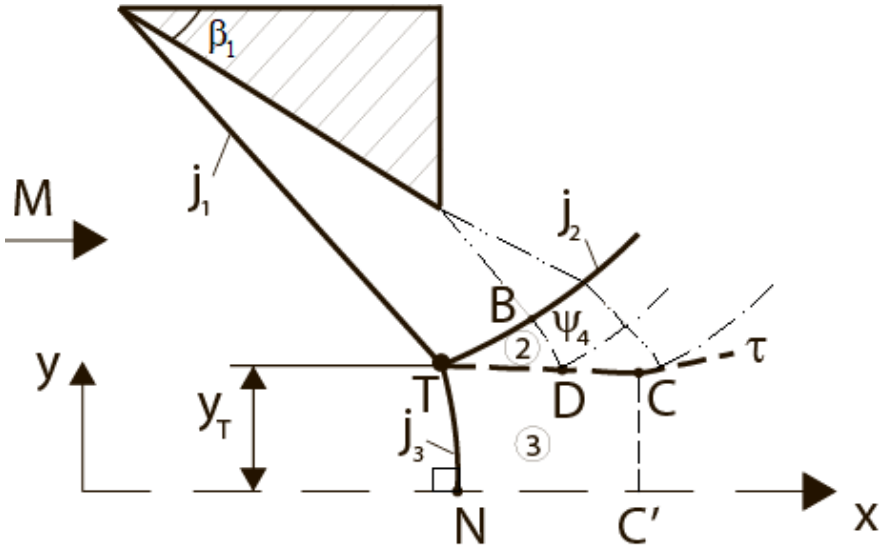

b)

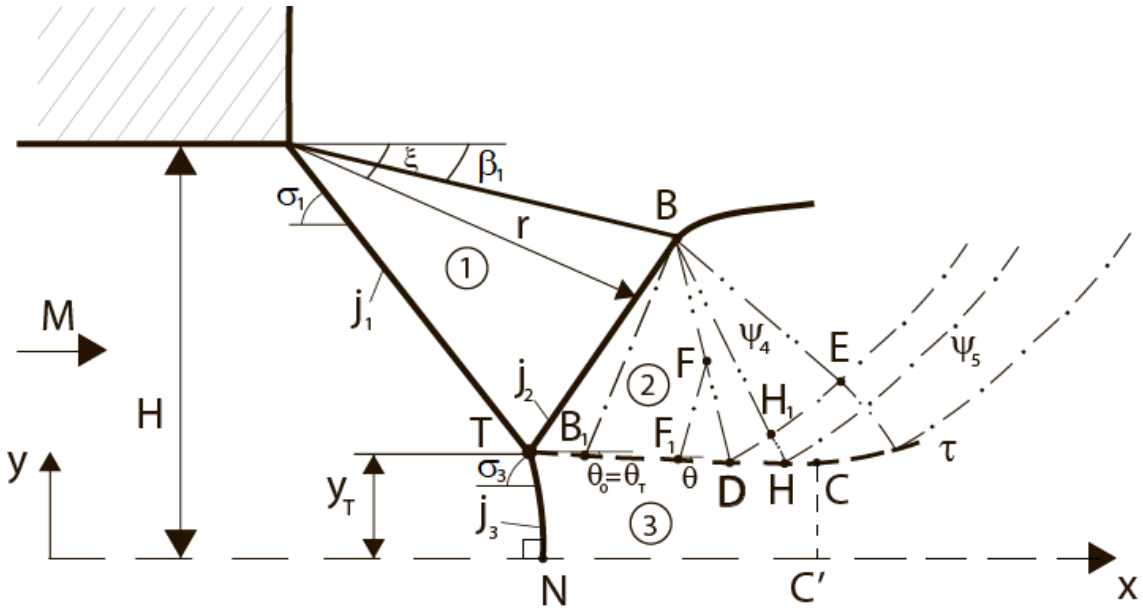

Figure 3.7. Flow diagram with Mach reflection in a narrowing channel between the wedges (a) and in a highly overexpanded jet (b)

The analytical model, described in detail in [56, 62, 145] and the materials of the Subsection 2.3, considers region 2 as a simple (non-centered) Prandtl-Meyer expansion wave, related with region 3 by the condition of equality of pressures across the upward-convex segment *TD* of the slipstream τ (the conjugation problem was solved in [64, 65]). Accounting for angle changes θ of the inclination of the slipstream significantly improves the accuracy of calculations of the supersonic part of the flow (as shown in [56, 62, 145], the error in determining the height of the triple point is on the order of 0.5-1% compared to the results of calculations by the method of characteristics). Reverse turn of the slipstream τ which takes place on its final segment *DC* is calculated based on the solution to the problem of the incidence of an expansion wave ψ_4 on the slipstream=

Interest in methods for quickly estimating the parameters of the shock wave structure of two-dimensional flows with Mach reflection, including asymmetric ones [66-68], has noticeably increased recently [58, 66-68]. It is apparently associated with the development of aviation and rocket vehicles flying at high supersonic speeds in the atmosphere. It is under such conditions that the presence of strong shocks in a supersonic flow of a reactive gas (fuel-air) mixture can initiate chemical reactions and detonation effects. In this regard, it is necessary to generalize the analytical

model [145], which has proven itself well for flows of perfect non-reacting gas, in the case of changes in the chemical composition and pulsed energy release at the emerging shocks. In [88, 89, 91], classical relations for shock waves are generalized to the case of changes in chemical composition and the presence of pulsed energy release, described within the Chapman-Jouguet model. In particular, instead of classical shock polars, “detonation” polars are constructed [91, 146]; generalized criteria for reflection transition of oblique shocks (regular or Mach one) are derived and their displacement is analyzed in comparison with a flow without energy release and changes in chemical composition.

Numerical and theoretical results achieved in [88, 89, 91, 128, 129, 146] are not always directly applicable in practice. In particular, important analytical relationships obtained in [88] are based on the assumption of the presence of detonation effects on the incident (j_1) and main (j_3) shocks. At the same time, as shown in [150, 152], a noticeably higher temperature of the gas mixture initiates detonation effects at the main shock primarily (see also Figure 3.8). In this case, no change in the chemical composition or energy release is observed either on the incident shock or on the reflected one, which is taken into account in [146]. The need to calculate the chemical kinetics of occurring reactions [128, 129] also does not contribute to the development of an approximate analytical technique for fast calculations.

In [143, 147] and, partially, in [161, 163, 164, 167, 169], an approximate analytical model of flow with Mach reflection [56, 145], also presented in the Subsection 2.3, is generalized to the case of changes in the chemical composition of the gas mixture and pulsed energy release at the main shock. Using the example of a highly overexpanded jet of methane-air or hydrogen-air mixture, an algorithm for calculating the parameters of the shock-wave structure is developed and the primary results of its application are shown, and a comparison is made with similar data for an overexpanded jet of non-reacting gas.

а) б)

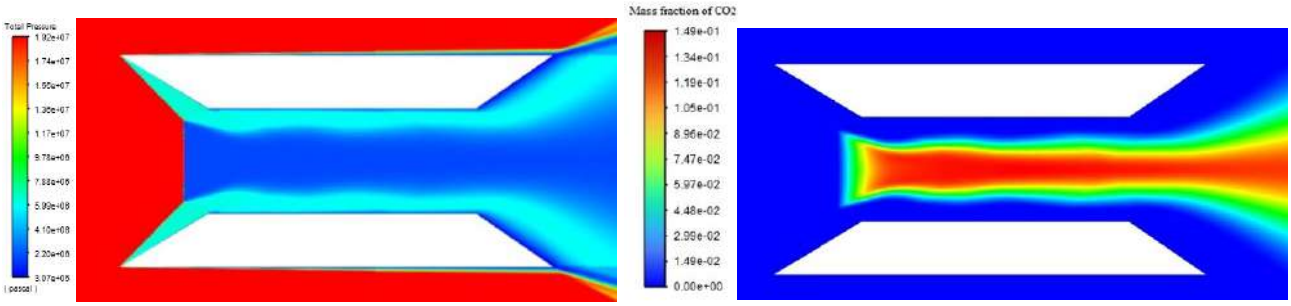

Figure 3.8. Distribution of total pressure (a) and mass fraction of carbon dioxide (b) in the flowfield of a stoichiometric methane-air mixture. Mach number of undisturbed flow $M = 6$, the angle at the top of the wedges forming the entrance to the narrowing channel, $\beta_1 = 24^\circ$. The stagnation pressure from above the slipstream is noticeably greater, but the chemical reactions with the formation CO_2 occur only after the main shock

3.2.1. Mathematical model of flow and algorithm for its application

Calculation of parameters in the vicinity of the triple point. As a sufficiently strong oblique shock wave j_1 falls in flow with Mach number M (Figure 3.7), a triple configuration of the second type (TC-2) is formed according to the classification [1, 10]. Parameters osf steady shocks $j_1 - j_3$ at their common (triple) point T are related by the conditions of equality of static pressures and co-direction of flows across the slipstream τ as in (1.18):

$$J_1 J_2 = J_3, \tag{3.24}$$

$$\beta_1 + \beta_2 = \beta_3. \tag{3.25}$$

Here $J_1 = p_1/p$, $J_2 = p_2/p_1$, $J_3 = p_3/p$ are the intensities (strengths) of the incident shock (j_1), the reflected one (j_2) and the main one (j_3), i.e. the ratios of static pressures on their sides, p is the free-stream static pressure, $p_1 - p_3$ are the pressures behind the shocks $j_1 - j_3$, and $\beta_1 - \beta_3$ are the flow deflection angles at those shocks in the vicinity of the triple point, related to their intensities by formulas of the form (1.4):

$$|\beta_1| = \arctan\left[\sqrt{\frac{(1+\varepsilon)M^2 - J_1 - \varepsilon}{J_1 + \varepsilon}} \cdot \frac{(1-\varepsilon)(J_1 - 1)}{(1+\varepsilon)M^2 - (1-\varepsilon)(J_1 - 1)}\right], \tag{3.26}$$

$$|\beta_2| = \arctan\left[\sqrt{\frac{(1+\varepsilon)M_1^2 - J_2 - \varepsilon}{J_2 + \varepsilon}} \cdot \frac{(1-\varepsilon)(J_2 - 1)}{(1+\varepsilon)M_1^2 - (1-\varepsilon)(J_2 - 1)}\right] \qquad (3.27)$$

on the incident and reflected shocks [1], and by the relation (1.12)

$$|\beta_3| = \arctan\left[\frac{(J_3 - 1)\sqrt{F - 1}}{\gamma M^2 - (J_3 - 1)}\right],\ F = \frac{2\gamma M^2\left[(\gamma - \gamma_3) + (\gamma - 1)\left((J_3 - 1) - (\gamma_3 - 1)\bar{\phi}\right)\right]}{(\gamma - 1)(J_3 - 1)\left[(\gamma_3 + 1)(J_3 - 1) + 2\gamma_3\right]} \qquad (3.28)$$

at the main shock [88]. Here $\varepsilon = (\gamma - 1)/(\gamma + 1);\ \varepsilon_3 = (\gamma_3 - 1)/(\gamma_3 + 1);\ \gamma$ is the adiabatic index of a gas mixture in the free flow, γ_3 is the adiabatic index of combustion products behind the main shock. Dimensionless quantity (1.11)

$$\bar{\phi} = \frac{\phi}{(p/\rho)} = \frac{\gamma\phi}{(\gamma - 1)c_p T} \qquad (3.29)$$

characterizes pulsed energy release ϕ per unit mass of the mixture; ρ is its density, T is its temperature, c_p is its isobaric specific heat capacity. Meaning ϕ is determined by the specific heat of fuel combustion λ, related to the entire mixture in the oncoming flow.

Mach numbers M_1 and M_{2T} of the flows behind the incident and reflected shocks are determined by relations of the form (1.6):

$$M_1 = \sqrt{\frac{(J_1 + \varepsilon)M^2 - (1-\varepsilon)\left(J_1^2 - 1\right)}{J_1(1 + \varepsilon J_1)}}, \qquad (3.30)$$

$$M_{2T} = \sqrt{\frac{(J_2 + \varepsilon)M_1^2 - (1-\varepsilon)\left(J_2^2 - 1\right)}{J_2(1 + \varepsilon J_2)}}. \qquad (3.31)$$

Relations (1.10) of the Chapman-Jouguet model of stationary detonation

$$\rho u_n = \rho_3 u_{3n},\ \ p + \rho u_n^2 = p_3 + \rho_3 u_{3n}^2,\ \ u_\tau = u_{3\tau},$$

$$\frac{u_n^2 + u_\tau^2}{2} + \frac{\gamma}{\gamma - 1}\frac{p}{\rho} + \phi = \frac{u_{3n}^2 + u_{3\tau}^2}{2} + \frac{\gamma_3}{\gamma_3 - 1}\frac{p_3}{\rho_3},$$

where the indices «n» and «τ» refer to the normal and tangential (to the shock surface) velocity components, determine the Mach number M_{3T} (1.15) in the vicinity of the triple point:

$$M_{3T} = \sqrt{\frac{\gamma M^2 \left(E_3^2 \sin^2 \sigma_3 + \cos^2 \sigma_3\right)}{\gamma_3 E_3 J_3}}. \qquad (3.32)$$

Here, according to (1.16),

$$\sigma_3 = \arcsin \sqrt{\frac{J_3 - 1}{\gamma(1 - E_3)M^2}}$$

is the angle of inclination of the shock to the flow in front of it, and

$$E_3 = 1 - \frac{2\left[J_3 - (\gamma_3 - 1)/(\gamma - 1) - (\gamma_3 - 1)\bar{\phi}\right]}{(\gamma_3 - 1) + (\gamma_3 + 1)J_3}$$

is th inverse ratio of gas densities on the sides of the shock (1.17), which reduces to the ordinary Rankine-Hugoniot adiabat at $\bar{\phi} = 0$ and $\gamma_3 = \gamma$.

As it is shown in [146] and in Subsection 3.1, a sufficiently large pulsed energy release $\bar{\phi}$ shifts the "detonation" polar III (Figure 3.9), reflecting the relation (3.28), inside the shock polar I, which corresponds to expression (3.26). In this case, the intensity of the steady shock j_3 must belong to the interval (1.13)

$$J_{3\min} \le J_3 \le J_{3\max}. \qquad (3.33)$$

Here the value $J_3 = J_{3\max}$ corresponds to a normal shock with pulsed energy release, and the triple configuration with $J_3 = J_{3\max}$ and $J_1 = J_{1N}$ (Figure 3.9) corresponds to the analogue of the von Neumann transition criterion eflection of the shock j_1 restablished in Subsection 3.1. Values $J_{3\min}$ and $J_{3\max}$, according to [146], are determined by the formula (1.14):

$$J_{3\min,\max} = \frac{\gamma + 1}{\gamma_3 + 1} \cdot \frac{J_m(M) + 1}{2} \mp \frac{\sqrt{\gamma^2 M^4 + \gamma_3^2 - 2\gamma M^2 \left[\left(\gamma_3^2 - 1\right)\bar{\phi} + \left(\gamma_3^2 - \gamma\right)/(\gamma - 1)\right]}}{\gamma_3 + 1}, \qquad (3.34)$$

here $J_m(M) = (1 + \varepsilon)M^2 - \varepsilon$.

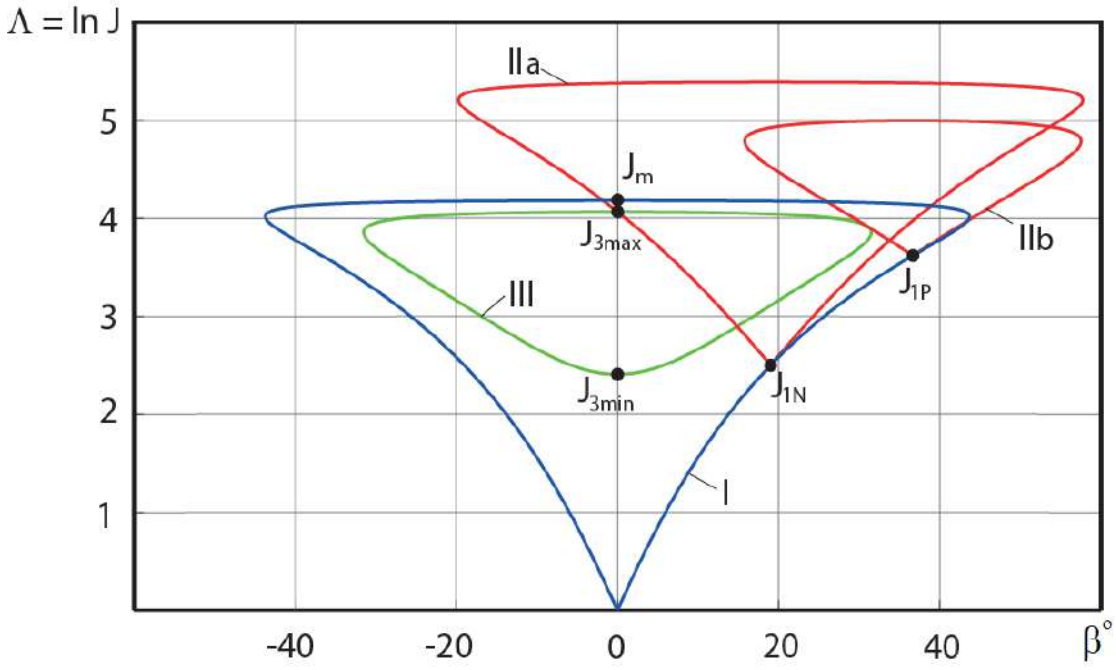

Figure 3.9. Solution of the problem of Mach reflection on the plane "shock intensity – flow deflecttion angle": I is the polar of the incident shock; IIa is the polarity of the reflected shock at minimum permissible intensity (J_{1N}) of the incident one; IIb – at its maximum permissible intensity (J_{1P}); III is the polar of the main (Mach) shock with pulsed energy release

The only solution to system (3.25-3.26) in the considered range of sufficiently large Mach numbers belongs to the interval of intensities

$$J_{1N} \le J_1 \le J_{1P}, \tag{3.35}$$

here the value $J_1 = J_{1P}$ corresponds to the limiting position of polar IIb of the reflected shock (its contact with polar III, see Figure 3.9). Flow behind the reflected shock j_2 at the same time it is supersonic ($M_{2T} > 1$), and it is subsonic ($M_{3T} < 1$) beyond the main shock j_3.

As a rule, for an approximate analytical description of the flow in region 3 (Figuse 3.7, a-b), a model of quasi-one-dimensional flow with a certain initial Mach number M_{30} immediately after the strong Mach stem is used. The value of M_{30} can be determined by formula (9), then $M_{30} = M_{3T}$, or by a similar ratio for $J_3 = J_{3\max}$, which corresponds to the flow at the point *N* after a normal shock (then $M_{30} = M_{3N}$), or as half the sum of these values: then

$$M_{30} = (M_{3T} + M_{3N})/2, \tag{3.36}$$

which corresponds to the approach adopted in [145, 58]. Initial value of M_{30} can also be based on more complex methods for averaging of flow parameters [5, 111]. Next, to determine the initial Mach number of the flow through the "virtual nozzle" 3, approximation (3.36) is used.

Thus, the application of the proposed model allows us to establish the initial flow angle ($\theta_0 = \beta_3$) and Mach numbers ($M_{20} = M_{2T}$ and M_{30}) in regions 2 and 3 behind the reflected shock and the main one.

Flow in an expansion wave behind a reflected shock. Relationships for flow angle θ in Prandtl-Meyer wave 2 with straight characteristics of the first family look as follows:

$$\theta = \theta_0 + \nu(M_{20}) - \nu(M_2),$$

here $\nu(M) = 1/\sqrt{\varepsilon}\,\mathrm{arctg}\sqrt{\varepsilon\left(M^2-1\right)} - \mathrm{arctg}\sqrt{M^2-1}$ is the Prandtl-Meyer function, together with a condition of the form (1.22)

$$y/y_T = q(M_{30})/q(M_3),$$

where $q(M) = M\left[1+\varepsilon_3\left(M_3^2-1\right)\right]^{-1/2\varepsilon_3}$ is the isentropic flow rate function, and equality (1.23) of pressures across the slipstream τ:

$$\pi(M_2)/\pi(M_{20}) = \pi_3(M_3)/\pi_3(M_{30}).$$

Here $\pi(M) = \left[1+(\gamma-1)M^2/2\right]^{-\gamma/(\gamma-1)}$ and $\pi_3(M) = \left[1+(\gamma_3-1)M^2/2\right]^{-\gamma_3/(\gamma_3-1)}$ are the isentropic pressure functions written for gases above and below the slipstream. Those relations lead to equations of the form (1.35-1.38), which describe the shape $y(x)$ of the slipstream τ and changes in flow parameters on both its sides:

$$\frac{dy}{dx} = \tan\theta,\ \ \frac{d\theta}{dx} = -\frac{\gamma_3 M_3^2\sqrt{M_2^2-1}\tan\theta}{\gamma M_2^2\left(M_3^2-1\right)y}, \tag{3.37}$$

$$\frac{dM_2}{dx} = \frac{\gamma_3 M_3^2\left[1+\varepsilon\left(M_2^2-1\right)\right]\tan\theta}{(1+\varepsilon)M_2\left(M_3^2-1\right)y},\ \ \frac{dM_3}{dx} = \frac{M_3\left[1+\varepsilon_3\left(M_3^2-1\right)\right]\tan\theta}{(1-\varepsilon_3)\left(M_3^2-1\right)y}.$$

If we consider the Mach number M_3 below the slipstream as an independent variable, equations (3.37) are similar to (1.39-1.42):

$$\frac{dx}{dM_3}=\frac{(1-\varepsilon_3)\left(M_3^2-1\right)y}{M_3\left[1+\varepsilon_3\left(M_3^2-1\right)\right]\tan\theta},\quad \frac{dy}{dM_3}=\frac{(1-\varepsilon_3)\left(M_3^2-1\right)y}{M_3\left[1+\varepsilon_3\left(M_3^2-1\right)\right]},$$

$$\frac{d\theta}{dM_3}=-\frac{(1+\varepsilon_3)M_3\sqrt{M_2^2-1}}{\gamma M_2^2\left[1+\varepsilon_3\left(M_3^2-1\right)\right]},\quad \frac{dM_2}{dM_3}=\frac{(1+\varepsilon_3)M_3\left[1+\varepsilon\left(M_2^2-1\right)\right]}{(1+\varepsilon)M_2\left[1+\varepsilon_3\left(M_3^2-1\right)\right]}. \qquad (3.38)$$

At the same chemical composition of the flows across the slipstream, the ratios (3.37) and (3.38) take the form (2.31-2.34), known from [64, 65, 145]. Integration of equations (3.37) or (3.38) is to be performed up to the point *D* of the intersection of the slipstream τ with boundary characteristic *BD* of the second family which incides from the exit point of the reflected shock j_2 (*TB*) to the jet boundary (Figure 3.7,b). The flow from below from the slipstream should remain subsonic ($M_3<1$); reaching critical speed indicates that the proposed altitude y_T of the triple point is significantly underestimated.

As calculations show, the angle of rotation of the slipstream τ on its segment *TD* if usually small in absolute value, but can be 1.5-2 times more than the initial angle θ_0 the slope of this discontinuity at the exit from the triple point. Therefore, ignoring the curvature of the slipstream leads to a significant underestimation of the resulting height of the main shock (namely, of the value of y_T).

An analysis of the differential characteristics of the flow in a Prandtl-Meyer wave, similar to that obtained in [64, 65, 145] with $\gamma=\gamma_3$, leads to the following equations to determine the shape $y_F(x_F)$ of the boundary acoustic characteristics of the second family *BD* and variation in flow parameters along the its direction φ:

$$\frac{dx_F}{d\varphi}=\cos(\theta-\alpha_2),\frac{dy_F}{d\varphi}=\sin(\theta-\alpha_2),\ \frac{d\theta}{d\varphi}=-\frac{2\gamma_3M_3^2\left(M_2^2-1\right)\sin\theta}{\gamma M_2^3\left(M_3^2-1\right)y_{F_1}}\cdot\left[\frac{y_F-y_{F_1}}{\Delta y}+1\right]^{-1},$$

$$\frac{dM_2}{d\varphi}=\frac{2\gamma_3M_3^2\left[1+\varepsilon\left(M_2^2-1\right)\right]\sqrt{M_2^2-1}\sin\theta}{(1+\varepsilon)M_2^2\left(M_3^2-1\right)y_{F_1}}\cdot\left[\frac{y_F-y_{F_1}}{\Delta y}+1\right]^{-1}, \qquad (3.39)$$

$$\frac{dM_3}{d\varphi}=\frac{2M_3\left[1+\varepsilon_3\left(M_3^2-1\right)\right]\sqrt{M_2^2-1}\sin\theta}{(1-\varepsilon_3)M_2\left(M_3^2-1\right)y_{F_1}}\cdot\left[\frac{y_F-y_{F_1}}{\Delta y}+1\right]^{-1},$$

which are consistent with the equations (1.51-1.59). Here $\alpha_2 = \arcsin(1/M_2)$ is the Mach angle, M_2 is flow Mach number at an arbitrary point F on the characteristic BD, M_3 is Mach number of the flow on the other side of the slipstream τ at the point F_1 its intersection with the corresponding straight characteristic FF_1. Coordinate y_{F_1} point F_1 obeys the formula

$$y_{F_1} = y_T q(M_{30})/q(M_3),$$

and the distance Δy from this point to the envelope line of the family of the straight characteristics obeys the relation

$$\Delta y = \frac{(1+\varepsilon)\sqrt{M_2^2-1}\left(M_3^2-1\right)y_{F_1}\sin(\theta+\alpha_2)}{\gamma_3 M_2 M_3^2 \sin\theta}.$$

The system of equations (3.39) is integrated starting from the point B of the intersection of the reflected shock with the jet boundary and finishing at the point D of the incidence of the characteristic BD on the slipstream. If we take the distance L between the curvilinear characteristic BD and slipstream as an independent variable, then the equations (3.39) are recorded in the form

$$\frac{dx_F}{dL} = \frac{dx_F/d\varphi}{dL/d\varphi}, \quad \frac{dy_F}{dL} = \frac{dy_F/d\varphi}{dL/d\varphi}, \quad \frac{d\theta}{dL} = \frac{d\theta/d\varphi}{dL/d\varphi}, \quad \frac{dM_2}{dL} = \frac{dM_2/d\varphi}{dL/d\varphi}, \quad \frac{dM_3}{dL} = \frac{dM_3/d\varphi}{dL/d\varphi}, \quad (3.40)$$

here the value

$$\frac{dL}{d\varphi} = \sin(\alpha_2-\theta) + \frac{2\sqrt{M_2^2-1}\sin\theta}{M_2}\cdot\left[\frac{y_F - y_{F_1}}{\Delta y}+1\right]^{-1}$$

characterizes the decrease in distance L as the curved characteristic BD approaches to the slipstream. Integrating of equations (3.40) is produced starting from the value L and flow parameters which correspond to the point B after the reflected shock, up to the value L=0, which corresponds to the point D.

Equation of the shape of a reflected shock. It has been repeatedly shown [113, 137] that the reflection coefficient of expansion or compression disturbances overtaking the preceding oblique shock wave is very small (if only the flow behind the shock is not transonic, which is not the case considered here). In addition, the

expansion wave part acting on the reflected shock j_2 in a triangle TBB_1 (Figure 3.7,b), is weak itself. Therefore, according to the method first proposed in [9], the shape of the reflected shock is determined basing on the condition of flow conjugation in direction (i.e., the flow angles behind each point of the reflected shock j_2 and at the corresponding points the Prandtl-Meyer expansion wave 2 must coincide). Analysis of the differential characteristics of the flowfield in wave 2 [64, 65, 145], together with the compatibility conditions on the oblique shock, determines the shape of the reflected shock in polar coordinates (r, ξ):

$$\frac{dr}{d\xi} = r\cot(\sigma_2 - \beta_1 - \xi), \tag{3.41}$$

$$\frac{d\theta_2}{d\xi} = \frac{K_s M_2 r \sin(\alpha_2 + \beta_2 - \sigma_2)}{\sin(\sigma_2 - \theta_1 - \xi)}. \tag{3.42}$$

Here r is the distance from the edge of the nozzle to the considered point on shock surface, ξ is the polar angle measured from the horizontal direction (see Figure 3.7,b), and $\alpha_2 = \arcsin(1/M_2)$ is the Mach angle. In this case, the angle β_2 of the flow deflection on the reflected shock is related to its intensity J_2 by (3.27), and the angle σ_2 of the shock clope to the flow in front of it – by dependence (1.1):

$$J_2 = (1+\varepsilon)M_1^2 \sin^2\sigma_2 - \varepsilon.$$

Mach number M_2 at the corresponding point of the expansion wave behind the shock obeys the dependence

$$\nu(M_2) = \nu(M_{20}) + \theta_0 - \beta_2,$$

here $\nu(M)$ is the Prandtl-Meyer function. Corresponding Mach number M_3 on the other side of the slipstream obeys the relation

$$\pi(M_3) = \pi(M_2)\cdot\pi_3(M_{30})/\pi(M_{20}).$$

The curvature K_S of the streamline behind an arbitrary point on shock surface, which is present in (3.42), is determined according to the results of the analysis in [65]:

$$K_S = \frac{\gamma_3 M_3^2\sqrt{M_2^2-1}\sin\theta}{\gamma M_2^2\left(M_3^2-1\right)y_A}\cdot\frac{y_A - y_{A_1}}{y - y_{A_1}},$$

here $y = H + r\sin\xi$ is the ordinate of a given point downstream the shock, $\theta = \theta_0 + \nu(M_{20}) - \nu(M_2)$ is flow angle at this point, $y_A = y_T q(M_{30})/q(M_3)$, $y_{A_1} = y_A\left[1 - (1+\varepsilon)\sqrt{M_2^2 - 1}\left(M_3^2 - 1\right)\sin(\alpha_2 + \theta)\Big/\left(\gamma_3 M_2 M_3^2 \sin\theta\right)\right]$, H is a half-width of the nozzle exit section.

Integration of (3.41-3.42) is carried out from the value $\xi = -\sigma_1$ at the triple point T to the value $\xi = -|\beta_1|$ at point B of the exit of the shock j_2 onto the jet boundary with subsequent reflection in form of the expansion wave ψ_4.

The incidence of an expansion wave on slipstream. Many modern approximate models of flows with Mach reflection [66-68] actually replace the fast analytical assessment for the interaction of the rarefaction wave ψ_4 with a sleepstream τ (Figure 3.7, a-b) for its numerical calculation using the method of characteristics. However, on the other hand, the reduction of the area *DCE* of this interaction to a single point *D*, which ignores the finiteness of the *DC* secot of the inverse turn of the sleepstream in the horizontal direction [52, 53], also leads to significant errors in determining the parameters of the shock-wave structure. By analogy with the model [145] set out in Subsection 2.3, the calculation of the wave interaction ψ_4 with a sleepstream τ is performed as follows. It is assumed that the wave ψ_4 is the Prandtl-Meyer flow, and the Mach number M_{2BD} flow in front of this wave corresponds to the average slope angle of the characteristic *BD* in area 2:

$$\nu(M_{2BD}) + \alpha(M_{2BD}) = \left[\nu(M_{2B}) + \alpha(M_{2B}) + \nu(M_{2D}) + \alpha(M_{2D})\right]/2. \qquad (3.43)$$

Initial Mach number M_{3D} and width y_D of flow area 3 along the “virtual nozzle” are determined from previously obtained solutions to problems about the shape of the slipstream *TD*, boundary characteristics BD and variations of flow parameters along them.

Arbitrary Mach number $M_{3H} \in [M_{3D}; 1]$ on the lower side of the slipstream corresponds to the Mach number M_{2H} from its upper side. It is determined by the relation

$$\pi(M_{2H})/\pi_3(M_{3H}) = \pi(M_{2BD})/\pi_3(M_{3D}), \qquad (3.44)$$

and width y_H area 3 is such that

$$y_H / y_D = q(M_{3D}) / q(M_{3H}). \tag{3.45}$$

In this case, the abscissa x_H of point H is approximately determined from the condition of straightness of the incident characteristic BH_1H:

$$(y_H - y_B)/(x_H - x_B) = \mathrm{tg}\left[\zeta + \nu(M_{2BD}) + \alpha(M_{2BD}) - \nu(M_{2H_1}) - \alpha(M_{2H_1})\right], \tag{3.46}$$

here $\tan\zeta = (y_D - y_B)/(x_D - x_B)$, and the slope $y'_H(x_H)$ of the slipstream at this point obeys the condition

$$y'_H(x_H) = \tan\left[\theta_D + 2\nu(M_{2H_1}) - \nu(M_{2BD}) - \nu(M_{2H})\right], \tag{3.47}$$

taking into account the turn of streamlines in the waves which are incident on the slipstream τ (ψ_4) and reflected from it (ψ_5). Here M_{2H_1} is Mach number on the characteristic BH_1, θ_D is the previously determined angle of inclination of the sleepstream at point D.

System of equations (3.44-3.47) defines the shape $y_H(x_H)$ of the sleepstream τ and is to be integrated until the value $M_{3H} = 1$ is reached.

If the expansion wave ψ_4 undergoes refraction at the reflected shock j_2 before falling onto the sleepstream(see, for example, Figure 3.7,a), then we should add to system (3.44-3.47) the analytical solutions to the problem of the interaction of a shock with an expansion wave of counter direction, obtained in [60, 61].

Algorithm for applying an approximate analytical model. To quickly estimate the parameters of the shock-wave structure of a supersonic flow with Mach reflection, pulsed energy release and changes in the chemical composition at the main shock, first of all, the parameters of the free-stream flow of the initial mixture (values M and γ) should be set, as well as the adiabatic index γ_3 of the combustion products, dimensionless pulse energy release $\bar{\phi}$ and intensity J_1 of the incident shock, satisfying inequality (3.35). Next, the flow parameters are to be determined as follows:

1. Let us set the height y_T of the triple point to a first approximation.

2. The problem (3.24-3.30) of calculating flow parameters in the vicinity of the triple point is to be solved. Relations (3.25), (3.31), (3.32) and (3.36) determine the initial Mach numbers $M_{2T} = M_{20}$ and M_{3T} on the sides of the slipstream, as well as the initial Mach number M_{30} of the flow along the "virtual nozzle" 3 and angle $\theta_0 = \theta_3$ of inclination of slipstream in the vicinity of the triple point.

3. Relations (3.41-3.42) establish the shape of a slightly curved (convex upward) reflected shock wave j_2 (*TB*), as well as the coordinates of the point *B* and flow parameters behind the shock at this point.

4.Shapes of the boundary characteristic *BD* (3.39-3.40), of the slipstream τ (3.38) and flow parameters on their sides are to be determined jointly. Integration of equations (3.38) and (3.39-3.40) finishes at point *D* of intersection of the boundary characteristic with the slipstream. The flow through the "virtual nozzle" 3 can reach a critical speed ($M_3 = 1$) to this point, indicating a significant underestimation in the value y_T in the accepted approximation.

5. The problem (3.43-3.48) about the incidence of a expansion wave ψ_4 which causies a reverse turn of the slipstream τ is solve,. If it is discovered that the critical flow speed in region 3 is reached before the sleepstream turns horizontally ($M_{3H} = 1$ at $y'_H(x_H) < 0$), suggested height y_T is overestimated, otherwise it is underestimated.

6. Based on the results of the iteration, the value y_T is specified, after which calculations are performed in the next approximation.

3.2.2. Results of applying an approximate analytical model of the shock-wave structure of a flow with pulsed energy release and a change in the chemical composition of the gas at the main shock

As an example of using the presented model, the outflow of a uniform (in the outlet section) planar jet of a fuel-air gas mixture is calculated. The adiabatic indices of the mixture in the free flow and behind the main shock wave were assumed to be equal $\gamma = 1.396$ and $\gamma_3 = 1.290$, which approximately corresponds to a stoichiometric methane-air mixture (mass fractions – 4.856% CH_4, 74.212% N_2,

19.980% O_2, 0.951% of other impurities) and products of its complete combustion, including carbon dioxide and water vapor. The specific heat of combustion of fuel was taken equal to $\lambda = 55.266$ MJ/kg, which corresponds to the value $\phi = 2.684$ MJ/kg in terms of the entire gas mixture and the dimensionless value (3.29) of the pulse energy release $\overline{\phi} = 30.045$ at T=300 K. This value of specific energy release is an order of magnitude higher than that considered in [88].

Due to the rather large value of the pulsed energy release, the solution to system (3.24-3.30), which describes the stationary Mach reflection, under the conditions under consideration exists only for $M > 5.436$. According to inequality (3.33), which limits the range of possible intensities of the main shock with an energy supply, at $M = 5.436$ the detonation polar III (Figure 3.9) is compressed into a point

$$J_{3\min} = J_{3\max} = \frac{\gamma + 1}{\gamma_3 + 1} \cdot \frac{J_m(M) + 1}{2} = \frac{\gamma + 1}{\gamma_3 + 1} \cdot \frac{(1+\varepsilon)M^2 + (1-\varepsilon)}{2} = \frac{\gamma M^2 + 1}{\gamma_3 + 1},$$

and at lower Mach numbers it disappears. The solution describing the triple configuration of the Mach reflection, with $M < 5.436$ should be sought by allowing the movement of the main shock wave j_3 upstream, i.e. unsteadiness of the emerging flow.

Figure 3.10 shows examples of calculating the dimensionless (relative to the half-width of the outlet section) height of the triple point y_T depending on intensity J_1 of the incident shock (provided that there is a non-separated outflow of the highly overexpanded jet under consideration). Curves 1-6 correspond to the outflow with Mach numbers M=6; 6.5; 7; 8; 9 and 10 over the entire range (3.33) of incident shock intensities.

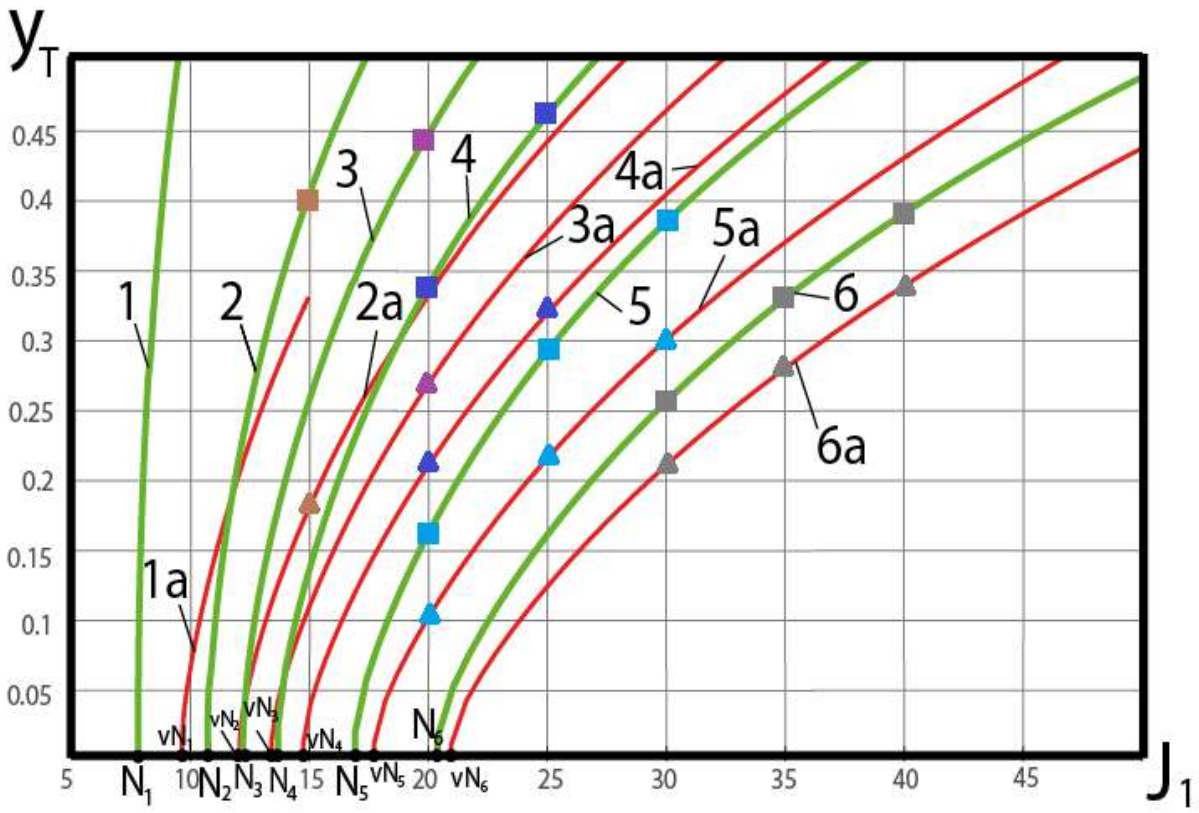

Figure 3.10. Values of the triple point height depending on the intensity of the incident shock in the presence (curves 1-6) and absence (curves 1a-6a) of pulsed energy release and changes in the chemical composition of the methane-air mixture. Squuares and triangles correspond to numerical results in CFD package ANSYS Fluent

For comparison, curves 1a-6a show the values $y_T(J_1)$, calculated for the same outflow parameters, but in the absence of energy release ($\phi = 0$) and without changes in the chemical composition of the mixture ($\gamma_3 = \gamma = 1.396$), that is, according to the algorithm [145] (Subsection 2.3), a generalization of which is presented in this section. From a comparison of curves 1-6 and 1a-6a, it is obvious that a significant pulsed energy release noticeably shifts the conditions for the occurrence of Mach reflection (from points vN_1-vN_6, corresponding to the "classical" von Neumann criterion, to points N_1-N_6), which completely corresponds to the conclusions and relationships obtained in Subsetion 3.1. In addition, the energy release leads to a significant increase in size of the main (Mach) shock and in the width of the subsonic flow region after it.

The following example of verification of the developed analytical model is presented in Figure 3.8. Using a software package ANSYS Fluent 2020 R2, the

planar flow of a stoichiometric methane-air mixture in a symmetrical narrowing duct between the wedges was calculated. The angles at the tops of the wedges are $\beta_1 = 24^\circ$, the distance between their leading edges is 200 mm, and the minimum channel width is 100 mm. The oncoming flow had normal atmospheric parameters, the dynamic viscosity of the gas was changed according to the Sutherland formula, and $\kappa - \omega$ SST-turbulence model was applied. The calculations were obtained on an unstructured grid consisting of $2 \cdot 10^6$ cells. In this case, chemical reactions initiated by high temperature behind the Mach shock were calculated using a finite kinetics model. The results of the calculations were compared with those obtained under similar conditions for a non-reacting mixture of similar composition. The calculated values of the dimensionless (relative to the width of the channel inlet section) length of the main (Mach) shock were approximately 0.377 (in the presence of exothermic reactions) and 0.207 (in the case of their absence). From Figure 3.8b, it is obvious that in this case chemical reactions are initiated only behind the main (Mach) shock, but not behind the incident and the reflected shocks (since carbon dioxide, which is their product, is present only in the flow region behind the main shock).

Application of the approximate analytical model presented here (as well as in [143, 147]) made it possible to obtain the values $y_T = 0.412$ (in the first case) and $y_T = 0.215$ (in the second one). Thus, the comparison of numerical (also demonstrated by squares and triangles in Figure 3.10) and analytical results seems satisfactory.

At the next verification step, the results of applying the proposed analytical model and the calculations given in [138] were compared. First, the flow of a lean hydrogen-air mixture was calculated (0.4 H_2 + 4.772 Air) with Mach numbers *M*=3.0 and *M*=3.15. According to [138] , a steady numerical solution with Mach reflection was not obtained in both cases (a transition to regular reflection occurred, or oscillatory movements of the Mach shock with chemical reactions behind it began). Assuming complete combustion of hydrogen with specific heat $\lambda = 141.8$ MJ/kg, it is easy to establish that the energy release per unit mass of the gas mixture is $\phi = 0.821$

MJ/kg. This is significantly greater than the critical value corresponding to the maximum dimensionless energy release $\overline{\phi}_*$ (3.18) which is 0.538 MJ/kg at M=3.0 and 0.477 MJ/kg at M=3.15. At the indicated values, the "detonation polar" of the main shock [24] degenerates into a single point and disappears, which leads to the absence of a solution for a steady shock-wave structure (at least at $\gamma = 1.403$ in the free stream and $\gamma_3 = 1.322$ in the mixture behind the main shock). Thus, a "negative" (reducing to the absence of both analytical and numerical solution) agreement between the numerical and analytical results was obtained. More "positive" results (expressed in the presence of a steady solution with Mach reflection and pulsed energy release) for a mixture of a given composition should be sought, for example, at M = 4.0.

Lastly, the flows of a stoichiometric mixture of hydrogen and oxygen were calculated ($2H_2 + O_2$), also considered in [138]. At M=4.0, the estimated energy release also exceeds the critical value (3.18). Therefore, the numerical result obtained in [138] for $\beta_1 = 25^\circ$ (unsteady flow regime) is quite consistent with the proposed model.

At Mach number *M*=7.0, according to the data of [138], stationary detonation took place only in a narrow range of flow deflection angles on the incident shock (between $\beta_1 = 20^\circ$ and $\beta_1 = 23.5^\circ - 24^\circ$). The upper limit is fully consistent with the data of the proposed model, in particular, the equation (3.34): $J_1 = J_{1P}$ at $\beta_1 = 23.824^\circ$. According to numerical experiments in [138] and analytical results of applying the proposed model, at $J_1 = J_{1P}$ the Mach shock occupies almost the entire cross-section of the channel, gradually turning into the bow detached shock.

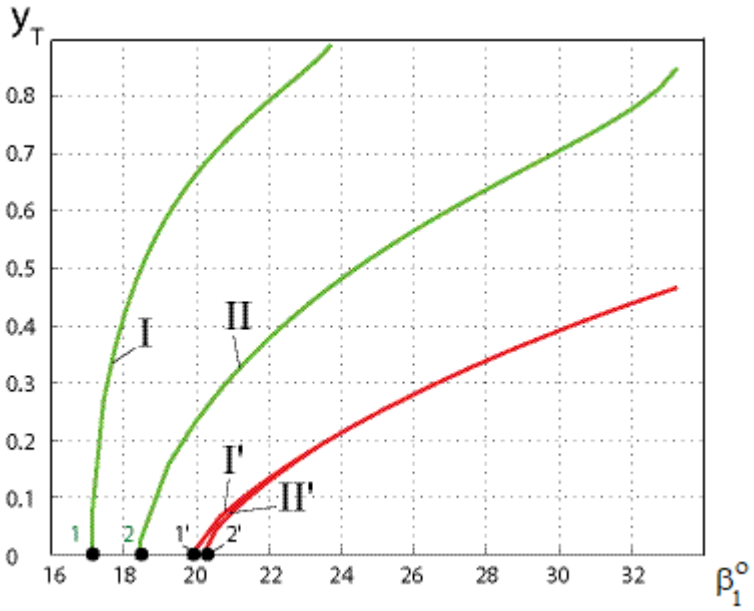

Figure 3.11. Dimensionless height of the triple point depending on the angle of flow deflection at the incident shock in the presence (curves I, II) or absence (curves I', II') of energy release and changes in the chemical composition of ga mixture behind the main shock in the jet flow of a stoichiometric mixture of hydrogen and oxygen at M=7.0 (curves I, I') and M=8.0 (curves II, II')

Bottom line ($\beta_1 = 20^\circ$) of the region of existence of stationary detonation in a stoichiometric mixture of hydrogen and oxygen at M=7.0 corresponds to formation of "classical" stationary Mach configuration in a perfect diatomic gas ($\beta_1 = 19.716^\circ$), i.e. to von Neumann criterion. According to the results of Subsection 3.1, in the presence of a pulsed energy supply, this boundary shifts to the value $\beta_1 = 17.104^\circ$ (from point 1' in Figure 3.11 to point 1). It should be noted that at *M*=7.0 wide range of angles β_1 (up to $\beta_1 = 30.245^\circ$) belongs to the domain of "dual solution" for Mach and regular reflections. Therefore, in a number of cases, numerical solutions with regular reflection are obtained, for example, at $\beta_1 = 22^\circ$, although in the case of the implementation of the Mach reflection, the height of the main shock should be quite large (see, for example, the curve in Figure 3.11). In addition, at M=7.0 or M=8.0 and normal free-stream temperature, chemical reactions in a stoichiometric mixture of hydrogen and oxygen take place not only behind the main shock, but also behind the incident one.

The dependence $y_T(\beta_1)$ of the dimensionless height of the triple point on the flow deflection angle at the incident shock in a supersonic jet of a stoichiometric

mixture of hydrogen and air is shown in Figure 3.11 for Mach numbers M=7.0 (curves I and I') and M=8.0 (curves II and II'). In this case, curves I and II correspond to a mixture with a change in chemical composition and pulsed energy release at the main shock (the results of applying the model discussed in Point 3.2.1). Curves I' and II' correspond to the Mach reflection in a non-reacting mixture of the same chemical composition (the results of applying the model outlined in Subsection 2.3).

Thus, the flow emperature behind the main shock of the Mach reflection, formed in high-speed supersonic gas flows, is significantly higher than behind the incident and reflected shocks. For this reason, detonation effects (pulse energy release and changes in the chemical composition of the reactive gas mixture) are initiated, first of all, after the main (Mach) shock. An analysis of the resulting triple configurations using the Champan–Jouguet model of stationary detonation to the main (Mach) shock shows that a significant pulsed release of energy leads to a shift in the criteria of the oblique shock reflection transition. The shocks, which reflect regularly according to the classical theory, can reflect with the formation of a triple point, if we allow pulse energy release at the Mach shock.

The presented approximate analytical model for quickly calculating the parameters of the shock-wave structure of the flow of a reactive gas mixture with Mach reflection takes into account for the first time the change in chemical composition as well as pulsed energy release at the main shock. The primary results obtained when calculating a supersonic jet flow of a stoichiometric composition of methane-air, hydrogen-air or hydrogen-oxygen gas mixtures show not only an earlier occurrence of Mach reflection compared to a similar flow without chemical reactions, but also a significant increase in the geometric dimensions of the Mach stem.

3.3. On the possibility of applying the obtained results in the design of a combined jet engine

3.3.1. The idea of the combined engine

Traditional jet engines working on chemical fuel have largely reached the limit of their efficiency. There is an opinion that in order to significantly increase thrust and to improve efficiency, it is necessary to develop fundamentally new types of jet engines, including through a combination of thermodynamic cycles that underlie traditionally used designs.

The concept of a ramjet detonation engine was previously discussed in [86, 89, 150, 152, 153-156]. Despite the theoretical simplicity of the device, its operation in practice is difficult due to the formation of complex shock-wave structures with different temperatures of the gas mixture, as a result of which the chemical reactions (for example, at gas detonation) are excited only in the part of the flow that has the highest temperature [76, 79 , 92]. In particular, at a stationary Mach reflection, the temperature of the flow behind the main (Mach) shock is always (especially at high flow Mach numbers) significantly higher than behind the system of incident and reflected shocks. As a result, only part of the fuel-air mixture in the flow behind the Mach shock detonates first. It is this part of the flow that is advisable to use in the thermodynamic cycle of a ramjet detonation engine (so-called Fickett-Jacobs cycle).

In itsw turn, as theoretical and numerical studies of flows in supersonic air intakes show, the loss of total pressure (stagnation pressure) in the system of the incident shock and the reflected one is significantly less than in the Mach stem [76, 78, 79, 92]. This part of the flow is preferable for subsequent use in the combustion chamber of a “classical” ramjet engine (in the Brayton thermodynamic cycle).

Significant differences (at least in several times, but sometimes in tens of times) in total pressures and static temperatures of gas flows separated by tangential discontinuities behind triple configurations (TC) of different types (for example, with Mach reflection) are discussed in [9, 10] . The extreme properties of shock=wave systems and structures have been previously used to optimize the shapes of

streamlined bodies [118, 119], supersonic air intakes [80–83], in jet technologies and other applications of gas dynamics.

Based on the noted features of the emergence of shock-wave structures, the concept of a combined jet engine with detonation of a reactive gas mixture behind a Mach shock and using a flow behind an oblique reflected shock according to the scheme of a “classical” air-breathing engine was proposed in [86, 150, 152] .

The practical implementation of the idea of a combined engine requires the separation of streams with different values of temperature, stagnation pressure (and with different chemical compositions as chemical reactions are excited), separated by a slipstream beyond the triple point. The conditions for the existence of Mach reflection in the presence of exothermic reactions and changes in the chemical composition of the gas mixture at the main shock can be determined based on the data discussed in Subsection 3.1. The dimensions of the flow regions used in various thermodynamic cycles are determined based on the algorithm for calculating the triple point height discussed in Subsection 3.2. The same algorithm determines the shape of the sleepstream along which the streams should be divided.

Below are several examples of calculating an idealized (to the model of flow with Mach reflection in a narrowing channel between the wedges) model of the air intake of a prospective combined jet engine, both in the presence of pulsed energy release at the main shock and without it.

3.3.2. Flow without chemical reactions in an idealized air intake of a prospective engine

To analyze the operation of an idealized (model) air intake of a prospective propulsion system, it was necessary to obtain a series of gas-dynamic calculations in standard and most common computational fluid dynamics packages.

In the first calculation, the steady problem of planar of supersonic air flow into a narrowing channel between wedges is solved. Air was considered as a perfect gas, there were no chemical reactions.

During the numerical simulation of the process under consideration, the averaged Navier-Stokes equations [139] for a compressible perfect gas are used, which are represented by the following system (the averaging signs are omitted):

$$\begin{cases} \dfrac{\partial \rho}{\partial t} + \nabla \cdot (\rho \vec{u}) = 0 \\ \dfrac{\partial (\rho \vec{u})}{\partial t} + \nabla \cdot (\rho \vec{u}\vec{u}) = -\nabla p + \nabla \cdot (\tau_m + \tau_t) + \rho \vec{g} + \vec{F} \\ \dfrac{\partial (\rho E)}{\partial t} + \nabla \cdot (\rho \vec{u} H) = \nabla \cdot \left[\alpha_{эф} \nabla T - \sum_j h_j \vec{J}_j + \vec{u} \cdot (\tau_m + \tau_t) \right] + S_h \end{cases} \quad (3.48)$$

In (3.48), $\vec{u}$ is the averaged flow velocity vector with projections u, v и w on the coordinate axis, $\tau_m + \tau_t$ are the molecular and turbulent components of the viscous stress tensor, $E = C_v T + 0.5(u^2 + v^2 + w^2)$ is total gas energy, $H = E + p/\rho = C_p T + 0.5(u^2 + v^2 + w^2)$ is its total enthalpy, T is temperature, $C_v = (C_p - R)$ is the specific heat capacity of gas at constant volume, C_p is the specific heat capacity of gas at constant pressure, R is gas constant, $\rho \vec{g}$ is gravitational force per unit volume (here it is negligible), $\vec{F}$ are the external forces, $\alpha_{эф} = \alpha + \alpha_t$ is effective heat transfer coefficient, $\vec{J}_j$ is diffusion term, h_j is the enthalpy of formation of a component, S_h are quantitative characteristics of the energy source (allows us to take into account the process of formation and absorption of thermal energy).

The relationship between turbulent stresses and averaged flow parameters can be determined using various turbulence models. In those models, certain assumptions are made, on the basis of which the missing number of equations is introduced, which makes it possible to find all the unknowns. The work uses the tubulence model $k - \varepsilon$ Realizable [139].

The parameters of the free-stream flow correspond to the Mach number M=5 and the adiabatic index γ=1.4. The von Neumann criterion for the transition from a Mach reflection to a regular one for given flow parameters corresponds to the following parameters of the incident shock: deflection angle (the angle at the top of

the wedges shown in Figure 3.12,a-c) β_1=20.862˚, or intensity J_1=7.479, or slope angle (angle of incidence of the shock) σ_1= 0.796˚.

To obtain a Mach reflection with a sufficiently large height of the main shock, the angle at the wedge apex corresponded to the value β_1=31˚. The distance between the wedges was 200 mm, the internal section was 100 mm.

a)

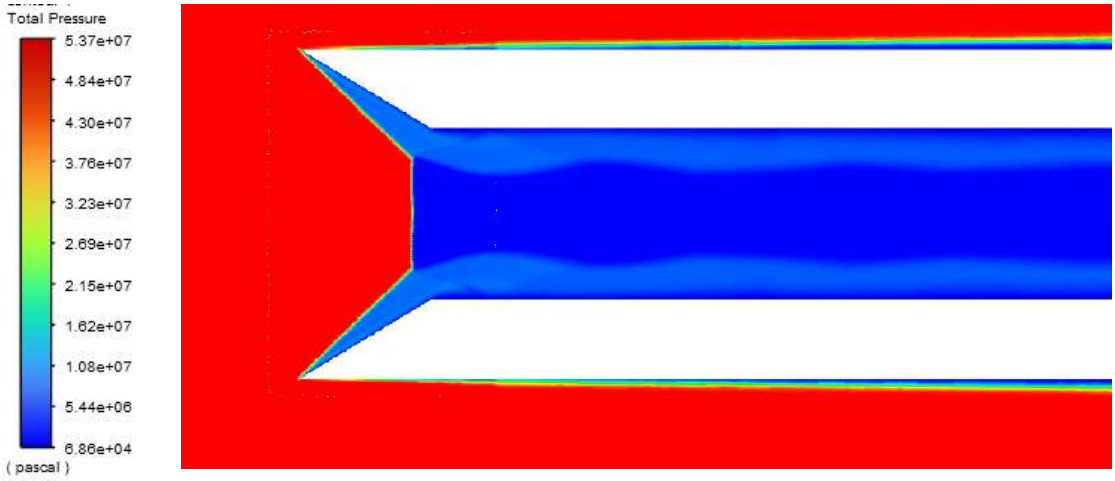

b)

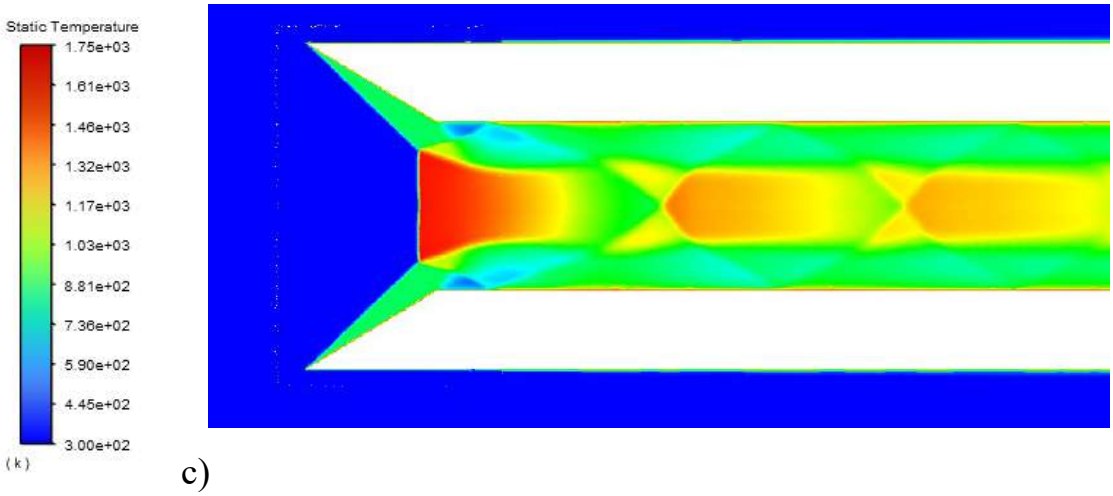

c)

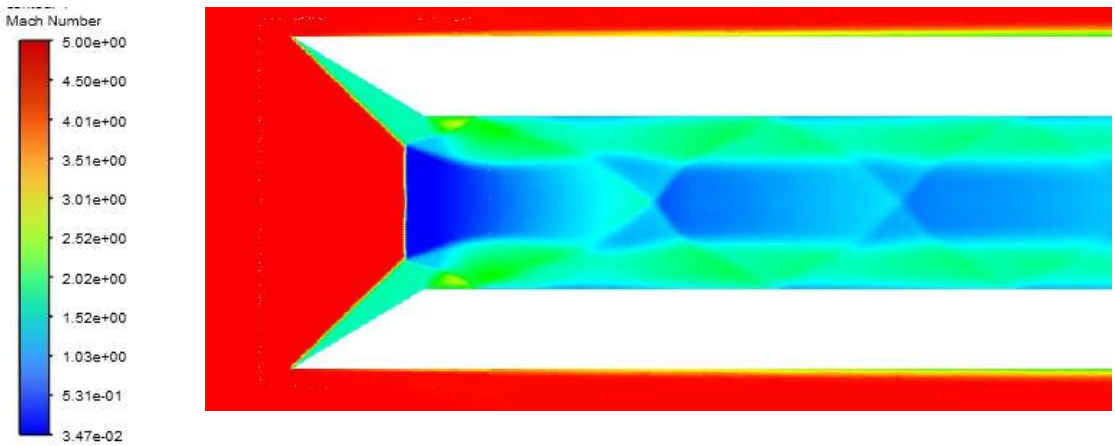

Figure 3.12,a-c. Field of stagnartion pressures (a), static temperatures (b) and Mach numbers (c) when air flows into the narrowing channel of a prospective engine

The resulting main, or Mach shock occupies approximately half of the inlet section. It can be noted that the flow behind the Mach shock resembles a quasi-one-dimensional flow through convergent-divergent nozzle with a transition from subsonic to supersonic flow ("virtual de Laval nozzle"). The inverse turn of the slipstream occurs under the influence of an expansion wave falling from the trailing edge of the wedge.

Figure 3.12a shows the distribution of total gas pressure (stagnation pressure of the gas flow). From the diagram above, it is obvious that the flow behind the reflected oblique shock has a stagnation pressure several times greater than the flow behind the "Mach stem" (main shock). Such a flow can be used with much greater efficiency in the combustion chamber of a "classical" ramjet engine.

According to Figure 3.12b, the gas temperature after the main (Mach) shock increases to 1750 K, which creates good conditions for ignition or detonation of the fuel-air mixture passing through that shock, compared to the flow overcoming the system of incident and reflected oblique shocks, where the gas temperature is noticeably lower. Thus, the flow in this part of the air intake can be used in a detonation engine cycle.

3.3.3. Influence of pulsed energy release on the parameters of the shock-wave structure

If a reactive fuel-air mixture is supplied to a strong shock, a sharp increase in temperature promotes its ignition and can initiate detonation.

In the example discussed in Figure 3.13 and 3.14, air flows in with the same Mach number (M=5) into a tapering channel formed by two wedges and similar to that discussed in Figure 3.12. After some time, when the calculation is established, fuel (a stoichiometric mixture of methane with air) is supplied into the central part of the channel through a slit (slot) 10 mm wide.

Figure 3.13 shows the dimensions of the input part and the calculation area. The calculation area is a rectangle with dimensions of 5 m by 10 m. All dimensions in Figure 3.13 are indicated in millimeters.

The problem is solved in a two-dimensional planar symmetric formulation.

A one-stage chemical reaction of combustion of a stoichiometric mixture of methane with air is simulated:

$$CH_4 + 2O_2 \Rightarrow 2H_2O + CO_2$$

To solve chemical reactions, a finite-rate chemistry model (Finite-Rate/No TCI) is used, which implies that the applied fluid dynamics package used takes into account the finite rate of chemical reactions, solving chemical kinetics equations using Arrhenius reaction rate constants, without attempting to additionally take into account the influence of turbulence.

Simulating the flow of a gas mixture, its multicomponence must be taken into account. The equation of the concentration change of each *i*-th component of the gas mixture is written as it follows:

$$\frac{\partial(\rho_i C_i)}{\partial t} + \nabla(\rho_i \vec{u} C_i) = -\nabla \vec{g}_i + \omega_i + S_i, \tag{3.49}$$

In (3.49), ω_i is the rate of formation of the *i*-th component, which is determined by the formula (3.50):

$$\omega_i = \mu_{mwi} \sum_{r=1}^{N_R} R_{ir}, \tag{3.50}$$

Here μ_{mwi} is the molar mass of the *i*-th component of the gas mixture, N_R is the number of chemical reactions, R_{ir} is the molar rate of formation/decay of the *i*-th component in the reaction r, which was calculated by equation (3.51) of chemical kinetics for the rate of formation of the *i*-th component during a nonequilibrium chemical reaction:

$$R_{ir} = \Gamma\left(\nu''_{jr} - \nu'_{jr}\right)\left(k_{fr}\prod_{j=1}^{N}\left[X_{jr}\right]^{\eta'_{jr}} - k_{br}\prod_{j=1}^{N}\left[X_{jr}\right]^{\nu''_{jr}}\right). \tag{3.51}$$

Here $\Gamma = \sum_{j}^{N} \gamma_{ir} X_j$ is a coefficient that takes into account the influence of third bodies on the rate of chemical reactions, ν''_{jr} is an exponent for product j in chemical reaction r, ν'_{jr} is a stoichiometric coefficient for the reagent j in reaction r, k_{fr} и k_{br} are, respectively, the rate constants of the direct and reverse reactions, X_{jr} is a molar concentration of component j in reaction r, η'_{jr} is an exponent for reagent j in reaction r, γ_{ir} is the efficviency of component j in reaction r as the third body.

The rate constants of the forward and reverse reactions are calculated according to the Arrhenius law:

$$k_{f,r} = A_r T^{\beta_r} e^{-E_r/RT}. \quad (3.52)$$

Here, A_r is the pre-exponential coefficient, β_r is the dimensionless exponent at the temperature T, E_r is the activation energy (J/kmol), R is the universal gas constant (J/kmol·K)

We used the combustion model Species Transport, Finite-Rate/No TCI, which was realized in CFD package ANSYS Fluent.

In the “Species Transport” model, the local mass of each of the reagents is calculated by solving the convection-diffusion equation (3.53):

$$\frac{\partial}{\partial t}(\rho Y_i) + \nabla \cdot (\rho \vec{v} Y_i) = -\nabla \cdot \vec{J_i} + R_i + S_i, \quad (3.53)$$

Here, R_i is the rate of additional production of reagent i during the chemical reaction, S_i is the rate of reagent production from the dispersed phase or the user-defined rate of reagent production. This equation is solved for N-1 reagents; N is the number of all reagents in the liquid phase included in the system to be solved. The mass of reagent N is equal to the difference between the total mass of the system and the mass of the other $N-1$ calculated reagents. In order to avoid numerical errors, it is recommended to set the n-th reagent to a substance with the maximum mass fraction in the system, for example, nitrogen for a reaction in which air is the oxidizer [26].

The diffusion of mass in turbulent flows is described by the equation

$$\vec{J}_i = -\left(\rho D_{i,m} + \frac{\mu_t}{Sc_t}\right)\nabla Y_i - D_{T,i}\frac{\nabla T}{T}, \tag{3.54}$$

where Sc_t is the turbulent Schmidt number, μ_t is the turbulent viscosity.

Density of the mixture:

$$\rho_{см} = \frac{P_{см}}{R_{см}T}. \tag{3.55}$$

Here, the pressure of the mixture

$$P_{см} = \sum_{i=1}^{n} P_i, \qquad M_{см} = \sum_{i=1}^{n} C_i P_i, \tag{3.56}$$

and $C_i = \rho_i / \rho_{см}$ is the mass concentration of the *i*-th component in mixture [11].

Thermodynamic enthalpy of the mixture:

$$i = \sum_{i=1}^{n} C_i \cdot i_i, \tag{3.57}$$

where $i_i = \int_{T_1}^{T_2} c_{p,i} \cdot dT$ is the enthalpy of the *i*-th component.

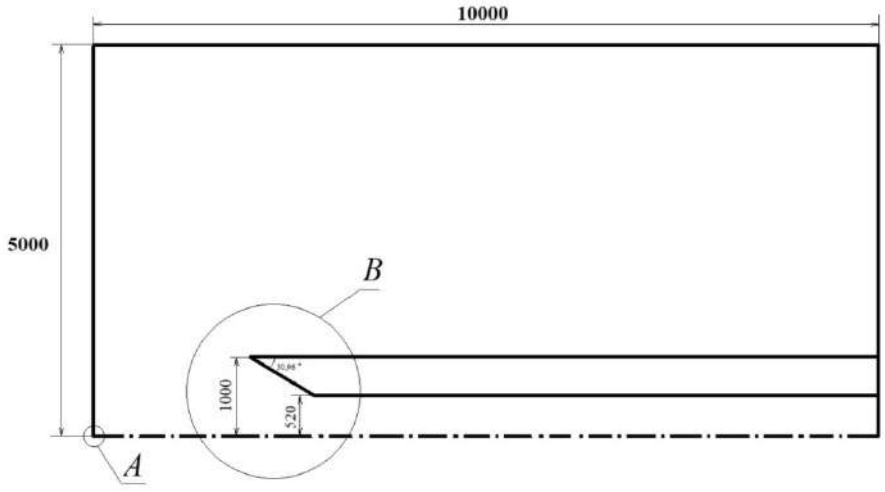

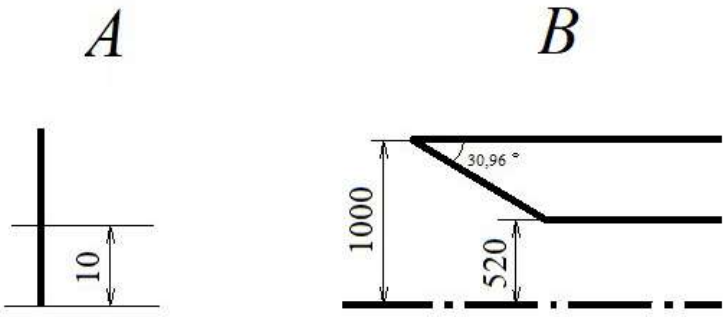

Figure 3.13 – Geometric parameters of the calculation area

The specific heat capacity $c_{p,i}$ of each *i*-th component is given according to a piecewise linear law as a function of temperature and pressure. Thus, the average specific heat of a gas mixture is calculated using the ratio

$$c_{p,i} = \sum_{i=1}^{n} C_i \cdot c_{p,i} . \tag{3.58}$$

Here, $c_{p,i}$ is the the specific isobaric heat capacity of each component [11].

The thermal conductivity λ_i of each *i*-th component is determined using the ratio from the kinetic theory of gases:

$$\lambda_i = \frac{15}{4}\frac{R_\mu}{M_i} \cdot \mu_i \left[\frac{4}{15}\frac{c_{p,i} M_i}{R_\mu} + \frac{1}{3} \right] \tag{3.59}$$

The thermal conductivity of the gas mixture is determined by the formula

$$\lambda_{см} = \sum_{i=1}^{n} \frac{X_i \lambda_i}{\sum_j X_i \varphi_{i,j}}, \tag{3.60}$$

X_i is the molar concentration of t *i*-th component; the parameter $\varphi_{i,j}$ was calculated using the ratio

$$\varphi_{i,j} = \frac{\left[1 + \left(\frac{\mu_i}{\mu_j} \right)^{1/2} \left(\frac{M_{w,i}}{M_{w,j}} \right)^{1/4} \right]^2}{\left[8 \left(1 + \frac{M_{w,i}}{M_{w,j}} \right) \right]^{1/2}} \tag{3.61}$$

The viscosity of each *i*-th component was calculated using Sutherland's formula:

$$\mu_i = \mu_{0i} \left(\frac{T}{T_0} \right)^{3/2} \frac{T_{норм} + S}{T + S} . \tag{3.62}$$

Here, μ_{0i} is the dynamic viscosity of the *i*-th component in normal conditions, *S* is the effective temperature (Sutherland's constant).

The dynamic viscosity of the gas mixture is calculated as follows:

$$\mu_{см} = \sum_{i=1}^{n} \frac{X_i \mu_i}{\sum_{j=1}^{m} X_j \varphi_{ij}} \tag{3.63}$$

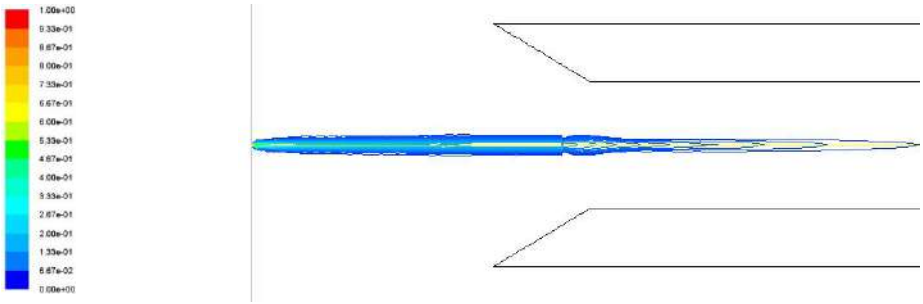

Figure 3.14. Distribution (mass fraction) of methane in the flow field

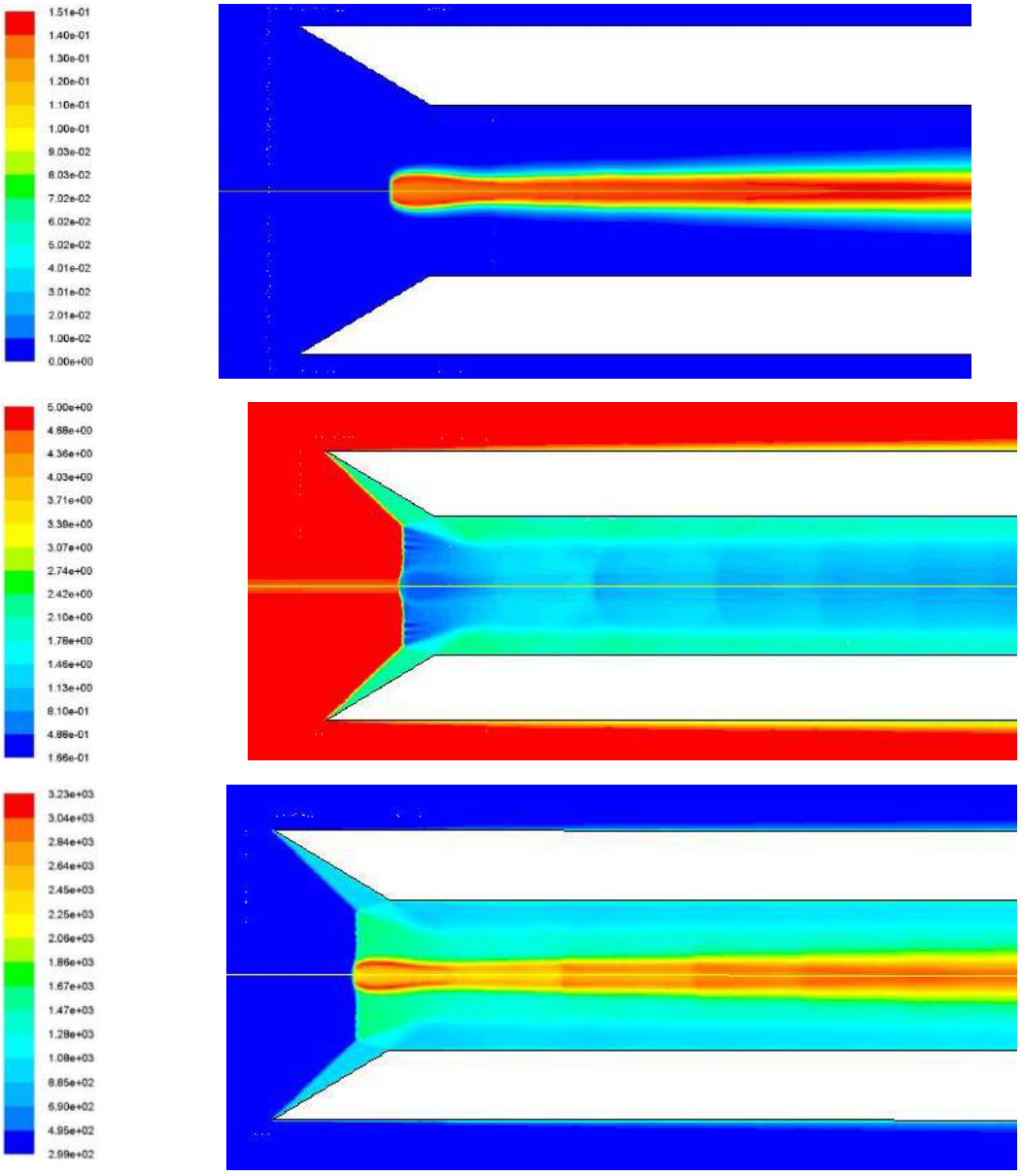

Figure 3.15. Distribution of the mass fraction of carbon dioxide (a), flow Mach numbers (b) and temperature, K (c) in the flow with the reactive mixture supplied to the central part of flowfield

Figure 3.14 shows the supply of a fuel-air mixture (a stoichiometric mixture of methane with air). The fuel is supplied from the right at an angle of 90° to the main

(Mach) shock, since in this way it is easier to check the possibility of its ignition. It can be seen that methane mixes with air as it moves to the air intake.

Figure 3.15,a-c shows the results of calculating the flowfield with fuel supplied to the central part of the Mach stem using the model (3.49-3.63). From the results obtained, it is clear that the mixture ignites at a strong shock, resulting in the formation of carbon dioxide (Figure 3.15a). In this case, the combustion surface does not come into contact with the channel body, and this fact has a beneficial effect on minimizing the cooling of the walls of the apparatus.

The flow pattern shown in Figure 3.15b-c shows that the main (Mach) shock bends upstream (to the left), which is not observed in Mach reflection without chemical reactions [1, 20, 44]. Thus, the main shock at Mach reflection becomes convex forward with respect to the oncoming flow – a fact that is not characteristic for flows of non-reacting gases which requires additional analysis using differential conditions of dynamic compatibility [1, 140-142].

Due to the relatively small size of the nozzle from which methane is supplied, there is a noticeable mixing of the mixture supplied through the slot with the surrounding air. The distance from the nozzle to the Mach shock is 2.6 m. At this distance, the methane flow dissipates, and an already mixed mixture with a methane concentration much lower than the stoichiometric one enters the main shock. However, the methane concentration is sufficient to initiate chemical reactions at the Mach stem.

The change in the position of the shock configuration is also noticeable. The reflected shock approaches the edge of the wedge, and the main shock moves upstream by 1 cm, thereby noticeably increasing in size.

Thus, it has been established through numerical simulation that the presence of energy release resulting from the excitation of chemical reactions at a strong Mach stem significantly increases the size of this shock (the height of the triple point), which is in good agreement with the materials in Subsection 3.2. This fact increases the significance of the flow region behind the Mach shock, which is proposed to use in the thermodynamic cycle of a ramjet detonation engine.

3.4. Conclusions to the Chapter 3

The pulsed energy release behind the main shock (Mach stem), as well as, to a much lesser extent, the decrease in the adiabatic index of the gas caused by physical and chemical effects, lead to an expansion of the region of existence of the Mach reflection, which, in the presence of energy release and physicochemical effects, can theoretically arise at all Mach numbers of supersonic flow. The possibility of energy release behind the main shock contributes to the Mach reflection of relatively weak incident shocks, which, in the absence of combustion, detonation and other physical and cchemical effects, reflect only regularly.

The presented thesis study proposes a new approximate analytical model for quickly calculating the parameters of the shock-wave structure of the flow of a reactive gas mixture with Mach reflection, which for the first time takes into account changes in the chemical composition and pulsed energy release at the main shock. The primary results obtained when calculating a supersonic jet flow of methane-air, hydrogen-air or hydrogen-oxygen gas mixture show not only an earlier occurrence of the Mach reflection compared to a similar flow without chemical reactions, but also a significant increase in the geometric dimensions of the main shock. Those primary results are confirmed by numerical simulation data.

In a number of works of the author of the dissertation and his supervisor, the idea of a combined ramjet engine which uses gas flows separated by slipstream behind the triple point of Mach reflection in different thermodynamic cycles was put forward. The development of such an engine is one of the possible practical applications of the results of this thesis study.

Conclusions

Research and optimization of shock-wave systems and structures using the mathematical apparatus of the modern theory of interaction of gas-dynamic discontinuities allows us to obtain theoretically important and practically valuable results.

In the presented dissertation study, an analysis of the shock-wave structures, that form at the reflection of oblique shocks, including under conditions of pulsed energy release and changes in the chemical composition of the gas at the main shock that occurs at Mach reflection, was carried out. A mathematical apparatus has been developed for quickly and accurately estimating the parameters of the resulting shock-wave structure and the integral characteristics of the flowfield as a whole.

For the regular shock reflection, analytical expressions have been obtained that describe structures with minimal dynamic and thermal loads on the affected object. The cubic equation in the variables “shock intensity – free-stream Mach number” determines both the parameters of the incident shocks with the minimum value of pressure and gas temperature behind them, and the angles of inclination of the obstacle at which the static pressure and temperature behind the point of regular reflection of a propagating shock wave of a given amplitude are minimal. Geometric optimization of the interaction of shock waves (in particular, blast ones) with obstacles can significantly reduce mechanical and thermal loads on structural elements.

For more complex shock-wave structures (in particular, triple shock-wave configurations with a negative slope angle of the reflected shock, which arise at irregular reflection in flows with high Mach numbers and a reduced adiabatic index), areas of solution ambiguity were identified. It has been established analytically and numerically that there is a wide range of problem parameters, within which for the same incident (branching) shock-wave the solutions for the following sturctures coexist:

- Mach reflection with subsonic flow after the main shock; the flow behind the reflected shock can be either supersonic or subsonic;

- regular reflection (as a rule, with a supersonic flow downstream the reflected shock);

- triple configuration of the third type, in most cases – with the subsonic flow after the resulting shock.

In addition, with similar problem parameters in real gas-dynamic devices, the formation of detached shocks, the formation of unsteady flows, as well as more complex and branched shock-wave configurations is not excluded. In particular, solutions corresponding to the formation of triple configurations of Mach reflection with a negative angle of inclination of the reflected shock are always ambiguous. Their realizability (as well as the stability of the emerging shock-wave structures) must be confirmed in each individual practically important case.

In the presented work, the conditions for the existence are identified and a parametric analysis is carried out for triple configurations of steady shocks that arise at Mach reflection with pulsed energy release and a change in the chemical composition of the gas mixture at the main shock. The cause of pulsed energy release and changes in chemical composition can be, for example, detonation phenomena excited by a strong increase in temperature at the main shock. The author of the study has shown analytically and numerically that the pulsed energy release behind the main (Mach) shock, as well as, to a much lesser extent, the decrease in the adiabatic index of the gas caused by real gas effects, lead to an expansion of the region of Mach reflectioexistence. The possibility of energy release after the main shock makes possible the Mach reflection of relatively weak shocks, which, in the absence of combustion, detonation and other physical and chemical effects, reflect only regularly.

Solutions to individual problems of interaction of gas-dynamic discontinuities and waves, previously obtained in the theory of interaction of stationary gas-dynamic discontinuities (solution for the triple configuration of Mach reflection, conjugation of a Prandtl-Meyer wave with a previous overtaking shock, counter shock and quasi-

one-dimensional flow, interaction of an incident centered or simple expansion wave with the slipstream, etc.), contributed to the development of a new analytical model of the shock-wave structure of a supersonic flow with Mach reflection. Based on the results obtained for a supersonic overexpanded jet or flow in a narrowing channel, we demonstrate its high accuracy, especially determining the size of the main shock (Mach stem).

The developed analytical model of the shock-wave structure of a supersonic flow with Mach reflection was generalized to the case of possible pulsed energy release at a Mach shock, as well as real gas effects that are significant for irregular reflection in flows with high Mach numbers. Thus, an approximate analytical model was obtained for quickly calculating the parameters of the shock-wave structure in the flow of a reactive gas mixture with Mach reflection, which for the first time takes into account the change in chemical composition and pulsed energy release at the main shock. The primary results obtained when calculating the supersonic flow of a methane-air, hydrogen-air or hydrogen-oxygen gas mixture show not only an earlier occurrence of the Mach reflection compared to a similar flow without chemical reactions, but also a significant increase in the geometric dimensions of the main shock. Those primary results are confirmed by numerical simulation data.

In a number of their studies, the author of the thesis and his supervisor put forward the idea of a combined ramjet engine using gas flows separated by a slipstream behind the triple point of Mach reflection in different thermodynamic cycles. In particular, the flow downstream the reflected shock, which has a relatively high stagnation pressure, is advisable, after further deceleration in a system of several shocks, to be used in the Brayton cycle of a classical ramjet engine. In the flow after the Mach shock, due to very high temperature values, detonation effects can be initiated, and it is more expedient to use this flow in the Fickett-Jacobs cycle of a ramjet detonation engine. The development of such an engine that combines the benefits of the advantages of two gas flows is one of the possible practical applications of the results of this dissertation study. It is easy to see that the developed analytical model of flows with Mach reflection in the presence of pulsed

energy release and changes in the chemical composition of the gas at the main shock can be used for the gas-dynamic design of such prospective devices.

From the point of view of theoretical gas dynamics, continuation of the ongoing research may include a complete parametric analysis of all types of triple shock-wave configurations with the possibility of pulsed energy release at individual shocks. In particular, it is necessary to analyze the ratios of the parameters of the flows formed behind the triple point and separated by the slipstream, and to identify triple configurations that are optimal for solving the assigned engineering problems. Of no less interest is the analysis of flowfield gradients in the vicinity of the triple point using differential conditions of dynamic compatibility.

In further studies of triple configurations with energy release and significant changes in the physical and chemical properties of the gas, the following should be taken into account:

- existence and development of more modern models of detonation transformations, which replaced the Chapman–Jouguet model applied here;

- a more complex nature of physical and chemical transformations at strong shocks, which is not always described with a sufficient degree of accuracy and reliability by the one-parameter model of the “effective adiabatic index” of the mixture downstream the main shock.

Bibliography

1. Adrianov A.L., Starykh A.L., Uskov V.N. Interference of Stationary Gasodynamic Discontinuities. Novosibirsk: Nauka, 1995. 180 p. (in Russian)

2. Omelchenko A.V. Non-Linear Extremal Problems of Gas Dynamics. Dr. Sci. (Phys & Math.) Thesis. Saint Petersburg: Saint Petersburg State University, 2002. 366 p.

3. Mostovykh P.S. The Theory of Shock-Wave Structures. Cand. Sci. (Phys & Math.) Thesis. Saint Petersburg: Saint Petersburg State University, 2012. 149 p.

4. Mach E. Über den Verlauf von Funkenwellen in der Ebene und im Raume // Sitzungsbr. Akad. Wiss. Wien. 1878. Vol. 78. Pp. 819-838. (in German)

5. Mach E., Salcher P. Optische Untersuchung der Luftstrahlen // Sitzungsbr. Akad. Wiss. Wien. 1889. Vol. 98. Pp. 1303-1309. (in German)

6. Reichenbach H. Contribution of Ernst Mach to fluid mechanics // Annual Review of Fluid Mechanics. 1983. Vol. 15. Pp. 1-28.

7. Krehl P.O.K. Hystory of Shock Waves, Explosions and Impact. A Chronological and Biographical Reference. Springer Science & Business Media, 2008. 1288 p.

8. von Neumann J. Oblique reflection of shock waves // Collected Works. London: Pergamon Press, 1963. Vol. 6. Pp. 238-299.

9. Courant R., Friedrichs K.O. Supersonic Flow and Shock Waves. New York: Springer, 1976. 464 p.

10. Landau L.D., Lifshitz E.M. Course of Theoretical Physics. Vol. 6. Fluid Mechanics. Oxford: Pergamon Press, 1987. 552 p.

11. Zel'dovich Ya.B. Theory of Shock Waves and Introduction to Gas Dynamics. New York: Academic Press, 1967. 231 p.

12. Zel'dovich Ya.B., Raizer Y.P. Physics of Shock Waves and High-Temperature Hydrodynamic Phenomena. Vol. II. New York: Academic Press, 1967. 478 p.

13. Pack D.C. The reflection and diffraction of shock waves // Journal of Fluid Mechanics. 1964. Vol. 18. Issue 4. Pp. 549-576.

14. Griffith W.C. Shock waves // Journal of Fluid Mechanics. 1981. Vol. 106. Pp. 81-101.

15. Hornung H.G. Regular and Mach reflection of shock waves // Annual Review of Fluid Mechanics. 1986. Vol. 18. Pp. 33-58.

16. Ben-Dor G., Takayama K. The phenomena of shock wave reflection – a review of unsolved problems and future research needs // Shock Waves. 1992. Vol. 2. Issue 4. Pp. 211-223.

17. Arutiutian G.M., Karchevsky L.V. Reflected Shock Waves. Moscow: Mashinostroenie, 1973. 376 p. (in Russian)

18. Bazhenova T.V., Gvozdeva L.G. Unsteady Interactions of Shock Waves. Moscow: Nauka, 1977. 274 p. (in Russian)

19. Lyakhov V.N., Podlubny V.V., Titarenko V.V. Effect of Shock Waves and Jet Flows of Structural Elements. Moscow: Mashinostroenie, 1989. 392 p. (in Russian)

20. Ben-Dor G. Shock Wave Reflection Phenomena. 1st Edition. NewYork: Springer, 1992. 307 p.

21. Hornung H.G., Oertel H., Sandeman R.J. Transition to Mach reflexion of shock waves in steady and pseudosteady flow with and without relaxation // Journal of Fluid Mechanics. 1979. Vol. 90. Part 3. Pp. 541-560.

22. Henderson L.F., Lozzi A. Experiments on transition to Mach reflection // Journal of Fluid Mechanics. 1975. Vol. 68. Part 1. Pp. 139-155.

23. Henderson L.F., Lozzi A. Further experiments on transition to Mach reflection // Journal of Fluid Mechanics. 1979. Vol. 94. No. 3. Pp. 541-560.

24. Hornung H.G., Robinson M.I. Transition from regular to Mach reflection of shock waves. Part 2: The steady-flow criterion // Journal of Fluid Mechanics. 1982. Vol. 123. No. 1. Pp. 155-164.

25. Chpoun A., Ben-Dor G. Numerical confirmation of the hysteresis phenomenon in the regular to Mach reflection transition in steady flows // Shock Waves. 1995. Vol. 5. Issue 4. Pp. 199-204.

26. Ivanov M.S., Gimelshein S.F., Beylich A.E. Hysteresis effect in stationary reflection of shock waves // Physics of Fluids. 1995. Vol. 7. Issue 4. Pp. 685-687.

27. Ben-Dor G., Elperin T., Li H., Vasiliev E. Downstream pressure induced hysteresis in the regular ↔ Mach reflection transition n steady flows // Physics of Fluids. 1997. Vol. 9. Issue 10. Pp. 3096-3098.

28. Ivanov M.S., Gimelshein S.F., Markelov G.N. Statistical Simulation of the Transition between Regular and Mach reflection in Steady Flows // Computer Math. Applic. 1998. Vol. 35. No. 1/2. Pp. 113-125.

29. Ivanov M.S., Markelov G.N., Kudryavtsev A.N., Gimelshein S.F. Numerical Analysis of Shock Wave Reflection Transition in Steady Flows // AIAA Journal. 1998. Vol. 36. No. 11. Pp. 2079-2086.

30. Gimelshein S.F., Markelov G.N., Ivanov M.S. Real Gas Effects on the Transition Between Regular and Mach Reflection in Steady Flows // AIAA Paper 98-0877. 9 p.

31. Kudryavtsev A.N., Khotyanovsky D.V., Ivanov M.S., Hadjadj A., Vandromme D. Transition Between Regular and Mach Reflections in Plane Overexpanded Jets // AIAA Paper 2002-0977. 11 p.

32. Hadjadj A., Kudryavtsev A.N., Ivanov M.S. Numerical Investigation of Shock-Reflection Phenomena in Overexpanded Supersonic Jets // AIAA Journal. 2004. Vol. 42. No. 3. Pp. 570-577.

33. Shimshi E., Ben-Dor G., Levy A. Viscous simulation of shock-reflection hysteresis in overexpanded planar nozzles // Journal of Fluid Mechanics. 2009. Vol. 635. Pp. 189-206.

34. Ivanov M.S., Vandromme D., Fomin V.M., Kudryavtsev A.N., Hadjadj A., Khotyanovsky D.V. Transition between regular and Mach reflection of shock waves: new numerical and experimental results // Shock Waves. 2001. Vol. 11. Pp. 199-207.

35. Chpoun A., Passerel D., Li H., Ben-Dor G. Reconsideration of the oblique shock wave reflection in steady flows. I. Experimental investigation // Journal of Fluid Mechanics. 1995. Vol. 301. Pp. 37-50.

36. Ivanov M.S., Kudryavtsev A.N., Nikiforov S.B., Khotyanovsky D.V., Pavlov A.A. Experiments on shock wave reflection transition and hysteresis in low-noise wind tunnel // Physics of Fluids. 2003. Vol. 15. Pp. 1807-1810.

37. Mouton C.A., Hornung H.G. Experiments on the mechanism of inducing transition between regular and Mach reflection // Physics of Fluids. 2008. Vol. 20. Paper No. 126103. 11 p.

38. Skews B.W. Aspect ratio effects in wind tunnel studies of shock wave reflection transition // Shock Waves. 1997. Vol. 8. Pp. 373-383.

39. Sudani N., Sato M., Karasawa T., Noda J., Tate A., Watanabe M. Irregular effects on the transition from regular to Mach reflection of shock waves in wind tunnel flows // Journal of Fluid Mechanics. 2002. Vol. 459. Pp. 167-185

40. Mouton C.A., Hornung H.G. Mach Stem Height and Growth Rate Predictions // AIAA Journal. 2007. Vol. 45. No. 8. Pp. 1977-1987.

41. Hornung H.G. On the stability of steady-flow regular and Mach reflection // Shock Waves. 1997. Vol. 7. Pp. 123-125.

42. Ben-Dor G. Hysteresis phenomena in shock wave reflection in steady flows // Journal of Materials Processing Technology. 1999. Vol. 85. Pp. 15-19.

43. Ben-Dor G., Ivanov M., Vasilev E., Elperin T. Hysteresis processes in the regular reflection ↔ Mach reflection transition in steady flows // Progress in Aerospace Sciences. 2002. Vol. 38. Pp. 347-387.

44. Ben-Dor G. Shock Wave Reflection Phenomena. 2nd Edition. Berlin – Heidelberg – NewYork: Springer, 2007. 342 p.

45. Teshukov V.M. Stability of regular shock wave reflection // Journal of Applied Mechanics and Technical Physics. 1989. Vol. 30. Pp. 189-196.

46. Ivanov M.S., Kudryavtsev A.N., Khotyanovskii D.V. Numerical Simulation of the Transition between the Regular and Mach Reflection under the Action of Local Perturbations // Doklady Physics. 2000. Vol. 45. No. 7. Pp. 353-357.

47. Kudryavtsev A.N., Khotyanovsky D.V., Ivanov M.S., Hadjadj A., Vandromme D. Numerical investigations of transition between regular and Mach reflections caused by free-stream disturbances // Shock Waves. 2002. Vol. 12. Pp. 157-165.

48. Henderson L.F., Menikoff R. Triple-shock entropy theorem and its consequences // // Journal of Fluid Mechanics. 1995. Vol. 366. Pp. 179-210.

49. Bulat P.V. Stationary Gasodynamic Discontinuities and Shock-Wave Structures. Dr. Sci. (Phys & Math.) Thesis. Saint Petersburg: Saint Petersburg State University, 2017. 361 p.

50. Bulat P.V. Rearrangements and transformations of shock-wave structures under the interference of oblique shocks under conditions of ambiguity and hysteresis // Aerospace Engineering and Technology. 2023. Vol. 1. No. 2. Pp. 12–32.

51. Ben-Dor G., Elperin T., Li H., Vasiliev E., Chpoun A., Zeitoun D. Dependence of Steady Mach Reflections on the Reflecting-Wedge Trailing-Edge Angle // AIAA Journal. 197. Vol. 35. No. 11. Pp. 1780-1782.

52. Azevedo D.J., Liu C.S. Engineering approach to the prediction of shock patterns in bounded high-speed flows // AIAA Journal. 1993. Vol. 31. No. 1. Pp. 83-90.

53. Medvedev A.E., Fomin V.M. Approximate analytical calculation of the Mach configuration of steady shock waves in a plane constricting channel // Journal of Applied Mechanics and Technical Physics. 1998. Vol. 39. No. 3. Pp. 369-374.

54. Schotz M., Levy A., Ben-Dor G., Igra O. Analytical prediction of the wave configuration size in steady Mach reflection // Shock Waves. 1997. Vol. 7. Pp. 363-372.

55. Li H., Ben-Dor G. A parametric study of Mach reflection in steady flows // Journal of Fluid Mechanics 1997. Vol. 341. Pp. 101-125.

56. Omel'chenko A.V., Uskov V.N., Chernyshev M.V. An Approximate Analytical Model of Flow in the First Barrel of an Overexpanded Jet // Technical Physics Letters. 2003. Vol. 29. No. 3. Pp. 243-245.

57. Bai C.-Y., Wu Z.-N. Size and shape of shock waves and slipline for Mach reflection in steady flow // Journal of Fluid Mechanics. 2017. Vol. 818. Pp. 116-140.

58. Choe S.-G. A method for predicting Mach stem height in steady flows // Proceedings of the Institution of Mechanical Engineers. Part G: Journal of Aerospace Engineering. 2021. Vol. 236. Issue 1. 095441002110015. 8 p.

59. Ivanov M.S., Ben-Dor G., Elperin T., Kudryavtsev A.N., Khotyanovsky D.V. Flow-Mach-Number-Variation-Induced Hysteresis in Steady Shock Wave Reflections // AIAA Journal. 2001. Vol. 39. No. 5. Pp. 972-974.

60. Li H., Ben-Dor G. Oblique Shock – Expansion Fan Interaction – Analytical Solution // AIAA Journal. 1996. Vol. 43. No. 2. Pp. 418-421.

61. Meshkov V.R., Omel'chenko A.V., Uskov V.N. The interaction of shock wave with counter rarefaction wave // Vestnik Sankt-Peterburgskogo Universiteta. Ser. 1. Matematika Mekhanika Astronomiya. 2002. No. 2. Pp. 101-109. (in Russian)

62. Chernyshov M.V. Interaction of the Elements of Shock-Wave Systems between Themselves and with Various Surfaces. Cand. Sci. (Phys & Math.) Thesis. Saint Petersburg: Baltic State University "VOENMEH", 2002. 173 p. (in Russian)

63. Silnikov M.V., Chernyshov M.V., Uskov V.N. Analytical solutions for Prandtl-Meyer wave – oblique shock overtaking interaction // Acta Astronautica. 2014. Vol. 99. Pp. 175-183.

64. Uskov V.N., Chernyshov M.V. Conjugation of Prandtl-Meyer wave with quasi-one-dimensional flow region // Mathematical Models and Computer Simulations. 2003. Vol. 15. No. 6. Pp. 111-119. (in Russian)

65. Silnikov M.V., Chernyshov M.V. The interaction of Prandtl-Meyer wave and quasi-one-dimensional flow region // Acta Astronautica. 2015. Vol. 109. Pp. 248-253.

66. Tao Y., Liu W., Fan X., Xiong B., Yu J., Sum M. A study of the asymmetric shock reflection configurations in steady flows // Journal of Fluid Mechanics. 2017. Vol. 825. Pp. 1-15.

67. Roy S., Gopalapillai R. An analytical model for asymmetric Mach reflection configuration in steady flows // Journal of Fluid Mechanics. 2019. Vol. 863. Pp. 242-268.

68. Lin J., Bai C.-Y., Wu Z.-N. Study of asymmetrical shock wave reflection in steady supersonic flow // Journal of Fluid Mechanics. 2019. Vol. 864. Pp. 848-875.

69. Gvozdeva L.G., Gavrenkov S.A. Formation of triple shock configurations with negative reflection angle in steady flow // Technical Physics Letters. 2012. Vol. 38. Issue 4. Pp. 372-374.

70. Gavrenkov S.A., Gvozdeva L.G. Numerical Investigation of the Onset of Instability of Triple Shock Configurations in Steady Supersonic Gas Flows // Technical Physics Letters. 2012. Vol. 38. No. 6. Pp. 587-589.

71. Gvozdeva L.G., Silnikov M.V., Gavrenkov S.A. Triple shock configurations with negative angle of reflection // Acta Astronautica. 2015. Vol. 116. Pp. 36-42.

72. Gvozdeva L., Gavrenkov S., Nesterov A. A study of slipstreams in triple shock wave configurations // Shock Waves. 2015. Vol. 25. Issue 3. Pp. 283-291.

73. Gvozdeva L.G., Gavrenkov S.A. New configuration of irregular reflection of shock waves // Progress in Flight Physics. 2015. Vol. 7. Pp. 437-452.

74. Azarova O.A., Gvozdeva L.G. Unsteady Triple-Shock Configurations and Vortex Contact Structures Initiated by the Interaction of an Energy Source with a Shock Layer in Gases // Technical Physics Letters. 2016. Vol. 42. No. 8. Pp. 799-803.

75. Sil'nikov M.V., Chernyshov M.V., Gvozdeva L.G. Analytic Description of the Domain of Existence of Triple Configurations with a Negative Slope of Reflected Shock // Technical Physics. 2016. Vol. 61. No. 11. Pp. 1633-1637.

76. Chernyshov M.V. Extreme Triple Configurations with Negative Slope Angle of the Reflected Shock // Russian Aeronautics. 2019. Vol. 62. No. 2. Pp. 259-266.

77. Shoev G.V., Ivanov M.S. Numerical study of shock wave interaction in steady flows of a viscous heat-conducting gas with a low ratio of specific heats // Thermophysics and Aeromechanics. 2016. Vol. 23. No. 3. Pp. 343-364.

78. Tao Gang. Triple Configurations of Steady Shocks in Non-Uniform Supersonic Streams. Cand. Sci. Thesis (Engr.). Saint Petersburg: Baltic State Technical University "VOENMEH", 2000. 162 p. (in Russian)

79. Uskov V.N., Chernyshov M.V. Special and extreme triple shock-wave configurations // Journal of Applied Mechanics and Technical Physics. 2006. Vol. 47. No. 4. Pp. 492-504.

80. Petrov G.I., Ukhov E.P. Calculation of pressure recovery during the transition from supersonic to subsonic flow with various systems of planar shock waves // Technical Papers of Research Institute No. 1. 1947. No. 1. Pp. 1-7. (in Russian)

81. Petrov G.I. Aeromechanics of Large Speeds and Space Research. Collected Works. Moscow: Nauka, 1992. 306 p. (in Russian)

82. Hermann R. Supersonic inlet diffusers and introduction to internal aerodynamics. Minneapolis: Minneapolis-Honeywell Regulator Company, 1956. 378 p.

83. Omel'chenko A.V., Uskov V.N. Optimal Shock Wave Systems // Fluid Dynamics. 1995. Vol. 30. No. 6. P. 905–911.

84. Bulat P.V., Ilina E.E. The problem of creating detonation engine – thermodynamic cycle // Fundamental Research. Vol. 10. No. 10. Pp. 2143-2146. (in Russian)

85. Bulat P.V., Denissenko P.V., Volkov K.N. Trends in the development of detonation engines for high-speed aerospace aircrafts and the problem of triple configurations of shock waves. Part I. Research of detonation engines // Scientific and Technical Journal of Information Technologies, Mechanics and Optics. 2016. Vol. 16. No. 1. Pp. 1-21. (in Russian)

86. Ivanov M.S., Kudrjavtsev A.N., Trotsjuk A.V., Fomin V.M. Method of organization of detonation combustion chamber of supersonic ramjet engine. Patent on invention RU 2285143 C2, Russian Federation. Federal Service for Intellectual Property, 2006 (effective date for property rights: December 10, 2004). 8 p. (in Russian)

87. Li H., Ben-Dor G., Grönig H. Analytical Study of the Oblique Reflection of Detonation Waves // AIAA Journal. 1997. Vol. 35. No. 11. Pp. 1712-1720.

88. Medvedev A.E. Reflection of an oblique shock wave in a reacting gas with a finite relaxation-zone length // Journal of Applied Mechanics and Technical Physics. 2001. Vol. 42. Issue 2. Pp. 211-218.

89. Trotsyuk A.V., Kudryavtsev A.N., Ivanov M.S. Mach Reflection and Detonation Waves in Steady Supersonic Chemically Reacting Flows // Proceedings of International Conference on Recent Advances in Space Technologies (IEEE Cat. No.03EX743). 2003. Pp. 495-503.

90. Trotsyuk A.V., Kudryavtsev A.N., Ivanov M.S. Numerical study of standing detonation waves // Journal of Computational Technologies. 2006. Vol. 11. Issue 52. Pp. 37-44. (in Russian)

91. Denisov Yu.N. Gas Dynamics of Detonation Structures. Moscow: Mashinostroenie, 1989. 176 p. (in Russian)

92. Chernyshov M.V., Gvozdeva L.G. Triple Configurations of Steady and Propagating Shocks // Russian Aeronautics. 2022. Vol. 65. No. 2. Pp. 319-344.

93. Ryzhov O.S., Khristianovich S.A. On nonlinear reflection of weak shock waves // Journal of Applied Mathematics and Mechanics. 1958. Vol. 22. No. 5. Pp. 826-843.

94. Loytsiansky L.G. Fluid Mechanics. Moscow: Drofa, 2003. 840 p. (in Russian)

95. Cherny G.G. Gas Dynamics. Moscow: Nauka, 1988. 424 p. (in Russian)

96. Henderson L.F. Exact Expressions for Shock Reflection Transition Criteria in a Perfect Gas // ZAMM – Journal of Applied Mathematics and Mechanics / Zeitschrift für Angewandte Mathematik und Mechanik. 1982. Vol. 62. No. 6. Pp. 258-261.

97. von Wuest W. Zur Theorie des gegabelten Verdichtungsstoßes // Zeitschrift für Angewandte Mathematik und Mechanik (ZAMM). 1948. Vol. 28. Issue 3. Pp. 73-80.

98. Kawamura R., Saito H. Reflection of shock waves – 1. Pseudo-stationary case // Journal of the Physical Society of Japan. 1956. Vol. 11. No. 5. Pp. 584-592.

99. Balagansky I.A., Merzhievsky L.A. The Effect of Weapons of Destruction and Ammunition. Novosibirsk: Novosibirsk State Technical University, 2004. 408 p. (in Russian)

100. Silnikov M.V., Mikhaylin A.I. Protection of flying vehicles against blast loads // Acta Astronautica. 2014. Vol. 97. Issue 1. P. 30-37.

101. Mölder S. Particular conditions for the termination of regular reflection of shock waves // Canadian Aeronautics and Space Institute Transactions. 1979. Vol. 25. Pp. 44–49.

102. Ben-Dor G., Takayama K. Application of Steady Shock Polars to Unsteady Shock Wave Reflections // AIAA Journal. 1985. Vol. 24. No. 4. Pp. 682-684.

103. Silnikov M.V., Chernyshov M.V., Mikhaylin A.I. Blast wave parameters at diminished ambient pressure // Acta Astronautica. 2015. Vol. 109. Pp. 235-240.

104. Bulat P.V., Silnikov M.V., Chernyshev M.V. Spherical Shock Wave – 2D Surface Interaction // Research Journal of Applied Sciences, Engineering and Technology. 2015. Vol. 9. No. 6. Pp. 428-433.

105. Gelfand B.E., Silnikov M.V. Barothermal Action of Blasts. Saint Petersburg: Asterion, 2006. 658 p. (in Russian)

106. Vasilev E. Four-wave scheme of weak Mach shock wave reflection under von Neumann paradox conditions // Fluid Dynamics. 1999. Vol. 34. No. 3. Pp. 421-427.

107. Hekiri H., Emanuel G. Shock wave triple point morphology // Shock Waves. 2011. Vol. 21. No. 6. Pp. 511-521.

108. Hekiri H., Emanuel G. Structure and morphology of a triple point // Physics of Fluids. 2015. Vol. 27. Issue 5. Article number 056102.

109. Henderson L.F. On the confluence of three shock waves in a perfect gas // Aeronautical Quarterly. 1964. Vol. 15. Pp. 181-197.

110. Gounko Yu.P. Patterns of steady axisymmetric supersonic compression flows with a Mach disk // Shock Waves. 2017. Vol. 27. Issue 3. Pp. 495-506.

111. Sedov L.I., Cherny G.G. Averaging of non-uniform gas streams in channels // Theoretical Hydromechanics. 1954. Vol. 12. Issue 4. Pp. 17-30. (in Russian)

112. Grib A.A., Ryabinin A.G. Approximate integration of the equations of steady supersonic gas flow // Dokl. Akad. Nauk SSSR. 1955. Vol. 100. Issue 3. Pp. 425-428. (in Russian)

113. Cherny G.G. Gas Flows with Large Supersonic Velocity. Moscow: FIZMATGIZ, 1959. 220 p. (in Russian)

114. Hayes W.D., Probstein R.F. Hypersonic Flow Theory. New York, London: Academic Press, 1959. 464 p.

115. Katskova O.N., Naumova I.N., Shmyslevsky Yu.D., Shulinshina N.P. Experience in Calculating Planar and Axisymmetric Supersonic Gas Flows by the Method of Characteristics. Moscow: Computational Center of the Academy of Sciences of the USSR, 1961. 60 p. (in Russian)

116. Vorozhtsov E.V., Yanenko N.N. Methods of Localization of Singularities in the Numerical Solution of Problems of Gas Dynamics. Novosibirsk: Nauka, 1985. 224 p. (in Russian)

117. Ben-Dor G. Reconsideration of the State-of-the-Art of the Shock Wave Reflection Phenomena in Steady Flows // JSME International Journal. Series B. 1995. Vol. 38. No. 3. Pp. 325-334.

118. Omel'chenko A.V., Uskov V.N. Maximum turning angles of a supersonic flow in shock-wave systems // Fluid Dynamics. 1998. Vol. 33. Issue 3. Pp. 419-426.

119. Chernyshov M.V. Theoretical analysis of shock wave systems on a plate with a shield in a supersonic flow // Bulletin of Young Scientists. Ser. Applied mathematics and mechanics. 2000. Vol. 3. No. 2. P. 105-110. (in Russian)

120. Uskov V.N., Chernyshov M.V. Extreme shockwave systems in problems of external supersonic aerodynamics // Thermophysics and Aeromechanics. 2014. Vol. 21. No. 1. Pp. 15-30.

121.Omel'chenko A.V., Uskov V.N. An optimal shock-expansion system in a steady gas flow // Journal of Applied Mechanics and Technical Physics. 1997. Vol. 38. Issue 2. Pp. 204-210.

122.Omel'chenko A.V., Uskov V.N. Optimal shock-wave systems under constraints on the total flow turning angle // Fluid Dynamics. 1996. Vol. 31. Issue 4. Pp. 597-603.

123. Azarova O.A., Gvozdeva L.G. Contron of triple-shock configurations and vortex structures forming in high speed flows of gaseous media past an AD body under the action of external energy sources // Aerospace. 2017. Vol. 4. No. 1. 9 p.

124. Azarova O.A. Numerical experiments on modelling of steady-state structures in supersonic flows with asymmetric energy supply // Computational Mathematics and Mathematical Physics. 2010. Vol. 50. No. 10. Pp. 1746-1759.

125. Uskov V.N., Mostovykh P.S. Triple configurations of travelling shock waves in inviscid gas flows // Journal of Applied Mechanics and Technical Physics. 2008. Vol. 49. Issue 3. Pp. 347-353.

126. Uskov V.N., Mostovykh P.S. The flow gradients in the vicinity of a shock wave for a thermodynamically imperfect gas // Shock Waves. 2016. Vol. 26. Issue 6. Pp. 693-708.

127. Uskov V.N., Chernyshov M.V. Stationary Mach configurations, their features and optimality // Problems of Defense Engineering. 2008. Issue 11-12. Pp. 22-25. (in Russian).

128. Li J., Ning J., Le J.H.S. Mach reflection of ZDN detonation wave // Shock Waves. 2015. Vol. 25. Issue 3. Pp. 293-304.

129. Jing T., Ren H., Li J. Onset of the Mach reflection of Zel'dovich – von Neumann – Döring detonations // Entropy. 2021. Vol. 23. Issue 3. Paper No. 314. Pp. 1-20.

130. Smirnov N.N., Betelin V.B., Nikitin V.F., Phylippov Yu.G., Koo J. Detonation engine fed by acetylene-oxygen mixture // Acta Astronautica. 2014. Vol. 104. Pp. 134-146.

131. Smirnov N.N., Penyazkov O.G., Sevrouk K.L., Nikitin V.F., Stamov L.I., Tyurenkova V.V. Detonation onset following shock wave focusing // Acta Astronautica. 2017. Vol. 135. Pp. 114-130.

132. Bulat P.V., Volkov K.N. Detonation jet engine. Part I – Thermodynamic cycle // International Journal of Environmental and Science Education. 2016. Vol. 11. Issue 12. Pp. 5009-5019.

133. Bulat P.V., Volkov K.N. Detonation jet engine. Part II – Construction features // International Journal of Environmental and Science Education. 2016. Vol. 11. Issue 12. Pp. 5020-5033.

134. Schepanovsky V.A. Gas-Dynamic Design. Novosibirsk: Nauka, 1991. 200 p. (in Russian)

135.Schepanovsky V.A., Gutov B.I. Gas-Dynamic Design of Supersonic Air Intakes. Novosibirsk: Nauka, 1993. 228 p. (in Russian)

136. Averenkova G.I., Ashratov E.A., Volkonskaya T.G., et al. Supersonic Flow of Ideal Gas. Part 2. Moscow: Moscow State University, 1971. 170 p. (in Russian)

137. Lighthill M.J. Higher Approximations. In book: General Theory of High Speed Aerodynamics. Princeton University Press, 1954. Pp. 345-489.

138. Trotsyuk A.V., Kudryavtsev A.N., Ivanov M.S. Numerical study of standing detonation waves // Journal of Computational Technologies. 2006. Vol. 11. No. 52. Pp. 37-44. (in Russian)

139. Korkodinov Ia.A. The review of set of k-ε models for modelling turbulence // Bulletin PNPU. Mechanical Engineering, Materials Science. 2013. Vol. 15. No. 2. Pp. 5-16. (in Russian)

140. Rusanov V.V. Derivatives of Gasodynamic Functions After the Curved Shock Waves. Moscow: Keldysh Institute for Applied Mathematics RAS, 1973. 18 p. (in Russian)

142. Emanuel G. Shock Waves Dynamics: Derivatives and Related Topics. Boca Raton: CRC Press, 2012. 232 p.

142. Emanuel G. Analytical extension of curved shock theory // Shock Waves. 2018. Vol. 28. Issue 2. Pp. 417-425.

Appendix A

Publications on the topic of the dissertation

Publications in publications recommended by the Higher Attestation Commission of the Ministry of Education and Science of the Russian Federation, as well as indexed in the international scientific citation databases SCOPUS and Web of Science

143. Chernyshov M.V., Savelova K.E. An Approximate Analytical Model of Jet Flow with Mach Reflection and Pulsed Energy Supply at the Main Shock // Russian Aeronautics. 2023. Vol. 66. No. 1. Pp. 51-63.
144. Chernyshov M.V., Kapralova A.S., Savelova K.E. Ambiguity of solution for triple configurations of stationary shocks with negative reflection angle // Acta Astronautica. 2021. Vol. 179. Pp. 382-390. (SCOPUS Q1, WoS Q1)
145. Chernyshov M.V., Savelova K.E., Kapralova A.S. Approximate Analytical Models of Shock-Wave Structure at Steady Mach Reflection // Fluids. 2021. Vol. 6. Issue 9. Paper No. 305. 18 p. (SCOPUS Q2)
146. Chernyshov M.V., Kapralova A.S., Matveev S.A., Savelova K.E. Stationary Mach Configurations with Pulsed Energy Release on the Normal Shock // Fluids. 2021. Vol. 6. Issue 12. Paper No. 439. 16 p. (SCOPUS Q2)
147. Chernyshov M.V., Savelova K.E. An Approximate Analytical Model of a Jet Flow with Mach Reflection and Pulsed Energy Supply at the Main Shock // Fluids. 2023. Vol. 8. Issue 4. Paper No. 132. 16 p.

Other publications on the topic of the dissertation
148. Chernyshov M.V., Savelova K.E., Fedosenko N.B. The extremal regular reflection of oblique steady and propagating shocks // Military Enginery. Ser. 16. Counter-Terrorism Technical Devices. 2019. Issue 3-4. Pp. 96-104. (in Russian)
149. Laptinskaya M.M., Savelova K.E., Chernyshov M.V. Shock-wave structure control methods in the input section of the aircraft high-speed intake // Engineering Journal: Science and Innovation. 2023. №. 2 (134). 12 p. (in Russian)
150. Chernyshov M.V., Murzina (Savelova) K.E., Matveev S.A., Yakovlev V.V. Shock-wave structures of prospective combined ramjet engine // IOP Conf. Series: Materials Science and Engineering. 2019. Vol. 618. Paper No. 012068. 10 pp.

151. Alekseeva M.M., Matveev S.A., Savelova K.E., Chernyshov M.V. Interaction of Steady Gasodynamic Discontinuities and Waves on Supersonic Gas Jet Flows from Rocket Engines // XLIV Academic Space Conference dedicated to Sergey Korolev. Moscow, 2020. AIP Conference Proceedings, 2021. Vol. 2318. Pp. 060004-1 – 060004-8.

152. Savelova K.E., Alekseeva M.M., Matveev S.A., Chernyshov M.V. Shock-wave structure of prospective combined jet engine // Journal of Physics: Conference Series. 2021. Vol. 1959. Paper No. 012043. 9 p. (The International Scientific Conference on Mechanics “The Ninth Polyakhov’s Readings” (ISCM), 9-12 March 2021, Saint Petersburg, Russian Federation)

153. Murzina (Savelova) K.E., Savelov V.A., Chernyshov M.V. Simulation of processes in a prospective detonation engine // Materials of the all-Russian Youth Scientific and Technical Conference “Start-2018”. Library of the Journal “VOENMECH. Bulletin of BSTU”. 2018. No. 51. Vol. 1. P. 58. (in Russian)

154. Murzina (Savelova) K.E., Chernyshov M.V. The prospective combined jet engine // The Eighth Utkin Readings: Proceedings of the All-Russian Scientific and Technical Conference / St. Petersburg: Balt. State Tech. Univ., 2019. Pp. 110-116. (in Russian)

155. Chernyshov M.V., Matveev S.A., Murzina (Savelova) K.E. Theoretical justification of a combined-type jet engine // All-Russian Youth Scientific Conference “Current Problems of Modern Continuum Mechanics and Celestial Mechanics”. November 26–28, 2018. Conference Proceedings. Tomsk: Krasnoe Znamya, 2019. Pp. 118-120. (in Russian)

156. Chernyshov M.V., Savelova K.E., Alekseeva M.M. Concept and theoretical substantiation of a combined jet engine // Current Problems of Protection and Safety: Proceedings of the XXII All-Russian Scientific and Practical Conference of the Russian Academy of Rocket and Artillery Sciences. Vol. 1. Armament and Military Equipment. St. Petersburg, 2019. Pp. 420-425. (in Russian)

157. Alekseeva M.M., Savelova K.E., Chernyshov M.V. Interference of stationary gas-dynamic discontinuities and waves in supersonic gas jets of rocket engines // XLIV Academic Readings on Cosmonautics, dedicated to the memory of S.P. Korolev and other outstanding domestic scientists – pioneers of space exploration: collected abstracts. M.: Bauman MSTU, 2019. Vol. 1. Pp. 317-319. (in Russian)

158. Savelova K.E., Savelov V.A., Chernyshov M.V. Simulation of fuel combustion on a shock wave in the air intake of a combined type engine // Current Problems of Protection and Safety: Proceedings of the XXIII All-Russian Scientific and Practical Conference of the Russian Academy of Rocket and Artillery Sciences. Vol. 1. Armament and Military Equipment. Saint Petersburg, 2020. Pp. 185-191. (in Russian)

159. Savelova K.E., Chernyshov M.V., Savelov V.A., Alekseeva M.M., Kapralova A.S. Analysis of shock-wave structures in the air intake channel of a prospective air-breathing engine // 19th International Conference “Aviation and Cosmonautics”. November 23-27, 2020, Moscow. Abstracts. M.: Pero, 2020. P. 187. (in Russian)

160. Savelova K.E., Alekseeva M.M., Chernyshov M.V., Yatsenko A.A. Shock-wave structures of the prospective combined jet engine // The Ninth Polyakhov’s Reading. Proceedings of the International Scientific Conference on Mechanics, 2021, Saint-Petersburg, Russia. Saint-Petersburg” VVM, 2021. Pp. 233-234. (in Russian)

161. Matveev S.A., Savelova K.E., Chernyshov M.V. Analytical models of supersonic flows with Mach reflection and pulsed energy supply // XLV Academic readings on astronautics, dedicated to the memory of S.P. Korolev and other outstanding domestic scientists – pioneers of space exploration: collected abstracts. Moscow: Bauman MSTU, 2021. Vol. 2. Pp. 50-52. (in Russian)

162. Gvozdeva L.G., Matveev S.A., Savelova K.E., Chernyshov M.V. Special and extreme triple configurations of shock waves in supersonic gas jets // Proceedings of the XXII International Conference on Computational Mechanics and Modern Applied Software Systems (VMSPPS’2021), September 4-13, 2021, Alushta. Moscow: MAI Publishing House, 2021. Pp. 333-334. (in Russian)

163. Savelova K.E., Savelov V.A., Chernyshov M.V. Shock-wave structures of internal supersonic flows with chemical reactions // Proceedings of the XXII International Conference on Computational Mechanics and Modern Applied Software Systems (VMSPPS’2021), September 4-13, 2021, Alushta. Moscow: MAI Publishing House, 2021. Pp. 450-452. (in Russian)

164. Savelova K.E., Chernyshov M.V. Approximate analytical model of supersonic flow with Mach reflection in the presence of pulsed energy supply // The 20th International Conference “Aviation and Cosmonautics”. Moscow: MAI, November 22-26, 2021. Collected Abstracts. M.: Pero, 2021. Pp. 140-141. (in Russian)

165. Savelova K.E., Chernyshov M.V. Analysis of shock-wave structures in the air intake channel of a combined air-breathing engine // Scientific Readings in Memory of Academician V.P. Glushko. Second All-Russian Scientific and Practical Conference. Saint Petersburg: Publishing house “Info-Da”, BSTU “VOENMEH”, 2021. Pp. 126-135. (in Russian)

166. Chernyshov M.V., Savelova K.E. Ambiguity of solutions for shock-wave structures // XXVI All-Russian Seminar with International Participation on Jet, Separated and Unsteady flows. Saint Petersburg: Balt. State Tech. Univ., 2022. Pp. 196-197. (in Russian)

167. Chernyshov M.V., Savelova K.E. New analytical models of supersonic flows with Mach reflection and energy supply at the main shock // XXVI All-Russian Seminar with International Participation on Jet, Separated and Unsteady flows. Saint Petersburg: Balt. State Tech. Univ., 2022. Pp. 197-198. (in Russian)

168. Savelova K.E., Chernyshov M.V. Shock-wave structures in supersonic aerodynamics and gas dynamics // Proceedings of the XXXIII Scientific and Technical Conference on Aerodynamics. Zhukovsky: TsAGI named after Professor N.E. Zhukovsky, 2022. Pp. 89-91. (in Russian)
169. Savelova K.E., Chernyshov M.V. Analytical study of triple-shock configurations with the possibility of pulsed energy release // XLVII Academic Readings on Cosmonautics 2023. Collected abstracts dedicated to the memory of S.P. Korolev and other outstanding domestic scientists – pioneers of space exploration. Moscow: Bauman MSTU, 2023. Vol. 1. Pp. 349-350. (in Russian)

Personal contribution of the author to publications

In joint publications, scientific supervisor M.V. Chernyshov owns the main idea of the work, statement of the problem and discussion of the results, part of the theoretical models and algorithms for quickly estimating the parameters of the shock-wave structure formed at the Mach shock reflection without energy release at the main shock. In the article [148], N.B. Fedosenko is responsible for the interpretation of the results obtained from the analysis of the regular reflection of an oblique shock wave in the case of refraction of a shock wave on an inclined surface (wedge) due to appropriate reversal of motion. In the works [149, 151, 152, 156, 157, 159, 160], M.M. Laptinskaya (Alekseeva) is responsible for the analysis of grid convergence and selection of turbulence models for numerical modeling in computational gas dynamics packages. In the works [144, 145, 146, 159] A.S. Kapralova is responsible for part of the work on the derivation of analytical relationships that describe the special properties, domain of existence and ambiguity of the shock wave structures under consideration, using methods of symbolic mathematics. In publications [151, 152, 146, 155, 161], S.A. Matveev is responsible for the analysis of the feasibility and practical applicability of the proposed type of combined air-breathing engines in engineering developments. In the work [150], V.V. Yakovlev owns a historical review and analysis of modern literature on the use of triple configurations of shock waves in gas-dynamic devices. In work [162], L.G. Gvozdeva was responsible for the discovery of the existence of triple configurations with a negative angle of inclination of the reflected shock in steady supersonic gas flows. In publications [158, 159, 163], V.A. Savelov is responsible for the verification of models of chemical kinetics in numerical experiments. In work [160], A.A. Yatsenko is responsible for the analysis of modern trends in the creation of detonation engines.

In all works the author of the dissertation owns:

- the idea of controlled combined applicatiob of flows behind shock-wave structures, which have different thermogasdynamic parameters, in different thermodynamic cycles;

- derivation, analytical and numerical solution of equations describing the region of existence of the shock-wave structures under study, including in conditions of ambiguity of the solution, and analysis of their realizability in steady flows;

- analytical and numerical description of changes in the criterion of shock reflection transition, similar to the von Neumann criterion, in the presence of pulsed energy release and changes in the chemical composition of the gas mixture at the main (Mach) steady shock;

- generalization of approximate analytical solutions describing the shock-wave structure of jet and channel flows with Mach reflection, for the case of the presence of pulsed energy release at the main (Mach) shock;

- numerical confirmation of the effect of transformation of the shock-wave structure (in particular, an increase in the size of the main (Mach) shock) in the presence of pulsed energy release, and determination of the region of existence of the Mach reflection under study with stationary detonation at the main shock.